Smartphone Nowcast Next Big Calamity

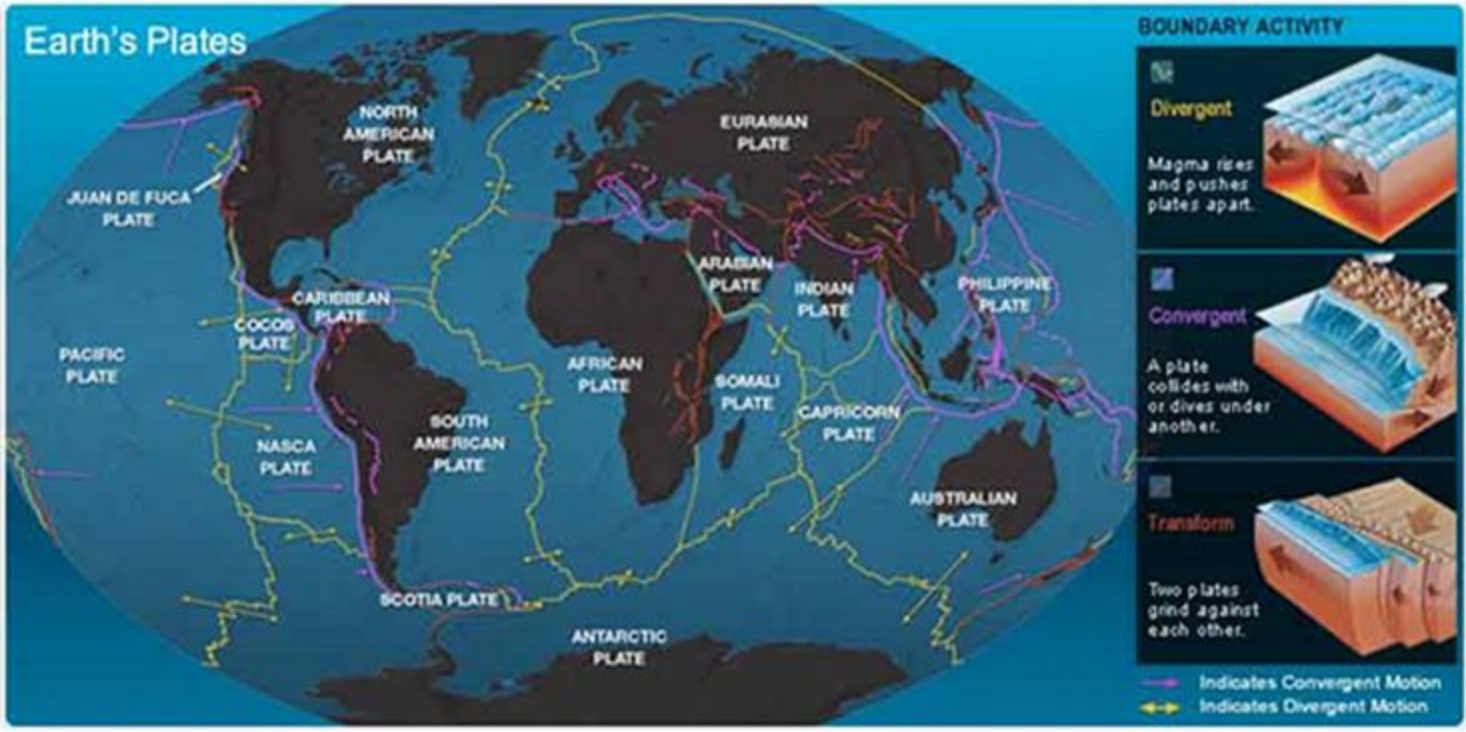

The contribution of :"Smartphones Nowcast Next Calamities," is to make sure that the next generation of Smartphones are active transceivers that can gather acoustic, optical, & seismological information for mankind's calamities (after minimizing the privacy, & false negative rate issues due to minority phones).

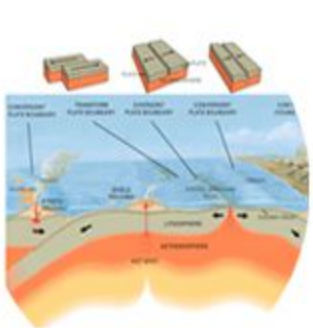

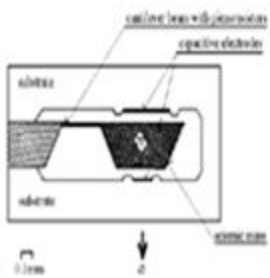

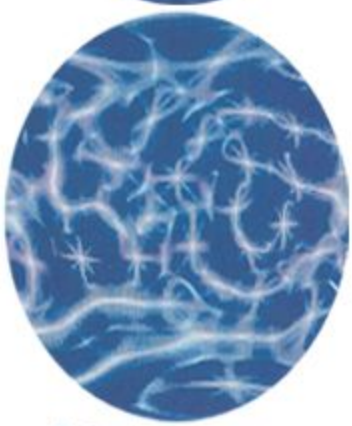

Dr Harold Szu

MedCrave

Step into the World of Research

Smartphone Nowcast Next Big Calamity

About the Authors

Dr Szu斯華齡 Harold

Ph. D. The Rockefeller Univ 1971; Res. Ord. Prof. EE, GWU, BME, CUA, Wash DC Fellows of IEEE (1075), OSA, SPIE, INNS (2010), AIMBE, AAIA, Academician Russian Nonlinear AS (#135, Jan15, 1999)

Several public websites are available for readers who are interested in the art and the author:

- "Nowcast natural resource and calamity warning," USPTO 8392122 B2, Apr. 29, 2008; USPTTO 0274493 A1, Oct. 28, 2010; USPTO 8,185,357 (2012); USPTO 8,392,122 (2013).
- http://www.usgs.gov/
- http://oregonstate.edu/instruct/oer/earthquake/04%20chapter%203_color.html
- http://www.crystalinks.com/platetectonics.html
- http://www.onrpao@onr.navy.mil (Oct. 2005)
- https://www.researchgate.net/profile/Harold_Szu2;
- http://www.ica-wavelet.org
- http://www.mathgeneology.org/harold_szu;
- https://www.youtube.com/watch?v=8Th2yqWt5mM
- R/D Funding Agency Federal Emergency Management Agency (FEMA): National Incident Management System (NIMA): as well as Defense Advanced Research Projects Agency (DARPA): or other appropriate ONR agencies in the United Nations and World. Our collective goal is to test Smartphone chain prototype and improve to reduce the False Negative Rate.

Correspondence: Harold H Szu, PhD (The Rockefeller U), BCC-YMCA, Bethesda MD, Fellows (AIAA, INNS, AIMBE, IEEE, OSA, SPIE) Academician (RAS) (RNL. S. V. Malrosov, 135, 1999), Res Ord Prof., CUA, Wash D.C, USA, Email szuharoldh@gmail.com

The contribution of : "Smartphones Nowcast Next Calamities," is to make sure that the next generation of Smartphones are active transceivers that can gather acoustic, optical, & seismological information for mankind's calamities (afterminimizing the privacy, & false negative rate issues due to minority phones).

Published By:

MedCrave Group LLC

November 09, 2023

Contents

Chapter 1: Why earthquake is periodic? Kitchen pot model

What is an Earthquake?

As Earth's plates move, the rocks in the crust gets pushed and pulled, scraped and jostled. Over time, strain slowly builds up inside the rocks and friction will hold the rocks in place for years. When they can't take it anymore, the rocks suddenly crack and shift. Their movement releases waves of energy called an earthquake.

Figure 1 Henri Bénard Cells in a Cooking pot convection mixing of viscous pea pot.

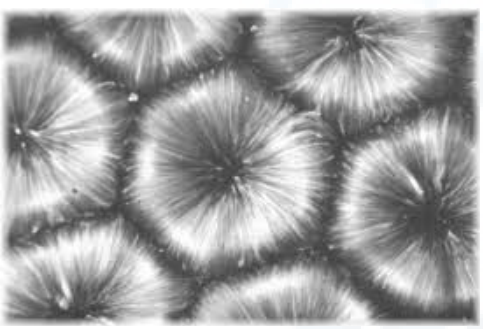

Figure 2 Although the earthquake mechanism is similar to a bubbling hot soup with a heavy (13 big 30 small) broken lid on.

It differs in the detail that is the rotation of the earth making those up and down motions no longer confined vertically, and, in fact, they drifted apart, by the **Coriolis force**, into a large vertical circular loop. A large thermal convection loops, the gravitational potential has revealed the differences at different places---weaker near the lighter upward dwelling and stronger at the heavier downward dwelling measured in the Space Satellite by *NASA*.

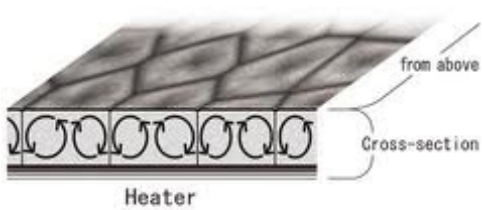

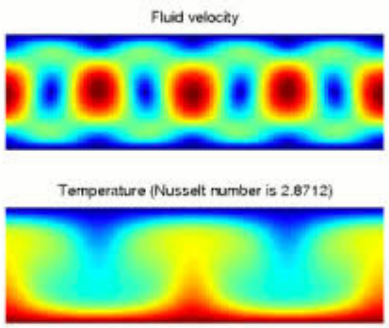

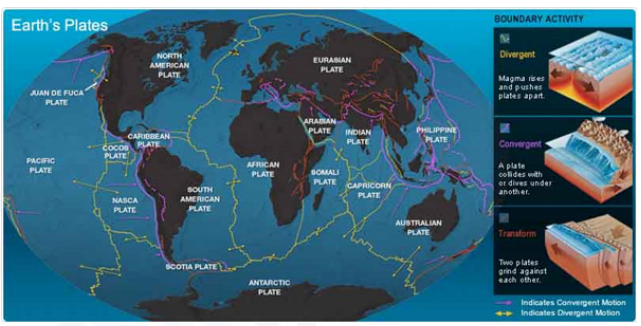

Figure 3 13 major tectonic plates, & 30 fragmented smaller plates replaced the classical continent drift theory (http://www.crystalinks.com/platetectonics.html).

Under Earth activity has several types: convergent push in; divergent out; and transform slide-pass. The lateral movement of the plates is typically at speeds of 0.66 to 8.50 centimeters per year.

Figure 4 Classical Land Instrument icative of a root mean square displacement of acoustic energy.

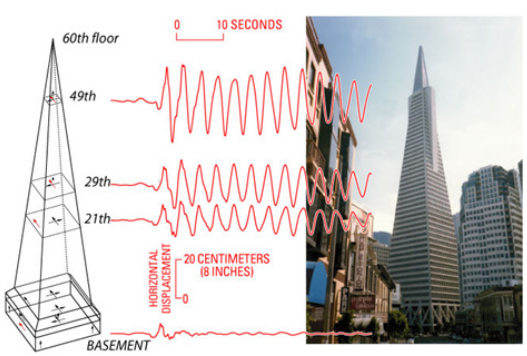

Figure 5 Sna Francisco Test Bed.

The 1989 Loma Prieta earthquake (magnitude 6.9) set San Francisco's Transamerica Pyramid swaying and rocking. An array of 22 sensors (small arrows) recorded horizontal movement on the 49th floor of the building five times greater than the 1.5 inches measured in the basement, as indicated by the recordings (red lines).

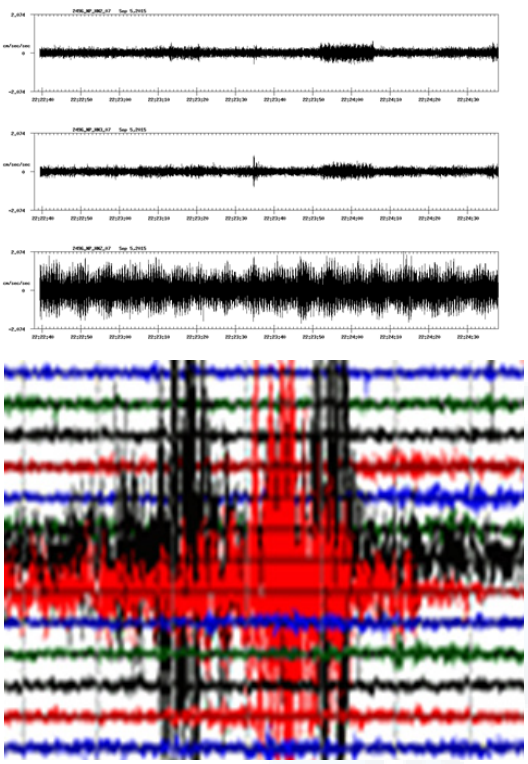

Figure 6 Seismogram displays.

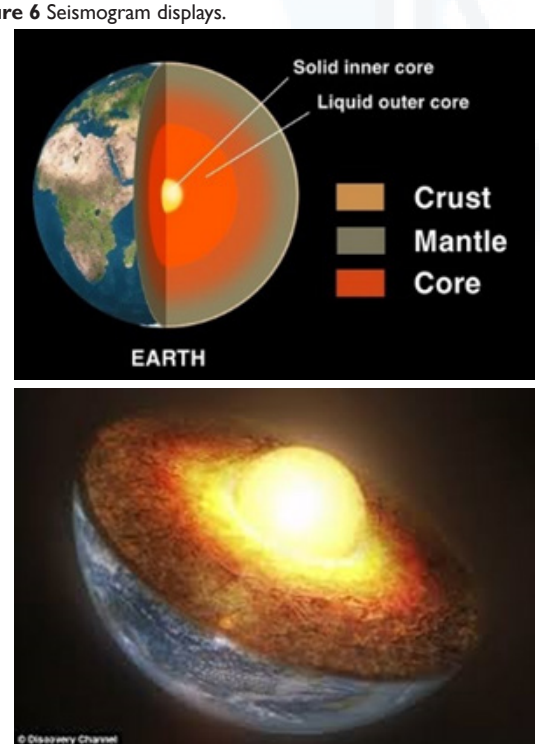

Figure 7 Earth Core is a hell fire ball like a cooked egg yoke.

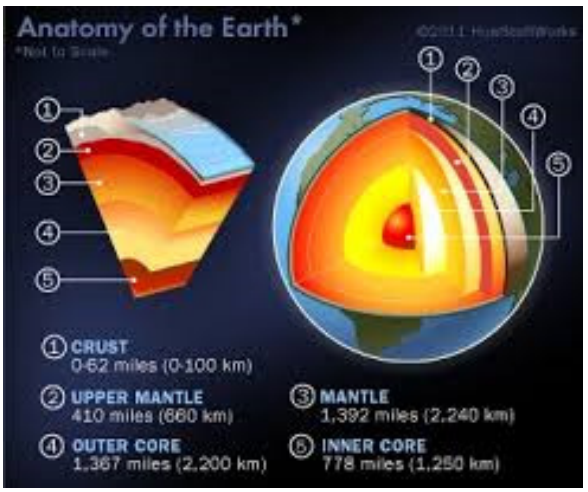

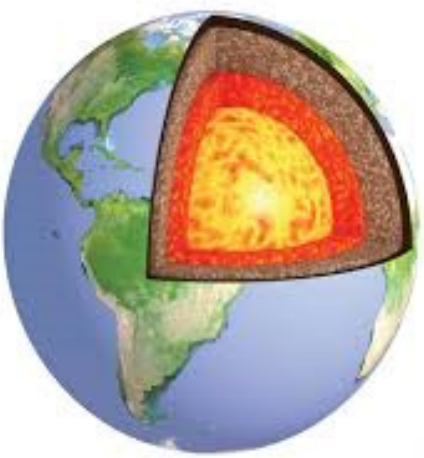

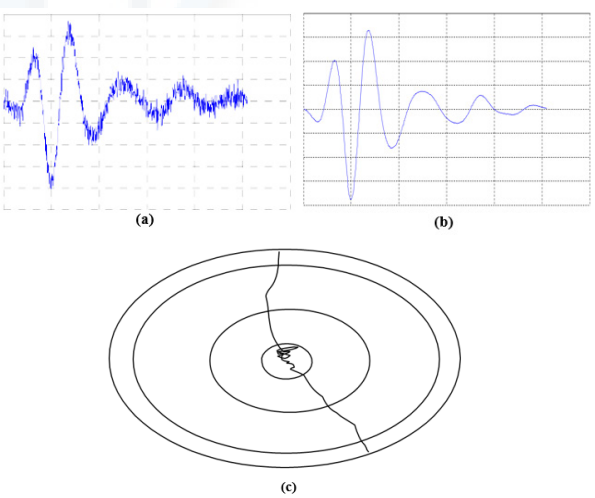

Figure 8 (a), (b), (c) How do we be sure the geologic model is true? (cf. *Wookey & Helffrich*, Nature V. 454, no. 7206, pp.873-876, 14 Aug 2008).

The book covers dummy common sense with dinner table conversations. The Earth Center is the biblical Hell with Fire at millions and millions degrees; Why it's so hot; How Iron was Formed in the Earth Core; 13 Helium fused into Iron Isotopes;

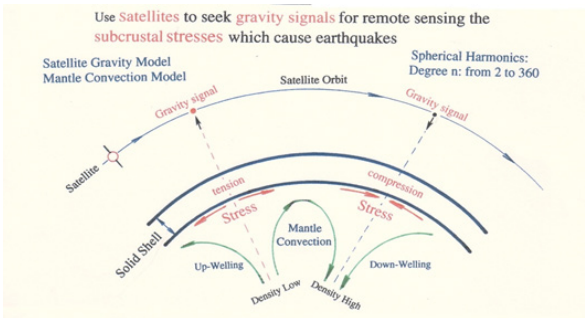

Figure 9 How NASA early measurement by Satellite flying over to detect abnormal compression and tension gravitational waves. The Earth has fireball core, layer III, molten rock mantel II and solid rock crust I.

Underlying course of Earthquake. Why Cyclic?

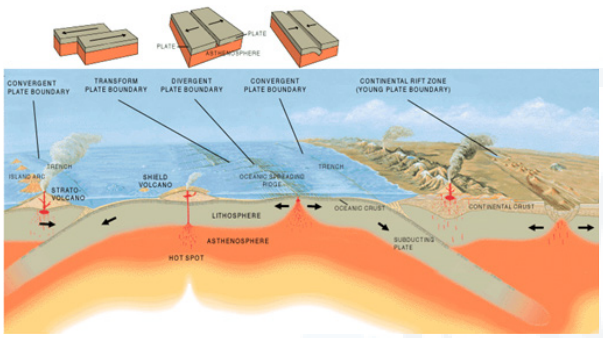

Figure 10 Earth Core Fireball as an active source of Earthquake.

To understand the Earthquake, we illustrated **Tsunami calamity** in 2004 because the India Plate buried under Burma Plate, Figure 3.

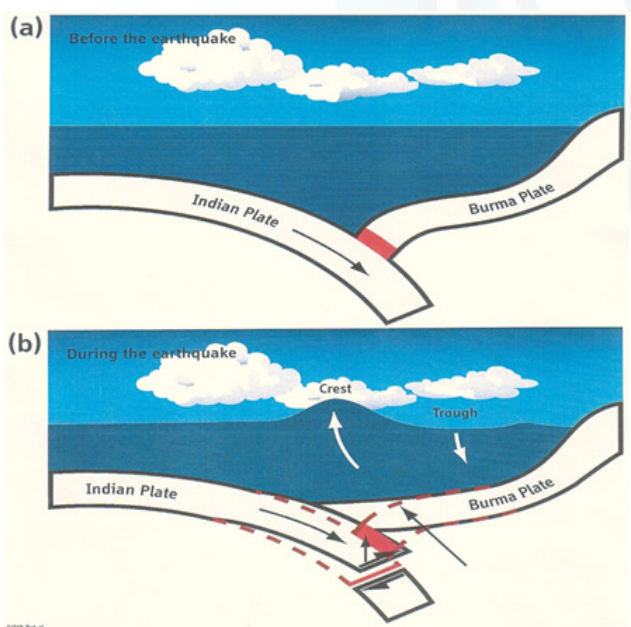

Figure 11 (a), (b) Tsunami is generated by earthquake mechanism e.g. Indian plate was sub-ducted by Burma plate under Indian Ocean **2004** (Szu & Liu 2008 SPIE Proc [2004 Charismas dar Indian Ocean earthquake1]).

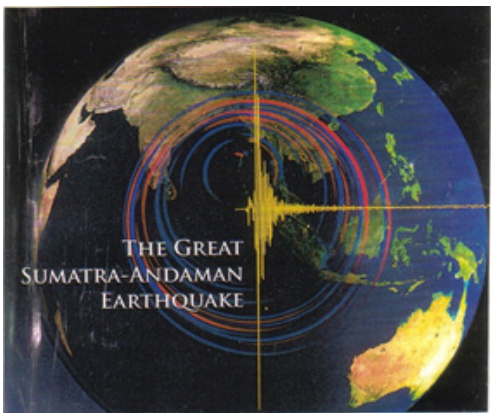

Figure 12

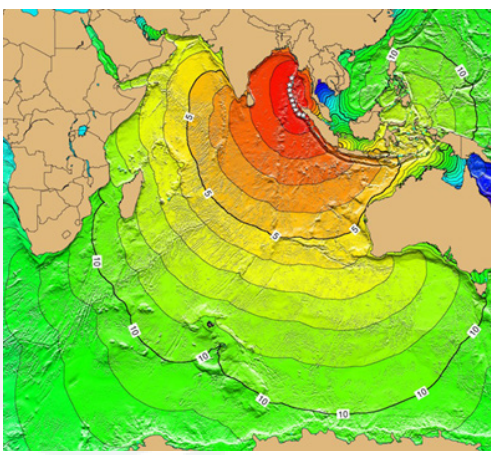

Figure 13

Figure 14

Figure 15 Ocean wave over 10 story high and generated by an Earthquake is called Tsunami in Japan over the holy Fuji Mountain in the background.

Figure 16 Tsunami on March 11, 2011 acclaimed 18,500 lives. Ōkuma, Infamous lesson learned is Japan 1st Nuclear Power Plant at Fukushima initiated primarily by the tsunami of the Tōhoku earthquake on **11 March 2011.**

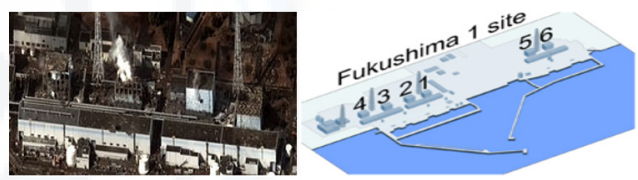

Figure 17 Fukushima Tsunami over the 1st Nuclear Power Plant with cooling melt down and radioactive leakage into ocean causing the death and subsequently cancer repercussion exceeding April 1986 disaster at the Chernobyl a nuclear power plant in Ukraine. The damage caused by the tsunami produced equipment failures, and without this equipment a loss-of-coolant accident followed with nuclear meltdowns. (The decay heat in the Unit 4 spent fuel pool had the capacity to boil about 70 tons of water per day (12 gallons per minute). The releases of radioactive materials began on March 12. It is the largest nuclear disaster since the Chernobyl disaster of 1986 and the second disaster (after Chernobyl) to measure Level 7 on the International Nuclear Event Scale, releasing an estimated 10 to 30% of the radiation of the Chernobyl accident.

On the ground Japan has the most experience in the earthquake detection and warning system Japan leads the ground **Earthquake Early Warning Technology (EEWT)**, since 1995 Kobe quake with 6000 causality& on March 2011 during Tohou-Oki Sendai epicenter of Richet magnitude **9** by gaining **15 second** early warning, informed worldwide in China, Taiwan, Mexico, Turkey and Romania.

(1) Early warning, (2) Emergence procedure: individual options for safety actions The Nuclear Power plant was located in Japan, which, like the rest of the Pacific Rim, is in an active seismic zone. and **worker operators took a wrong decision to save the PETO, rather Japan public** (3) **Mass Evacuation** The public need to know how to evaculate, and public evacuation streamline, that are just as important as the early detection and warning system.. Another lesson learned is about mass evacuation among 300,000 people who evacuated the area, approximately 1,600 deaths related to the evacuation conditions. **International Atomic Energy Agency** had expressed concern about the ability of Japan's nuclear plants to withstand seismic activity. At a 2008 meeting of the **G8's** in Tokyo, an expert warned that a strong earthquake with a magnitude above 7.0 could pose a "serious problem" for Japan's nuclear power stations The region had experienced three earthquakes of magnitude greater than 8, including the 1869 Jogan Sanriku earthquake, the 1896 Meiji-Sanriku earthquake, and the 1933 Sanriku earthquake. Fukushima Tokyo Electric Power Company (TEPCO) Generators but the design of motor cooling circulation system did not protect Tsunami waves. Six

GE light water, **boiling water reactors (BWR)** with a combined power of 4.7 gigawatts, making Fukushima Daiichi was the first GE-designed nuclear plant to be constructed and run entirely by the The **World Health Organization (WHO)** issued 2013 report and predicted that for populations living around the Fukushima nuclear power plant there is a 70% higher risk of developing thyroid cancer for girls exposed as infants, a 7% higher risk of leukemia in males exposed as infants, a 6% higher risk of breast cancer in females exposed as infants and a 4% higher risk, overall, of developing solid cancers for females.

In the US we have The San Andreas fault in central California. A "creeping" section separates locked stretches north of San Juan Bautista and south of Cholame. The Parkfield section is a transition zone between the creeping and southern locked section. Stippled area marks the surface rupture in the 1857 Fort Tejon earthquake.

Figure 18 San Andreas Fault California looking the North. San Andreas Fault near Park field California about 800 miles long suffered periodically large earthquake at Richter scale 5 and beyond.

The spatiotemporal varying **of Earthquake** spectrum in magnitudes and time is too complex to be statistically meaningful. Unless we take a cut at Richter scale M6 at Parkfield of San Andreas Fault., we can conduct Olympic and Beauty Pageant voting rule as follows:

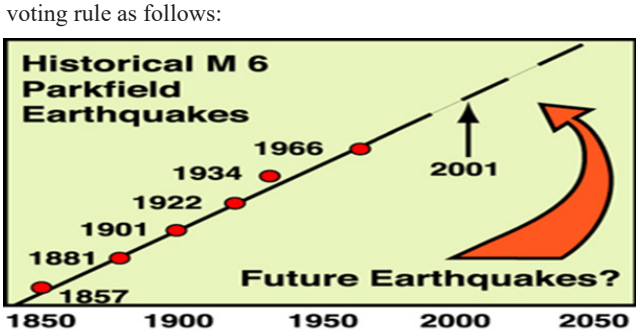

Figure 19 It seems to have 24 year period for large earthquake OD Richter scale 6 *1857, 1881, 1901, 1922, 1934, 1966, 2004.*

While little is known about the first three shocks, available data suggest that all six earthquakes may have been "characteristic" in the sense that they occurred with some regularity (mean repetition time of about 22 year) and may have repeatedly ruptured the same area on the fault. (See Bakun and Lindh, 1985 and Bakun and McEvilly, 1979) A complete record of the year of happening and the gap years of quiescence reveals the periodicity:

1857+24, 1881+20, 1901+21, 1922+12, 1934+32, 1966+38, 2004+?.

Firstly, a proper average method can produce more reliable forecast. We should adopt the score rule of Olympic and/or Beauty Pageant judges, namely by deleting the highest and the lowest biased scores; and average the rest. Deleting outliers 38 & 12, we obtain **two dozen magic number** of means & variance years among 4 remaining scores 24, 20, 21, and 32. Thus, the next large earthquake might be **24** years. Then, 2004+24= 2028, which subtract the current year 2015, would be about 13 years.

Figure 20 Great San Francisco Earthquake: Fire Hazard: On 5:12 am, April 18, 1906; Fire burned 3 days; claimed 3,000 lives. The enormous smoke coming from the lunchtime over turned stove fires after the San Francisco Earthquake in 1909.

Figure 21 Aftermath and re-build of San Francisco.

Its location near several of California's many faults, including the San Andreas Fault, made San Francisco prone to earthquakes. *Quakes shook the region in 1838*. But no one was prepared for what happened in the spring of 1906. At *5:12 am, on April 18*, underground rocks broke along the *San Andreas Fault* just ten miles from San Francisco. A loud roar could be heard as the Earth shook for a minute, toppling buildings. Within 15 minutes, dozens of fires were raging in downtown San Francisco. The *fires burned for three days* and were so intense that reddish smoke was visible to ships 100 miles out at sea.

The quake and fires destroyed much of San Francisco. Half the city's residents lost their homes. Many survivors fled San Francisco and never returned, making an accurate casualty count impossible. Although the death toll from the Great San Francisco Earthquake and Fire is often placed at *700*, some historians insist that more than *3,000* people died in this disaster.

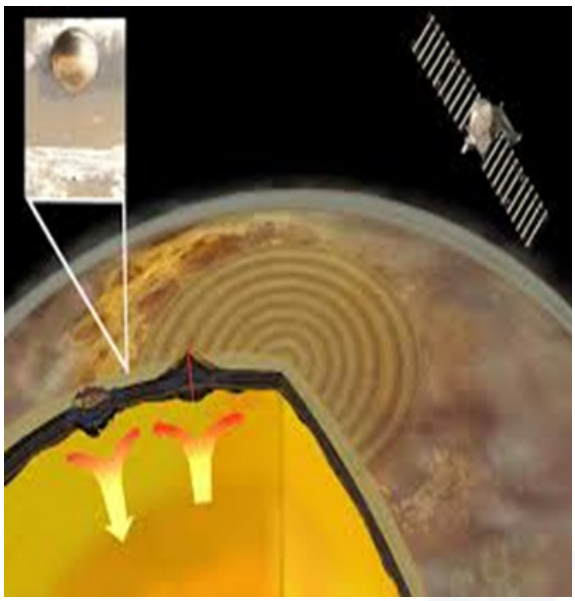

Figure 22 Tow down supervision would be the Satellite together with other seismology detonation wavelet probing for Earthquake detection.

When China completed the Great Three Georges Dam on the Yangtze River, China built more than three thousands dams in the province of Sichuan China since 1987 and completed in 2006 over the longest river Gorges Dam. Wenchuan (31N, 103E) located above the Dragon Gate fault in the north-east direction was the location of the 5/12/2008 Wenchuan Earthquake. In addition, large underground nuclear weapon facilities were constructed near the Dragon Gate Fault system. Therefore, the *gravity and stress fields* in that region (31° N, 103° E) in Sichuan was of great concern. The strength of this stress concentration approached $8x10^7$ dyne/cm^2, which is the fracture point of rocks. Therefore, the Dragon Gate fault system in this region may break up due to stress concentration. This stress concentration detected in 2006 by satellites was a precursor to the 5/12/2008 Wenchuan Earthquake in Sichuan. The predicted stress concentration pattern indicates that three cities of Wenchuan, Beichuan and Chinchuan above the Dragon Gate fault system could be destroyed NASA informed China Sichuan large stress underground but ignored from the Erroneous Judgment of Center Plate causing 88,000 deaths. Now there exist US-China bilateral calamity warning systems for the next large earthquake in a decade. NASA Satellite discovered Belgium Liege Earthquake in 1983 on **Eurasia Plate. Then 1983+ magic 24=2007 added 1 due to central plate immobility.**

In the space, US and World Wide Space Station Program have the system designed with a long baseline for low frequency stress wave tracking detection for early warning: Early satellite gravity data has discovered the convection model of molten mantle generating the Earth surface crustal stress fields. Theses stress fields have provided a unified forcing mechanism for deformation of the tectonic features on the surface of the Earth. Specifically, the crustal stress concentrations, as inferred from satellites gravity data, has explained the origin of 1976 Tangshan Earthquake in China, 1983 Liege Earthquake in Belgium, and 1993 Latur Earthquake in India. NASA Satellite discovered Belgium Liege Earthquake in 1983 on **Eurasia Plate. Then 1983+ magic 24=2007 added 1 due to central plate immobility.**

Figure 23 UN Environmental impact studies of Three Gorges Dam has recommended and eventually built the migration upstream side path for the Yangzi river bottom-dwelling man-size dragon fish from perished (cf. NGS Magazine). Do you Know "Three Gorges Dam" (China) has slowed down the rotation of earth.

Earthquake did happened on **15 May 2008 at Richet scale 7.8** took more than 80,000 human lives in Sichuan Province alone.

The NASA discovered from Satellite seismic wave measurement the abnormal increase of stress under the crust of Sichuan within China central plate and informed China weight of water might enhance the cooking pot theory. During 2006, China completed the Great Three Gorges Dam on the Yangtze River and built more than 3,000 dams in the Province of Sichuan. Furthermore, large underground nuclear weapon facilities were constructed near the Dragon Gate fault system. Therefore, geological instability in that region was of great concern. In order to evaluate potential risks of big earthquakes in Sichuan, it was of paramount importance to use satellites for synergetic detection of the deviations in the gravity and stress fields in China. In fact, during 2006, satellite gravity scanning discovered that stresses had concentrated under the crust of Sichuan. It was predicted that a big earthquake might hit Sichuan in China. Unfortunately, the Sichuan earthquake on 12 May 2008 with 8.0 logarithmic energy magnitudes at Richter scale had destroyed the infrastructure of more than 80,000 human lives in Sichuan Province. After this disaster, there were more than 33,000 aftershocks seismic events. Three are three common questions that need answers: #1. Why an 8.0 disastrous earthquake occurred in Sichuan? #2. Was there any precursor? #3. Where will be the next big earthquake in China? The purpose of this popular science book is to present the 2006 space images of the stress concentrations under Sichuan detected by satellites for addressing these three questions, and proposes a global solution.

This is a **wakeup call**, as seldom earthquake of that magnitude happened in the center of **Eurasia plate**. The delay of 8 years beyond fireball cycle at 2 dozen means & variance years implies a lot **more measurement labs and reinforcement building infrastructure** are needed. Since Smartphone is available to almost all in China, Smartphone Nowcast next big one can save lives. Within the framework of plate tectonics, there is little doubt that the massive plateau, **North of the Himalayas**, which maintains an elevation of 4.5 Km. over 600x1000 Km^2. This plate is anything but a direct consequence of the most spectacular **India-Eurasia plate collision** that must produce a stress field in the crust under China. Because a number of tectonic plates on the Earth move in a rather complicated way, the critical problem is how to derive the crusted stress field under China from the stress functions of the global plate boundaries.(2)

Figure 24 After the magic number ***means & variance years*** NASA *satellite gravity scanning* discovered the stresses concentrated under the crust of Sichuan within the *central Asian plate* near 3 Gorge Dam on the Yangtze River with 3000 dams.

Chapter 2: Why earth core is fireball?

Iron formation, isotope decay heat

We shall explain nuclear physics for dummy about the beginning of the universe as big bang theory, dark & bright matter comes from:

The so-called dark matter is a matter having no protons capturing neutrons forming the stable nuclei surrounded by the electronic orbital. The outer shell electron transition emits the optical light. Then, how we can see the light without electron orbits. . Without the light how can we detect the dark matter by telescope?

Figure 25 *Dark matter* is invisible. Based on the effect of gravitational lensing, a ring of *dark matter* has been inferred in this image of a galaxy cluster (CL0024+17) and has been represented in blue.

Astronomers using NASA's Hubble Space Telescope have discovered a ghostly ring of dark matter that formed long ago during a titanic collision between two massive galaxy clusters. The ring's discovery is among the strongest evidence yet that dark matter exists. Astronomers have long suspected the existence of the invisible substance as the source of additional gravity that holds together galaxy clusters. Such clusters would fly apart if they relied only on the gravity from their visible stars. Although astronomers don't know what dark matter is made of, they hypothesize that it is a type of elementary particle that pervades the universe. This Hubble composite image shows the ring of dark matter in the galaxy cluster CL 0024+17. The ring-like structure is evident in the blue map of the cluster's dark matter distribution. The map was derived from Hubble observations of how the gravity of the cluster Cl 0024+17 distorts the light of more distant galaxies, an optical illusion called gravitational lensing. Although astronomers cannot see dark matter, they can infer its existence by mapping the distorted shapes of the background galaxies. The map is superimposed on a Hubble Advanced Camera for Surveys image of the cluster taken in November 2004.

$$n \rightarrow p + e + \nu$$

Free neutron decay into proton, electrons and neutrino (proposed by Fermi to conserve the angular momentum) at 14 minutes & 42 seconds. When all neutrons disappear, then there will be no more atomic nuclei for light emitting matter. Thus, the majority universe is fill with dark energy 68%, and dark matters 27%, a small amount of atoms 5%, of which the miracle of life was born.

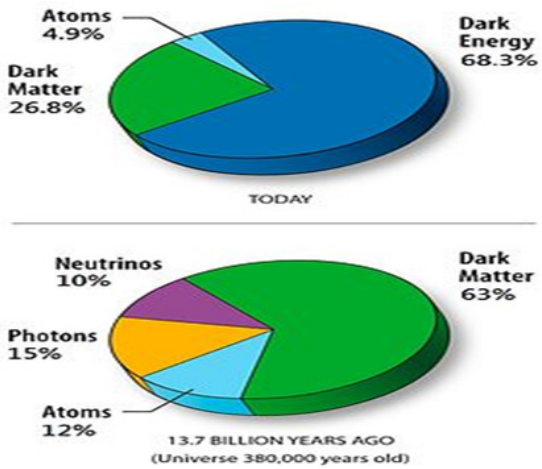

Figure 26

CMB Images IMAGES > CMB IMAGES > NINE YEAR MICROWAVE SKY http://map.gsfc.nasa.gov/media/121238/index.html Nine Year Microwave Sky The detailed, all-sky picture of the infant universe created from nine years of WMAP data. The image reveals 13.77 billion year old temperature fluctuations (shown as color differences) that correspond to the seeds that grew to become the galaxies. The signal from our galaxy was subtracted using the multi-frequency data. This image shows a temperature range of ± 200 microKelvin. Credit: NASA / WMAP Science Team WMAP # 121238 Image Caption 9 year WMAP image of background cosmic radiation (2012).

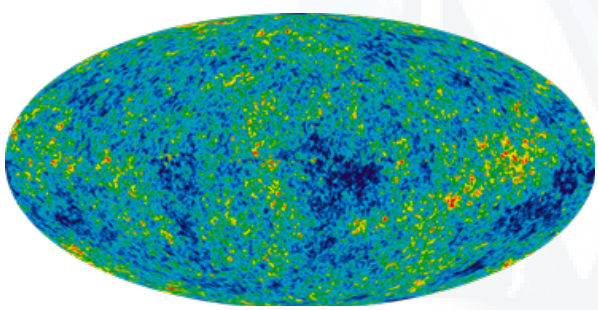

Figure 27

Dark matter was postulated by Jan Oort in 1932, albeit based upon flawed or inadequate evidence, to account for the orbital velocities of stars in the Milky Way, and by Fritz Zwicky in 1933 to account for evidence of "missing mass" in the orbital velocities ofgalaxies in clusters. Adequate evidence from galaxy rotation curves was discovered by Horace W. Babcock in 1939, but was not attributed to dark matter. The first hypothesis to postulate "dark matter" based upon robust evidence was Vera Rubin's in the 1960s–1970s, using galaxy rotation curves. Subsequently, many other observations have indicated the presence of dark matter in the universe, including gravitational lensing of background objects by galaxy clusters such as the Bullet Cluster, the temperature distribution of hot gas in galaxies and clusters of galaxies and, more recently, the pattern of anisotropies in the cosmic microwave background. According to consensus among cosmologists, dark matter is composed primarily of a not yet characterized type of subatomic particle. The search for this particle, by a variety of means, is one of the major efforts in particle physics today.

Although the existence of dark matter is generally accepted by the mainstream scientific community, some alternative theories of gravity have been proposed, such as MOND and TeVeS, which try to account for the anomalous observations without requiring additional matter. However, these theories cannot account for the properties of galaxy clusters.

Where earthquake come from?

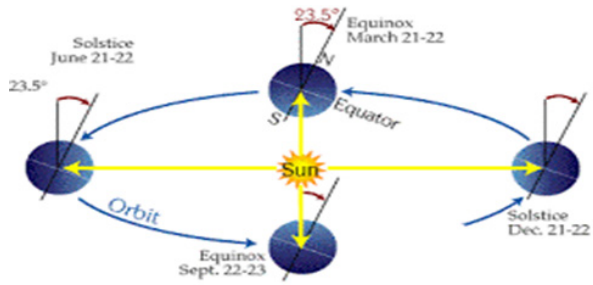

Figure 28 Kepler astronomy of the Earth rotating daily in a tilt axis 23.5 degree around the massive Sun solar orbit produced annually 4 Seasons.

----------**Excursion** ----------

Cosmological origin for dummy:

Figure 29 Discovery of hiss cosmic radiation background by Penzias and Wilson 1964.

In the late 1940s and early 1950s, George Gamov suggested that the elements in the Universe were "cooked" via nuclear reactions in the hot Big Bang. Later, Gamov and Alpher showed that actually the Big Bang could not create all the elements, but that the lighter elements, helium in particular, could have formed in this way. 1964, unaware of the cosmological predictions by, Penzias and Wilson discovered a persistent "hiss" in their radio antennae used to communicate with the Telstar satellite. The cosmic microwave background radiation (CMB) had been detected at Way at 3° K Cosmic Background Radiation.

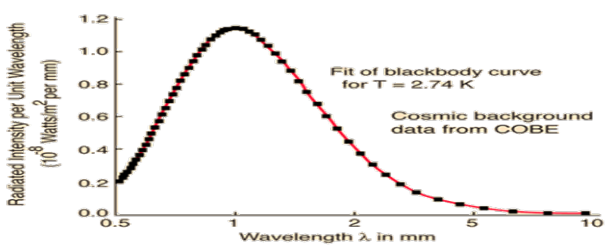

Figure 30 Cosmic background radiation happens to be Planck Black body radiation at the temperature of absolute 2.74=3 degree Kelvin.

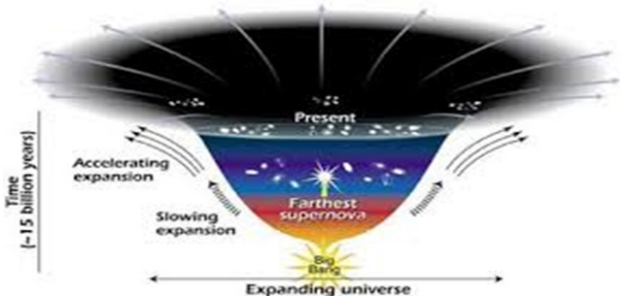

Figure 31 The expanding universe at the 15 billion years ago big bang, and the half-life, 7.5 billion years the celestial objects have been attracted away faster due to near the other heavy massive black holes.

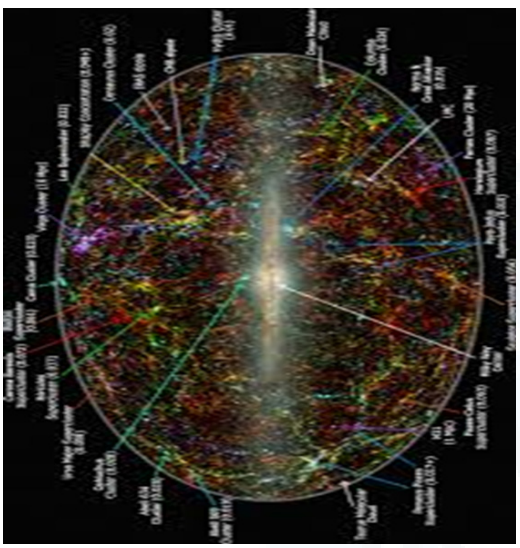

Figure 32 Big bang birth of our universe 15 billion years ago.

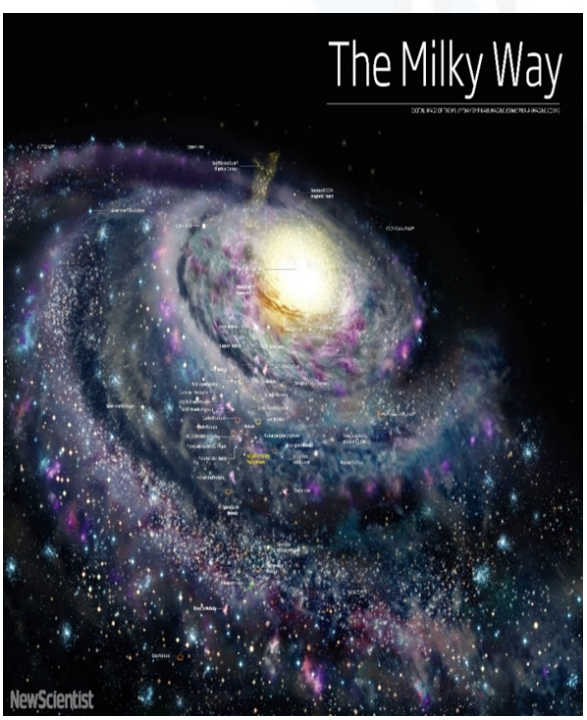

Figure 33 Our solar system Milky Way.

NASA/Ann Feild plotted the diagram 15 billion times versus size reveals changes in the rate of expansion since the universe's birth **15 billion years ago**. The more shallow the curve, the faster the rate of expansion. The curve changes noticeably about a half-life at **7.5 billion years ago**, when objects in the universe began flying apart as a faster rate. Astronomers theorize that the faster expansion rate is due to a mysterious black hole's gravitational attraction force that is pulling our galaxies apart.

Nuclear physics for dummy:

Our universe has more than half 68% bachelors, called dark matter, than married protons-neutrons nucleus, called light matter. The dark matter is like bachelors without family of male protons and female neutrons. It could not be surrounded with fighting transition of offspring of electrons, generating electromagnetic radiation called light. However, bachelor dark matter attracts by ubiquitous Newtonian gravitational force to married couples light matter. Thus, the astronomical observation of the light matter sluggish motions revealed the dark matter inertial mass. This phenomenon is similar to "***a dark matter river reflecting floating light matter leafs***."

An unbounded Neutron is not stable in a free space and will decay in 13 seconds; and the decay is predicted by Enrico Fermi:

$$N \rightarrow p^{+} + e^{-} + n.$$

He postulated the existence of neutrino, according to the conservation of angular momentum. Furthermore, he designed the experiment to prove the existence. He explore under deep salt mine cavern in Southern Italy, where all extra-terrestrial charged particles have been blocked, except the charge-less neutrino. He used tons of liquid detergent buckets as if bubble chambers deep down the salt-mine to capture the neutrino. For which he received the Noble Prize in experimental physics.

On the other hand, a free proton having positive charge will capture an electron in Hydrogen atom of which the ground state at 13 eV.

A dynamic balance keeps stable nuclear. Whenever proton fights in repulsing each other, nuclei castrated the positrons taking away their positive charges. The stripped charge gives to a neighborhood neutron making it a proton. The abundance of the universe indicates Hydrogen H, Helium He, Oxygen O_2, and Nitrogen N_2, However, when more neutrons available called **iron isotope**, and sometime neutrons competing pairing with protons have to decay, releasing large radiation heat energy. This is the source of earth core melting iron core.

Particle physics for dummy:

When Prof. CS Wu of Columbia Univ. Verified in the low temperature physics lab at NIST the theory that Prof. TD Lee of Columbia Univ. and Prof. CN Yang of NYSU Stony Brook postulated together the neutron decay theory, which violated the mirror-symmetry parity. They won the 1st Noble Prize in Theoretical Physic circa 1957. This is a decade before Feynman computing Quantum Electrodynamics (QED) by a re-summation of divergent Feynman diagrams; and Gel 'man proposed with SU3-8-fold way as the group theory organization of nucleons in 3 quarks and mason particles with fractional spin quantum numbers 1/3. (A. Pairs missed the race at the publication at PRL)

Earth core is about the size of moon, but is ultra-hot at millions degree and under exceedingly high pressure. Both conditions are similar after big bang making possible of nuclear fusion of 13 helium He_2^4 plus 4, 5, 6 more neutrons into the nuclei iron Fe_{26}^{56}, indicating atomic number 56 and proton 26. The iron has ore neutrons becomes the iron isotopes Fe_{26}^{57}, Fe_{26}^{58} that will decay generating enormous heat. That's how he earth core becomes molten iron inner core.

Iron neuclei composed of 13 **Heliums:**

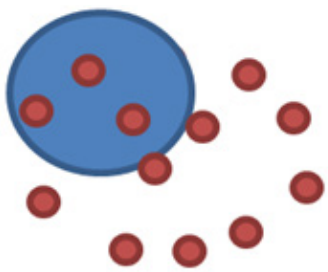

Figure 34 Iron composed of 13 Helium and 4 more neutrons to be Fe_{26}^{56}.

Iron is called iron because of 26 protons from the 13 Helium fused together under the tremendous pressure and temperature. The big bang helps fuse the gaseous ***Helium of 2 protons and 2 neutrons*** He_2^4 together to generate other chemical elements. For example, ***13 Helium*** fused into iron nucleus that has ***26 positron-charged protons***. **To keep peace** among protons from repelling one another in a closely packed living quarter of the nuclei. The nuclei must have at least equal and number of charged-neutral Neutrons. When protons are in trouble, their charge positron will be taken away from a proton to give to a neutron, making a neutron into a proton at a slightly distance apart.

An unbounded Neutron is not stable in a free space and will decay in 13 seconds; and the decay is predicted by Enrico Fermi:

$$N \rightarrow p^+ + e^- + n.$$

He postulated the existence of neutrino, according to the conservation of angular momentum. Furthermore, he designed the experiment to prove the existence. He explore under deep salt mine cavern in Southern Italy, where all extra-terrestrial charged particles have been blocked, except the charge-less neutrino. He used tons of liquid detergent buckets as if bubble chambers deep down the salt-mine to capture the neutrino. For which he received the Noble Prize in experimental physics.

On the other hand, a free proton having positive charge will capture an electron in Hydrogen atom of which the ground state at 13 eV.

A dynamic balance keeps stable nuclear. Whenever proton fights in repulsing each other, nuclei castrated the positrons taking away their positive charges. The stripped charge gives to a neighborhood neutron making it a proton. The abundance of the universe indicates Hydrogen H, Helium He, Oxygen O_2, and Nitrogen N_2, However, when more neutrons available called **iron isotope**, and sometime neutrons competing pairing with protons have to decay, releasing large radiation heat energy. This is the source of earth core melting iron core.

These thermodynamic mixing force generated movement slowly and the uprising thrust hit the pot cover periodically generating large earthquakes with the magic cycle **2 dozen years**. Why the earthquake is periodic? Knowing the cycle of Earthquake may help Nowcast. To answer this curiosity, we note that the Earth solid mantel mechanics become similar to viscous fluid in turns of the geological million-year time scale.

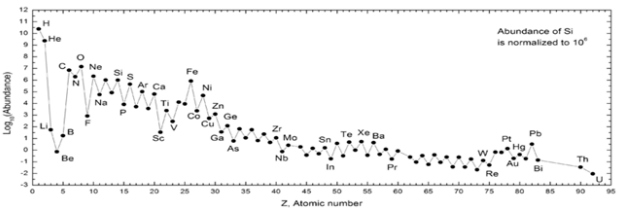

Figure 35 Abundance of chemical elements plotted against proton atomic numbers.

The upwelling of lesser density matter from the heated bottom layer generating the Earthquake. Henri Bénard, a French physicist, in 1900 studied such a "cooking pot mixing" hydrodynamic theory.

Common sense

There were seldom 4 leg animals discovered in earthquake remains. 4 bare feet on the ground without shoes and sense the trembling direction and run away. This is nowcast capability---discovery of the happening of large earthquake and the direction of arrival.

Figure 36 Vesuvius Volcano in the background where the eruption on 5 February 62 AD buried Pompeii city, now an archeologic site.

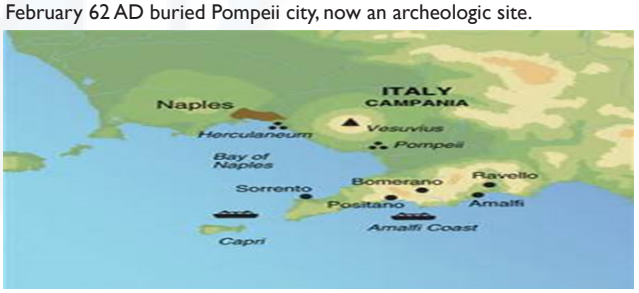

Figure 37 European Mediterranean Sea Naple Bay shows active earth crust stress map in lighter color.

Figure 38 Archeology remains reveal no wild animals.

Why animals seem to be able to escape buried under Earthquake archeological remains? What do animals have that we don't? For example, historically the most famous is the *Pompeii earthquake* occurred on 5 February 62 AD. It had an estimated a maximum intensity of XI or X on the *Mercalli intensity scale*, versus the squared intensity called *Richet energy scale*. The towns of *Pompeii* and *Herculaneum* completely damaged and buried underneath. However, among archeology remains, there were no 4 legs animals, except 2 legs. One explanation is that the animals having 4 bare feet on the ground sensing the trembling and the propagation direction finding to run away for life. Since modern human could not live with bare feet, a natural question could be whether or technology can help.

Three we never heard that "***Science has nothing to do with the Truth, but the Consistency***," said by Albert Einstein, according to Abraham Pairs who is his colleague at the Princeton Advanced Studies. While the Theologies and Philosophers deal with the Truth of Why and Who; but the Scientists and Engineers answer the rest of 4W's: What, Where, When and how. Accordingly, "Engineering has nothing to do with the Truth, but Consistent Approximations for Real World Applications." The book has mixed "something new, something old; something borrows & something blues," with many archival pictures, and descriptions taken from Internet Wikipedia. While the technology is domestic, the science is international. No one owns the science, but shares them. The more you share, the more you gain. In other words, the arts and the literature, as well as the math and the science are belonging to the public.

While forecast of Earthquake is not reliable; but nowcast of few minute ahead is absolute possible and useful to save life.

Since the Earth is a large nonlinear complex chaotic system, a long range large area forecast may not be reliable beyond the acoustic horizon. Nowcast is possible based on available Smartphone worldwide. It is always on everywhere. Especially, we anticipate a smarter version of Smartphone can be more than a passive transceiver of newscast, but also actively gather the scientific data. For example, we demand the next gen Smartphone to equip a miniaturized Seismic wave sensor, e.g. every car-seat airbag equipped with an ***Inertial Motion Unit (IMU)*** made of a small proving mass suspended in piezoelectric material that can turn the inertia distortion of material into electric signals made of dipole displacement current. Then, Smartphone can participate the cell tower network processing seismic wave data using the ***computational intelligent (CI)*** of modern ***Artificial Neural Network (ANN)*** technology where every node is Smartphone forming ***massive parallel and distributed (MPD)*** architecture. Smartphone Nowcast is possible because animals can, and why can't we?

Thus, such a compilation of common sense dummy book is ***"free to*** region.

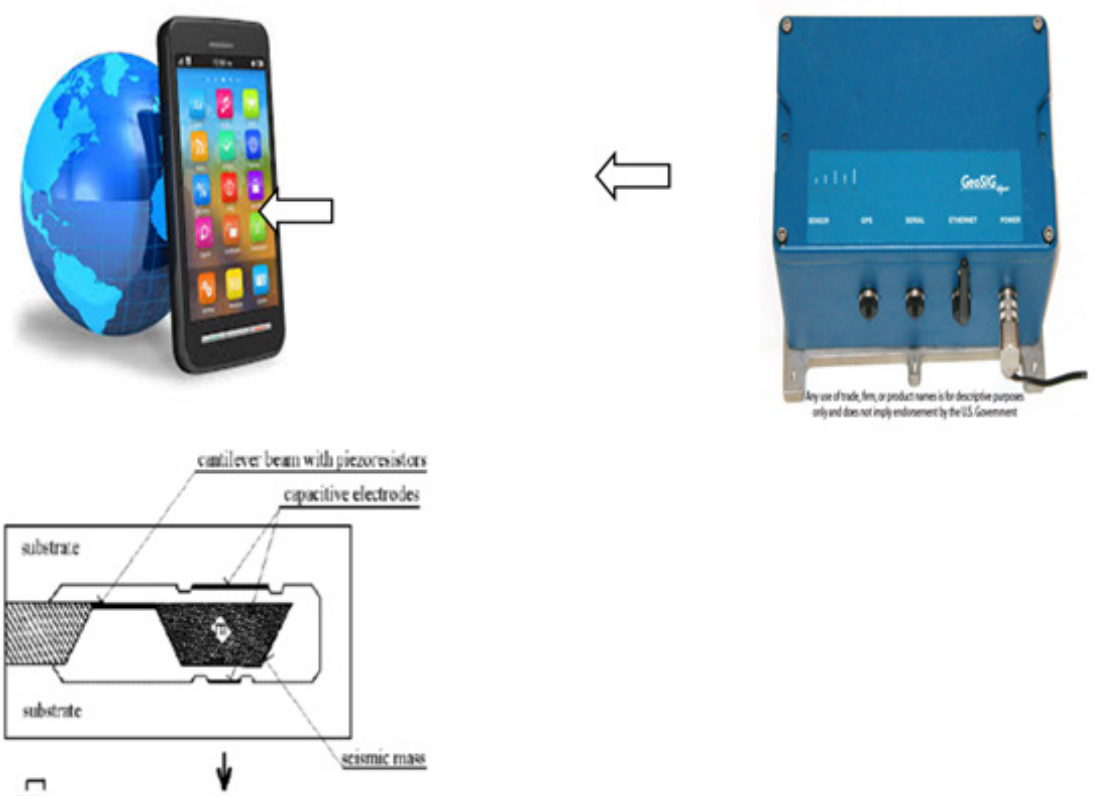

Figure 39 Inertial Motion Unit (IMU) has schematically a small proofing ball packaged within piezoelectric material in Micro-Electro-Mechanic System (MEMS). One needs to be tested & evaluated such a package in Next Gen Smartphone that are ubiquitous always on and everywhere. It would be a MPD supplement to Earthquake stations and effective Nowcast transceivers. A key algorithmic would be the nontraditional Computation Intelligence (CI) that is based on MPD asynchronously artificial neural network (ANN) where every node is Smartphone.

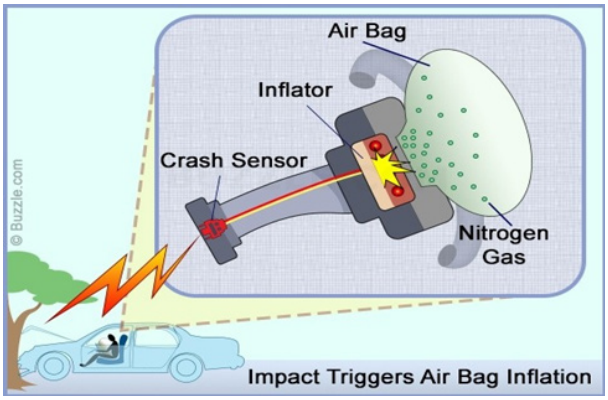

Figure 40 Chemistry explosive can help save life in car accidents.

Moreover, every car seat has safety airbag that detonated under a sudden deceleration, sensed and triggered by an Inertial Motion Unit (IMU) in the Micro-Electro-Mechanical System (MEMS) technology using a proving mass ball suspended in the piezoelectric bracket material. Thus, we suggested to improve IMU sensitivity and embedded in every Smartphone that can together build a netted sensing Nowcast system can provide a precious few minutes (longer than Japan record 15 seconds) during the imminent earthquake event.

The necessary and sufficient condition for Nowcast is also an emergence procedure must be drilled and known to all involved. Nowcast is just-in-time happening for taking lifesaving actions--running up-hill in beach, hiding under a sturdy metal desk upstairs, rushing to the open space in house, etc.

We will explain why in every region on the Earth there exists a set of mean and variance dates $\mu \mp \sigma$ based on the local statistics of big earthquakes. The exact happening time of next big one is almost unpredictable. The forecast is almost like the unpredictable chaos; but can be bounded, e.g. San Andrew Fault Parkfield $\mu \mp \sigma \cong 24 \mp 4$ yrs. The precise happening seems to be 4 bare feet animals on the ground sensing the actually happening in real time. We wish to emulate the animal capability with the next gen Smartphone that has built-in IMU and relayed through the MPD Cellular Towers. This is what we are anticipate the Nowcast Next Big One capability?

In God, we trust; all the rest, show data," Professional geologists have done what they can in decades to develop sensing, measurement instruments, and install seismological station nationwide. Nothing beats the real thing.

The data collected will help USGS scientists locate buried geologic features associated with the August 23, 2011 earthquake and its aftershocks.

August 23, 2011 Virginia Earthquake of M5.8. The instruments in the airplane recorded Earth's gravitational and magnetic fields as well as natural background radioactivity. Gravity and magnetic data can be analyzed to locate faults up to several miles underground.

What is Richter scale?

The magnitude of earthquake was defined first by Charles Richter of Caltech in 1935 as an integer logarithmic scale, and each integer 7 to 6 is 31 fold increase of seismic energy, in the unit of the Natural e=3.1-based logarithmic wave amplitude ratio, as an end y.

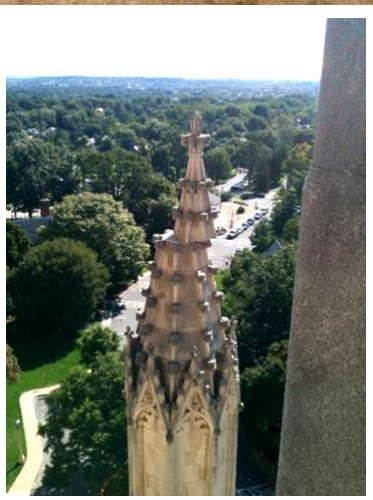

Damage to Washington National Cathedral August 23, 2011 M5.8

Also, in the US East Coast Virginia has the magnitude 5.8 happened few months later on **August 2011**.

Shake Table Parkfield, CA, USA

NetQuakes strong-motion instruments enable seismologists to collect extensive data in urban areas where installing traditional seismographs is not practical.

National strong motion project

Latest significant earthquakes					
Location	**Date**	**Time**	**Event ID**	**Magnitude**	
34 km (21.3 mi) ESE of Lamjung, Nepal	04/25/2015	06:11:26.270 UTC	us20002926	7.8	
8.0 km (5.0 mi) SSW of Napa, CA	08/24/2014	03:20:44 PDT	72282711	6.0	
78km (48mi) WNW of Ferndale, CA	03/09/2014	22:18:13 PDT	72182046	6.8	
16 km NNE of Van, Turkey	10/23/2011	10:41:22 UTC	usb0006bqc	7.1	
Earthquake Name	**Date**	**Time**	**Latitude**	**Longitude**	**Magnitude**
Lamjung_us20002926	4/25/2015	06:11:26.270 UTC	28.147	84.708	7.8
SouthNapa_24Aug2014	8/24/2014	03:20:44 PDT	38.22	-122.313	6
Ferndale_09Mar2014	3/9/2014	10:18:13 PM PDT	40.829	-125.134	6.8
EasternTurkey_23Oct2011	10/23/2011	10:41:22 UTC	38.722	43.513	7.1
MineralVirginia_23Aug2011	8/23/2011	17:51:04 UTC	37.936	-77.933	5.8
Japan_11Apr2011	4/11/2011	8:16:13 UTC	37.007	140.477	6.6
Japan_07Apr2011	4/7/2011	14:32:41 UTC	38.25	142.64	7.1
Japan_11Mar2011	3/11/2011	5:46:24 UTC	38.297	142.373	9
NewZealand_03Sep2010	9/3/2010	16:35:46 UTC	-43.53	172.12	7
Calexico_04Apr2010	4/4/2010	3:40:42 PM PDT	32.259	-115.287	7.2
Chile_27Feb2010	2/27/2010	06:34:14 UTC	-35.909	-72.733	8.8
HaitiRegion_12Jan2010	1/12/2010	12:21:53 UTC	18.457	-72.533	7
Ferndale_09Jan2010	1/9/2010	4:27:38 PM PST	40.645	-124.763	6.5
SamoaIslands_29Sep2009	9/29/2009	17:48:10 UTC	-15.509	-172.034	8
LAquilaItaly_06Apr2009	4/6/2009	01:32:39 UTC	42.334	13.334	5.8
ChinoHills_29Jul2008	7/29/2008	11:42:15 AM PDT	33.955	-117.765	5.4
Sumatra_Aftershock	9/12/2007	23:49:04 GMT	-2.506	100.906	7.9
Sumatra_12Sep2007	9/12/2007	11:10:26 GMT	-4.52	101.374	8.4
Hawaii_15Oct2006	10/15/2006	7:07:48 AM HST	19.82	-156.027	6.7
Parkfield_28Sep2004	9/28/2004	10:15:24 AM PDT	35.815	-120.374	6
SanSimeon_22Dec2003	12/22/2003	11:15:56 AM PST	35.706	-121.101	6.5
HectorMine99	10/16/1999	2:46:45 AM PDT	34.6	-116.27	7.1
Northridge_17Jan1994	1/17/1994	4:30:55 AM PST	34.209	-118.541	6.4
Landers92	6/28/1992	4:57:31 AM PDT	34.216	-116.433	7.3
BigBear92	6/28/1992	8:05:31 AM PDT	34.201	-116.826	6.5
Petrolia_25Apr1992	4/25/1992	11:06:05 AM PDT	40.38	-124.23	7.1
SierraMadre91	6/28/1991	7:43:00 AM PDT	34.262	-118.002	5.8
LomaPrieta_17Oct1989	10/17/1989	5:04:00 PM PDT	37.037	-121.883	7
Whittier87	10/1/1987	7:42:20 AM PDT	34.067	-118.078	6.1
MorganHill84	4/24/1984	2:15:19 PM PDT	37.317	-121.68	6.2
Coalinga_02May1983	5/2/1983	4:43:00 PM PDT	36.25	-120.3	6.5
Livermore80B	1/26/1980	6:33:35 AM PST	37.76	-121.7	5.8
Livermore80A	1/24/1980	11:00:09 AM PST	37.84	-121.8	5.9
ImperialValley79	10/15/1979	4:16:00 PM PDT	32.64	-115.33	6.6
SanFernando_09Feb1971	2/9/1971	6:00:00 AM PST	34.4	-118.4	6.6
KernCounty_21Jul1952	7/21/1952	4:52:14 PM PDT	34.958	-118.998	7.5
ElCentro_18May1940	5/18/1940	8:36:40 PM PST	32.844	-115.381	6.9
LongBeach_10Mar1933	3/10/1933	5:54:00 PM PST	33.7	-118	6.4

Space observation has predicted by the *satellite gravity scanning* discovered during November 8, 1983 Liege, Belgium that stresses concentrated under the crust of Liege in Belgium, an orderly evacuation has executed.

If the magic curse were consistent, the next big one will be 2004+24=2028.

Internet free publication is 'to level the playfield' like the e-commerce with a 'fat tai distribution' (due to every items has its own pair correlation, e.g. tourist-camera, or biker-sneaker. Rather than without the hindrance by traditional business bricks & mortars, winner takes all. We anticipate the Smartphone to be owned by everyone with 99% correlation. It is more than passively warning Newscast system, it can actively sense with inertial motion unit (IMU) used already in every car safety airbag that can likewise sensing the trembling direction finding of Earthquake arrival precisely over a large cellular towers. For example, the famous Vesuvius volcano of Northern Italy erupted on Feb 5, 62 AD, and unfortunately buried the whole Pompeii city under the volcano molten rocks and ashes. Archeologist discovered buried under the remains no 4-leg animals except 2-leg homosapiens. We have a simple message: "***Let's build a Smartphone Newscast & Nowcast System with computational natural intelligence (NI; not AI),*** emulating the Pompeii animal instincts." To achieve on a formidable task, "a journey of thousand miles begins with the first step," as one of my teachers, Mac Kac President of Am. math Soc., quickly added: "so long as it began with the right direction." We think, we did if we make Smartphone smarter.

We will cover topics for dummy, such as BIG BANG--BIRTH of THE UNIVERSE, DARK and BRIGHT MATTERS; IRON FORMATION AT EARTH CORE; IRON ISOTOPE DECAY HEAT; ANIMAL INSTICTS; (WHY NO 4-FOOT ANIMAL REMAINS BURIED UNDER ITALY POMPEII EARTHQUKE); COMPUTATIONAL INTELLIGENCE; UNSUPERVISED LEARNING; ARTIFICIAL NEURAL NETWORK (ANN) NATURAL INTELLIGENCE (NI) versus ARTIFICIAL INTELLIGENCE AI); etc.

They are relevant to our understanding of what the causes of Earthquakes are to explain the periodicity, and how we can do accurate Nowcast, among all clutters and noises. In short, we developed a '***kitchen cooking green pea soup theory***. ***While the hot pea expanded, and became buoyant, the cold pea, contract, became heavy and sunk. That cycle took the magic number of means & variance, 2 dozen, years to happen***. The uprising peas hit ***13 big +30 fragmented the pot cover in*** clashing one another, ***known as the tectonic plate's*** theory of the Earthquake. Where does the inferno 'heat' of Earth cores come from? We provide a rudimental Nuclear Physics for dummies. Big Bang of the Steve Hawkins black hole generated our Universe that happened at 15 billion years ago, and only $2.74^{o}K$ Cosmic Radiation Background remained. The major heat contribution is a sort of ***Helium fusion bomb***, namely 13 of the Helium nucleus, and each has 2 Protons P=2 indicated the 2nd location on the periodic table, and 2 neutrons N=2, making the atomic weight P+N=4; Thus, helium is denoted as He_2^4. When 13 of them were fused into iron P=26, N=26 and the atomic weight P+N=52 which must further captured 4, 5, and 6 more charge-neutral Neutrons into $Fe_{26}^{56}\ Fe_{26}^{57}; Fe_{26}^{58}$ isotopes to balance the electric repulsion Coulomb force among those positive-charged Protons. The rest of 2 dozen iron isotopes are less stable and would decay by fission atomic bomb and generate enormously large amount of heat. Now we can explain the reason why the periodicities of larger Earthquakes (at Richter scale $M \geq 6$) happen regularly at means & variance years? The magic number means & variance is statistically based on Olympic & Beauty Pageant voting rule: we deleted the longest delay 38 yrs. and the shortest 12 yrs. between 2 consecutive large Earthquakes in St Andreas Fault about 800 miles long in CA. Since the last one happened in 2004, which add mean 24 yrs. & variance -5 favor shorter period become 2023, which minuses the current year 2015, we discover 8 years of Next Big One. Of course, the exact time of the "Next Big One" required the modern Computational Intelligence (CI). The CI architecture is layer by layer brain-style artificial neural networks(ANN) to achieve the unsupervised learning blind sources separation (BSS) for de-clutter and de-noise among all kind of seismic waves Smartphone node equipped with sensitive Inertial Motion Unit (IMU) (used already in every airbag of car seats).

We take the input of terrestrial cellular towers and the space satellite seismic measurement. Of course, "***the devil, if any, is in the detail***."

We are grateful to the Gravity-Stress Theory that Han-Shou Liu, Chandrasekhar, O"Keefe and Runcorn, who taught the author (cf. SPIE Proc. Wavelet Aero-sense **2008** (Orlando FL)).

Chapter 3: Animal instinct, smartphone nowcast

We can't tell when a large Earthquake is. In other words, we can't "Nowcast," but some animal's instinct can. There are reports of cats, dogs, cockroaches, and rats becoming disoriented and disturbed prior to big earthquakes. It is well-known that a few seconds ahead of those calamities can save lives. What does animal know that we don't? Can modern technology help the animal's survival instinct? We suggest that the handy Smartphone that is not only useful for passive broadcast of Earthquake but also for active gathering seismic wave information. This network advantage is like a hurricane chaser forecast system, when somewhere is Nowcast hurricane, elsewhere will be reliable hurricane forecast.

Smartphone companies world-wide are proudly competing with a plenty of wedges and gadgets from GPS to Map Navigation. Shouldn't we ride the tidal wave and demand a robust capability of Earthquake Nowcast? In dummy fashion, the Author's advent of unsupervised learning Natural Intelligence (NI, not rule-based Artificial Intelligence (AI)), Artificial Neural Network (ANN) that emulates all animals instinct based on (1) the constant temperature of brains minimum free energy to do self-referencing voting work, and (2) the power of pair sensors as the vector time series. We can solve Blind Sources (Earthquake or not) Separation (BSS). These are the main points we wish to encourage the community to learn and prompt the vendors with a smarter Smartphone with NI.

Figure 41 Does a dog hunt by sights and smells? Dogs use the sights and smells in the chase. What happen to a dog seating and waiting on hind legs? Dog senses ground vibrations on the stomach and sampling the prey ode by nose when the wind is in the right direction.

Figure 42 Elephants communicate low rumbles (25fps) sound & stamp on marching.

These elephant rumbling sounds are low frequencies, similar to the Earthquake seismic waves. Computer simulations indicated these seismic waves generate by a human versus an elephant are quite different. The former is playing, the latter is communication.

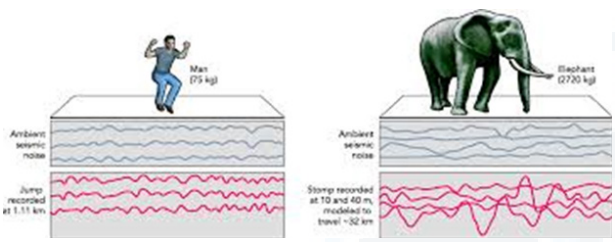

Figure 43 Comparison between human tramping with body weight, versus elephant using their toes and fingers scratching.

Historically, a famous earthquake buried Pompeii city 5 February 62 AD finding no 4 legs wild animals

Seldom have wild four leg animal skeleton but domesticated. Although no one knows exactly forecast where and when, not even the 4-leg creature but their bare feet on the ground provided a reliable Nowcast happening, as the animal sensed directly the trembling vibration with a specific direction finding among 4 leg animals.

Also, Smartphone have Earthquake warning display information. On the other hand, beside standard transceiver at L-band 1.8GHz capability, Smartphone should have their own IMU with mobile uniqueness and advantage. There are million Smartphone users nationwide. Smartphone enjoy the law of large number.

1. Massively parallel and distributiveness (MPD) Architecture;
2. Sensitive IMU that can adaptively sense beyond mobile movement and vibrations, the typical large seismic vibrations.
3. Robust nature comes from the law of large number.
4. Overcome variation of arrival time (AT) at local cellular phone tower level.
5. Improved by the fixed locations from tower to tower communication network**.**

USGS has Earthquake Hazards Program inform residence, and early warning on ShakeAlart that shall connrct Smartphone in two way street in the near future

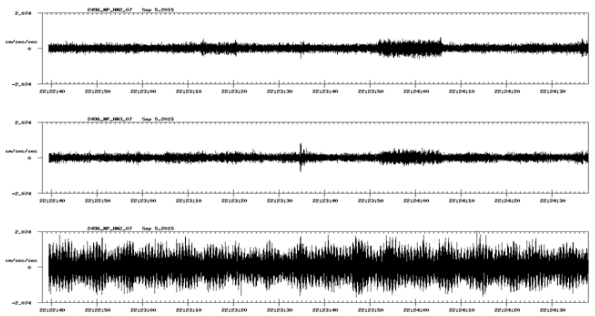

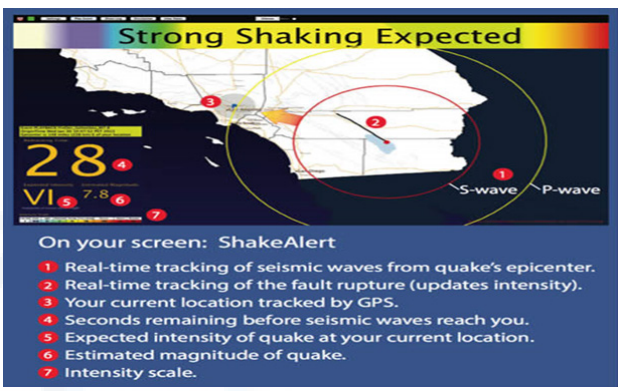

A user of Shake Alert receives a message like this on the screen of his computer. The message alerts the user to how many seconds before the shaking waves arrive at their location and the expected intensity of shaking at that site. The shaking intensity follows the Modified Mercalli scale; an intensity of VI, as shown here, would mean the shaking is felt by everyone, people find it difficult to stand, and structures may suffer some damage. Earthquake early warning systems use earthquake science and the technology of monitoring systems to alert devices and people when shaking waves generated by an earthquake are expected to arrive at their location. The seconds to minutes of advance warning can allow people and systems to take actions to protect life and property from destructive shaking.

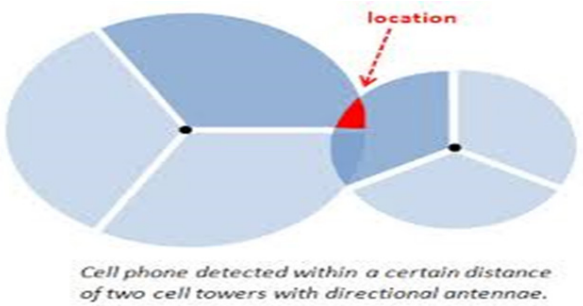

Cell phone detected within a certain distance of two cell towers with directional antennae.

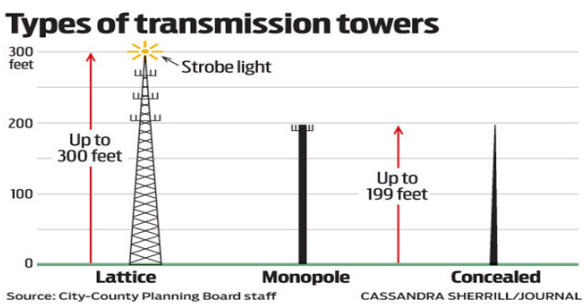

Microwave 1900 MHz=1.9GHz L band.

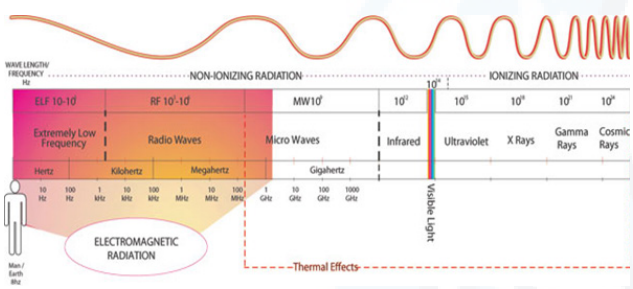

Body resonates with the earth's magnetic field at **10Hz**

What is Smartphone Nowcast technology?

Besides usual engineer's design considerations for Size, Weight and Power, Cost (SWaPC), Smartphone technologists shall consider miniaturized silicon piezoelectric material. This technology has already used in every car safety airbag detonation mechanism. The device can convert proving mass stress-strain to the electricity in every Inertial Motion Unit (IMU) embodying Micro Electric-Mechanic System (MEMS). Smartphone lab will take into account of the robustness versus the sensitivity trade-off according to earthquake magnitudes and frequencies statistics compared against car accident frequency (cf. earthquake dispersion spectrum, cf. USGA archival data).

The morale of our story is that "educated consumers wish to emulate animal instincts, and demand a technology help human with the miniaturized MEMS/IMU installed in **Next Gen Smartphone**." **How can Smartphone technology help Nowcast?** Since everyone and everywhere have Smartphone and cell towers. Smartphone Nowcast at some place becomes the Smartphone forecast at elsewhere (related by Coriolis force of Earth Mental Convection Model. Consequently, we could "Nowcast" ***precious 15 seconds*** ahead of the major Earthquake. We need demonstrate that measurement IMU proving mass will not perturbed the Earth Gravitational mass disturbance, so that it can be made small to increase the sensitivity, and yet the MPD NI architecture can increase the robust nature in our Cooking Pot Theory of Earthquake.

Figure 44 Smartphone is mounted with infrared (IR) filtered night vision camera, and weak short range microwave magnetron adopted in a save microwave oven at 2.4 GHz, together with long range communication at L band at 1 GHz Transceiver.

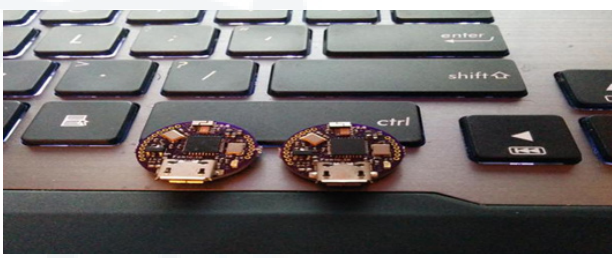

Figure 45 A small IMU compared to PC keyboard.

We can make NI ANN algorithm adaptive to SSSW, we need to improve the traditional deployment-control algorithm in the **sensing and diagnostic module (SDM)** in airbag in the tradeoff between the sensitivity and the robust when an internal accelerometer senses a ShakeAlart. After the algorithm is initialized, the microprocessor compares measured vehicle deceleration and other calculated values with calibration parameters stored in the SDM that were developed from many deployment and non-deployment crash events. To decide if bag deployment is warranted, the SDM considers signals from multiple accelerometers and door-pressure sensors. If the algorithm commands an airbag deployment and the arming function in the SDM concurs, electrical power is provided to the airbags to begin deployment." All that generally happens within 8 to 40 milliseconds of the initial impact.

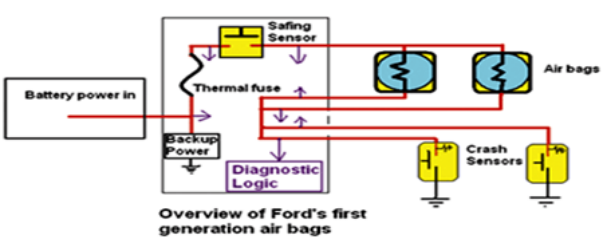

Figure 46 Simple Circuitry of Triggering Mechanism of Airbag needs to be improved for roaming Smartphone.

First, the sodium reacts with potassium nitrate (KNO_3) to produce potassium oxide (K_2O), sodium oxide (Na_2O), and additional N_2 gas. The N_2 generated in this second reaction also

fills the airbag, and the metal oxides react with silicon dioxide (SiO_2) in a final reaction to produce silicate, which is harmless and stable. (First-period metal oxides, such as Na_2O and K_2O, are highly reactive, so it would be unsafe to allow them to be the end product of the airbag detonation.)

We begin with well-known cellular phone tower for Wireless Communication Smartphone Architecture as follows: The capabilities that digital active array antennas bring to radar systems applied to communications systems**.** A great deal of active research is in the application of digital beam-forming to wireless communications systems. In a conventional wireless mobile telephone network, a large geographic area divided into a large number of cells, namely "cellular phones" as software defined radios.

Figure 47 Software defined radio.

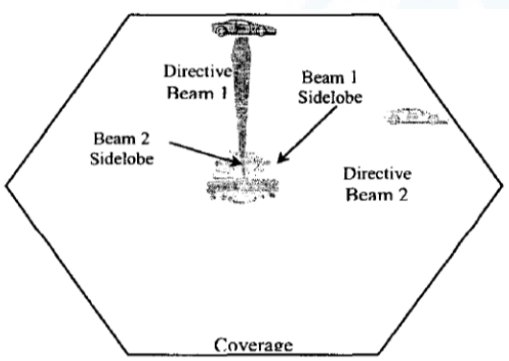

Figure 48 MPD Cell Towers.

Almost all information systems (music, phone, TV) have gone from analog to digital and why not RF device communication devices? We reviewed the Smartphone (cell tower CDMA) and Satellite (Iridium 66-like low-lying), as well as Future Space Station (having a long baseline for low frequency seismic waves earth core-mental trembling) Technology for dummies but smart buyers to demand early production of reliable IMU in every Smartphone, besides the legally requirement of GPS locator for emergency Smartphone call. Thus, smart buyer require a massively parallel & distributed Smartphone Smart Sensor Web, where every node is Smartphone in near field. We shall complete the *Near-Field Communication* with the Cellular *Far-Field Communication* with Cellular Tower and *Remote-Field Communication* with Satellite and Space station.

A single base station handles all of the mobile traffic within its cell. Frequency reuse is employed but in nonadjacent cells to minimize co-channel interference. *Azimuth coverage of 360 degrees* typically achieved in each cell by using between one and three *broad beam antennas***.** More complex antenna schemes, including diversity systems that mitigate multipath effects, and switched beam antennas that switch through an array of higher gain, narrower beam-width antennas to increase range coverage, have deployed. Adaptive beam-forming using conveniently digital device applied to a base-station antenna array in a scheme known as Space Division Multiple Access (SDMA), which can also be used to provide enhanced performance. In the SDMA concept, multiple directive independent beams, all at the same frequency, are steered at each beam at the mobile user while steering antenna user. Frequency reuse within a cell achieved by providing spatial isolation.

The device design has taken into account of all Commercial Off-The-Self (COTS) component technologies: (1) the inexpensive and reliable digital electronics transceiver technology developed for wireless digital phone using GaAs p-chip; and (2) the back plane communication technology using matured fiber optics wires with precision laser clock, as well as (3) Arbitrary waveform synthesizer (like music-CD) in terms of binary bits or Direct Digital Synthesizers (DDS's), for a simple Continuous Wave (CW) and linear chirp.

Chapter 3.1: Why earthquakes seems to be quasi-periodic

Analogously, the kitchen cooking pot has real world Earthquake that monitored from Satellite flying over seeking gravity signal for remote sensing. In the book we further extrapolate the modern Earthquake cooking pot theory to implement it on Smartphone equipped with small and sensitive IMU for massively parallel and distributed (MPD) in-situ Computational Intelligence (CI) for solving Blind Sources Separation for accurate Nowcast to gain 15 second to save millions lives.

The Rayleigh–Bénard Instability

Since there is a density gradient between the top and the bottom plate, gravity acts trying to pull the cooler, denser liquid from the top to the bottom. This gravitational force opposes the viscous damping force in the fluid. The balance of these two forces is by a non-dimensional parameter called the Rayleigh number. The Rayleigh defined

The geophysics has the **Rayleigh** number for the Earth's mantle, due to iron radioactive heating, Ra_H is given by

$$Ra_H = \frac{g\rho_0^2 \beta H D^5}{\eta \alpha k}$$

where H is the rate of radiogenic heat production, η is the dynamic viscosity, k is the thermal conductivity, α is the thermal diffusivity, β is thermal expansion coefficient, and D is the depth of the mantle.

At a critical Rayleigh number of 1708 for certain simplified boundary conditions, the instability sets in, and convection cells appear. The simplest case is that of two free boundaries, which Lord Rayleigh solved in 1916, and obtained $R_c = {}^{27}/_4\,\pi^4 \approx 657.51$.

IIya Prigogine of UT Austin received the Nobel Prize in 1977. He solved the far-away equilibrium structure called the spontaneous symmetry breaking. Bénard cells are meta-stable called "dissipative structure" as the irreversible thermodynamic.

The measurable seismic waves behave similar to daily stock trade rippling adjustment effect. While a hotter commodity expands its mass inertia becoming lighter popular and buoyant up noticeable; a colder contracting mass becomes denser and sinking down in trade board listing. Such mixing convection instability is similar to major stock profit taking activities---"buy low and sale high." Both major seismic wave events and stoke market trades may likewise require the CI Nowcast Decision-Aid Algorithm (CI-NDAA). Someday, the CI-NDAA can help adjusting the prime interest rate, i.e. a job usually done by experience Chairman Greenspan of Federal Reserve Board.

Why periodic?

Since 1857, six similar, Richet 6 earthquakes have occurred on the San Andreas fault near Parkfield with apparent regularity -- one approximately every means & variance years. Secondly, waveforms recorded on regional seismographs are strikingly similar for the 1922, 1934 and 1966 earthquakes, suggesting that these earthquakes involved repeated rupture of the same area on the fault. These observations suggest that there may be some predictability in the occurrence of earthquakes, at least at Parkfield. In addition, much is being learned about the physics of earthquakes from advances at Parkfield, including the discovery of repeating micro-earthquakes (see Ellsworth, 1995) and earthquake "streaks" (see Waldhauser et al 1999, and Rubin, 1999).

Recordings of the east-west component of motion made by Galitzin instruments at DeBilt, the Netherlands. Recordings from the 1922 earthquake (shown in black) and the 1934 and 1966 events at Parkfield (shown in red) are strikingly similar, suggesting virtually identical ruptures. Moderate-size earthquakes have occurred on the Parkfield section of the San Andreas fault at fairly regular intervals - in

Smartphone Nowcast requires similarly the stable predictability like hurricane chasers, who took the Nowcast at a region as surely the Forecast of the other. This is also true in Earthquake as the Earth rotates counter-clockwise from the West towards East so that the Sun always rises in the East every day. It's the fixed tilt of Earth rotation axis at 23.5^o w.r.t. solar orbital plan, making spring, summer, fall and winter four seasons possible over 364+ days. Sun contains 99.86% of all of the mass of the entire Solar System. The Sun is 864,400 miles (1,391,000 kilometers) across. The Sun weighs about 333,000 times as much as Earth. It is so large that about 1,300,000 planet Earths can fit inside of it. Earth is about the size of an average sunspot! The fixed orbital geometry is important to provide us with a stable gravitational attraction force among heavenly bodies, of which any major perturbation, inside closer major or outside far away minor, disturb the solar flares in radio communication and Earthquakes.

A couple of historical Earthquakes are cursory reviewed.

- In 1975, Sichuan had Earthquake at Magnitude 7.5 Richet scale, people reported in northeastern China mice and rabbits leaving their burrows and snakes coming out of hibernation in the middle of the winter before a huge earthquake occurred.
- In 1906, the night before the big San Francisco earthquake, horses in San Francisco grew panicky.
- Other sign from animals that an earthquake is coming includes birds flying in circles, dogs barking for hours and elephants starting to run.
- The day before the 1964 Good Friday Earthquake, Alaska's Kodiak bears came out of hibernation weeks before schedule.
- The space gravity anomaly data revealed a catastrophic earthquake that calls for more research & development (R&D) programs toward building a Now-cast real-time warning system. It may require the collaboration among several international parties: For example, (i) the International Future Space Station (IFSS) agency sponsors specifically a program of satellite-like gravity monitoring program; (ii) the United Nations sponsors the supercomputing for the development of the earth crust, mantle, and core interaction dynamics for the global scale earthquake and tsunami; and (iii) the international Professional Societies sponsoring a forecasting competition for the real-world gravity vector time series data analysis. Some have been accomplished, but the more remains to be the R&D from sponsored by
- Smartphone Nowcast of the next big Earthquake at millions time powers (Richet scale 6 & beyond) which can be anywhere along 800 miles of San Andreas Fault in California. However, the precise timing of forecast would be challenging.
- The earthquakes were due to the imbalance generated by the earth fireball ***core*** about the size of moon, which is made of ***liquid metal*** layer generating electrical current producing by Faraday induction the geo-magnetic field of 50 micro Tessa in the North pole and a gravitationally compressed ***solid metal*** core freezing into a single giant iron crystal of hexagonal closed-packed having ~1% anisotropy. This model was recently discovered a century ago by Oldham 1906, verified by a natural impulse seismic wave. The natural seismic earthquake wave was generated on 22 Feb 2006 propagated all the way from Japan coast line, through the Earth core, to Mozambique of South America. It happened to be in the shape of Hermitian super-wavelet amenable to be easily teased out of seismic noise background by means of Donohue wavelet de-noise algorithm. This mathematic tool might provide more opportunity to provide solid evidence with other less prominent shear waves propagating through solid and liquid phase core of Earth.

- There is historically earthquake seismic wave measurement from Japan to South America passing thorough the Earth core. The clean-up experimental data (a) from *Japan coast line, through the Earth core, to Mozambique of South America*.
- This data is similar to the Hermitian wavelet data (b) (cf. Nowcast of natural resource and calamity warning, Harold Szu, USPTO 8392122 B2, Apr. 29, 2008). It revealed a dual polarizations shear wave through the mantle, liquid & solid iron core. Changing from p wave (low frequency)-s wave (high frequency inside solid core)-p wave respectively (c), producing the relative slowness about 1.5 second upon the arrival, in a large shallow event at Richter energy scale 7.

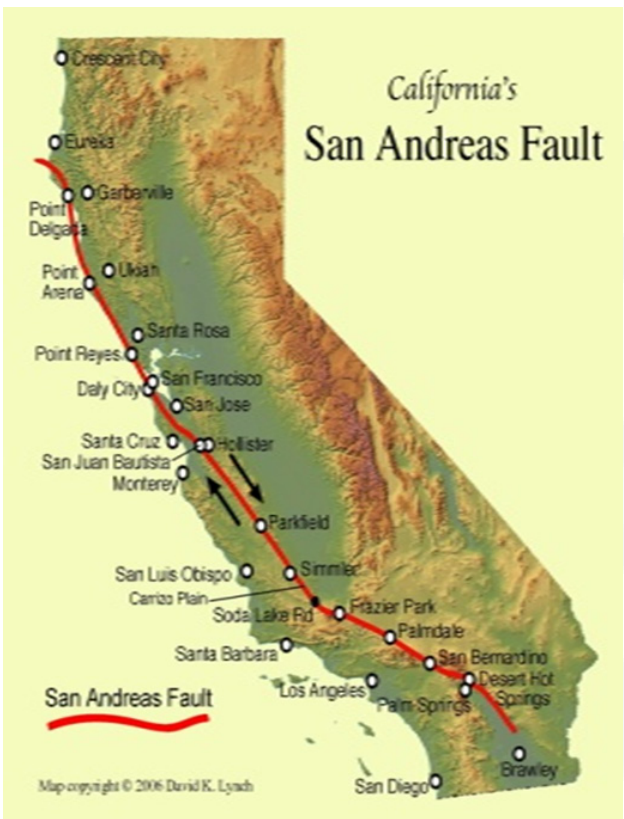

Figure 49 San Andreas Fault 800 mile long.

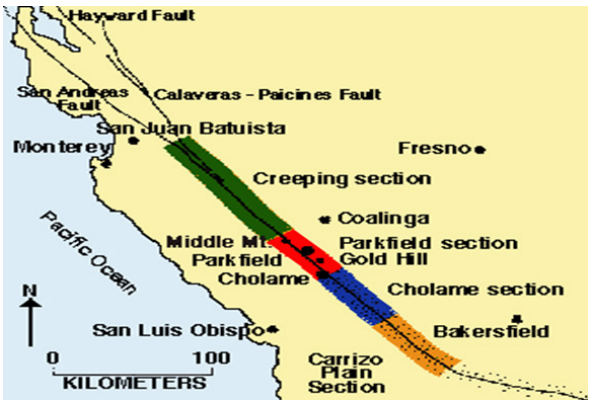

Figure 50 (a) (b) (c) (d) The San Andreas Fault defines an approximately 1300 km (800 mi) portion of the boundary between the Pacific and North American plates.

Earthquake Smartphone Nowcast: These natural disasters cannot be prevented. We can only learn from past earthquakes to predict where they might strike next and take precaution.

Chapter 3.2: Famous cases & lessons learned

To learn more about Earthquakes, here are some useful Internet places.

NASA established Space Observation Global Earthquake Satellite System (GESS) at California Institute of Technology, Pasadena CA.

NASA, cf. Han-Shou Liu NATO book, detected decades early under Liege Belgium an abnormal stress accumulation and evacuated the whole town orderly without human causality except 2 senior citizens.

We mentioned three famous earthquake cases as three **important lessons (in underlined)** learned in three countries in the Introduction. These cases are well known to anyone who lives on the Earth recently. Let's get over these preliminary so we can get on more series business lessoned learned and having anything to do with Smartphone Nowcast.

	Location	Date	Magnitude[2]
1	Chile	22-May-60	9.5
2	Prince William Sound, Alaska	March 28, 1964[3]	9.2
3	Andreanof Islands, Aleutian Islands	9-Mar-57	9.1
4	Japan	11-Mar-11	9
5	Kamchatka	Nov. 4, 1952	9
6	Off western coast of Sumatra, Indonesia	Dec. 26, 2004	9
7	Off the coast of Ecuador	Jan. 31, 1906	8.8
8	Offshore Maule, Chile	Feb. 27, 2010	8.8
9	Rat Islands, Aleutian Islands	Feb. 4, 1965	8.7
10	Northern Sumatra, Indonesia	28-Mar-05	8.7

http://www.infoplease.com/ipa/A0763403.html

Number of Earthquakes Worldwide for 2000 - 2012

Located by the US Geological Survey National Earthquake Information Center

(M4.5+ for most of the world; doesn't include US regional network contributions)

Magnitude	2000	2001	2002	2003	2004	2005	2006	2007	2008	2009	2010	2011	2012
8.0 to 9.9	1	1	0	1	2	1	2	4	0	1	1	1	2
7.0 to 7.9	14	15	13	14	14	10	9	14	12	16	23	19	11
6.0 to 6.9	146	121	127	140	141	140	142	178	168	144	150	185	96
5.0 to 5.9	1344	1224	1201	1203	1515	1693	1712	2074	1768	1896	2209	2276	1295
4.0 to 4.9	8008	7991	8541	8462	10888	13917	12838	12078	12291	6805	10164	13315	8710
3.0 to 3.9	4827	6266	7068	7624	7932	9191	9990	9889	11735	2905	4341	2791	2174
2.0 to 2.9	3765	4164	6419	7727	6316	4636	4027	3597	3860	3014	4626	3643	2721
1.0 to 1.9	1026	944	1137	2506	1344	26	18	42	21	26	39	47	34
0.1 to 0.9	5	1	10	134	103	0	2	2	0	1	0	1	0
No Magnitude	3120	2807	2938	3608	2939	864	828	1807	1922	17	24	11	6
Total	22256	23534	27454	31419	31194	30478	29568	29685	31777	14825	21577	* 22289	* 15049
Estimated Deaths	231	21357	1685	33819	228802	88003	6605	712	88011	1790	320120	21953	629

Starting in January 2009, the USGS National Earthquake Information Center no longer locates earthquakes smaller than magnitude 4.5 outside the United States, unless we receive specific information that the earthquake was felt or caused damage.

The values in the tables for the most recent years may fluctuate due to magnitude updates during the review process.

Number of Earthquakes in the United States for 2000 - 2012

Located by the US Geological SurveyNational Earthquake Information Center

(M2.5+; doesn't include US regional network contributions)

Magnitude	2000	2001	2002	2003	2004	2005	2006	2007	2008	2009	2010	2011	2012
8.0 to 9.9	0	0	0	0	0	0	0	0	0	0	0	0	0
7.0 to 7.9	0	1	1	2	0	1	0	1	0	0	1	1	0
6.0 to 6.9	6	5	4	7	2	4	7	9	9	4	8	3	4
5.0 to 5.9	63	41	63	54	25	47	51	72	85	58	89	51	25
4.0 to 4.9	281	290	536	541	284	345	346	366	432	288	631	347	250
3.0 to 3.9	917	842	1535	1303	1362	1475	1213	1137	1486	1492	3584	1838	1096
2.0 to 2.9	660	646	1228	704	1336	1738	1145	1173	1573	2379	4132	2941	1951
1.0 to 1.9	0	2	2	2	1	2	7	11	13	26	39	47	34
0.1 to 0.9	0	0	0	0	0	0	1	0	0	1	0	1	0
No Magnitude	415	434	507	333	540	73	13	22	20	14	12	8	5
Total	2342	2261	3876	2946	3550	3685	2783	2791	3618	4262	8496	* 5237	* 3365
Estimated Deaths	0	0	0	2	0	0	0	0	0	0	0	0	0

Earthquake Information for the 1990s

Graphs of Earthquake Statistics

http://earthquake.usgs.gov/earthquakes/eqarchives/year/eqstats.php

Magnitude vs. Ground motion and energy

Magnitude change	Ground motion change (Displacement)	Energy change
1.0	10.0 times	about 32 times
0.5	3.2 times	about 5.5 times
0.3	2.0 times	about 3 times
0.1	1.3 times	about 1.4 times

This table shows that a magnitude 7.2 earthquake produces 10 times more ground motion than a magnitude 6.2 earthquake, but it releases about 32 times more energy. The energy release best indicates the destructive power of an earthquake. See: How much bigger is a magnitude 8.7 earthquake than a magnitude 5.8 earthquake?

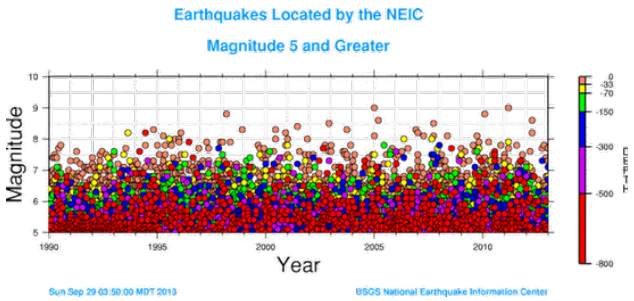

We need to understand the sources of large Earthquakes and then the reason large earthquakes are periodic. What's an Earthquake, and how large is large.

Seismicity of the Earth 1900-2013

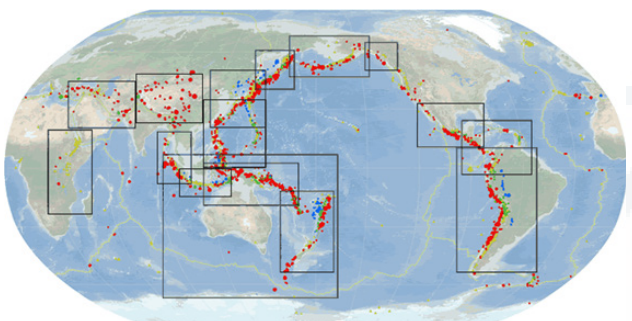

- Can we homosapiens forecast it? No, but.
- Why 4-leg fossil never been found under the historical ruin by Vesuvius Volcano, say, Italy Pompeii?
- What do wild animal know, we don't?
- O.K. they have 4 bare feet, don't wear shoe, they can sense the trembling and 4 feet sampling gives the direction of arrival to run away. A Great theory! But when comes to human lives, it's too important to just believe it. "In God, We trust; All the rest, Show data." (NIH Doctrine). Is there gold standard experiments? NIH defined the gold standard as: double blind (DB), with negative control (NC), and sufficient statistics (SS).
- Can modern technology in Smartphone, Cellular Tower Net, and Low Flying Satellite Iridium help?
- Cooking Pot Theory of Earthquakes;

Last Big One happened in 2004, so Dummy can figure out the next big one will be in a decade $2015 - 2004 \cong 13$ Years;

To know the source of Earth Core Iron, Dummy must know from the common sense book about Origin of the Universe; Big Bang, Nucleus Physics; as well as Dark Matter.

Whoever has a right mind would claim any cost from those borrowed references, materials, and pictures used in the book. They who want money should have their right-side emotional-IQ brains or the left-side logical-IQ brain examined; "making profit out of others misery is socially unacceptable and immoral." Any K-12 kid knows how to compute zero dollar multiplying any percentage profit sharing remains to be zero dollar. How wonderful is the math when it is used to the advantage of argument! Just image the insidious smile of the Judge and those surprise face on greedy souls in the Intellectual Property Right Court. "In God, we trust; all the rest, show data." This data-driven common sense knowledge (know the logic), even a dummy wouldn't be stupid. Of course, we know "the devil, if any, is in the details."

Back to the Future:

Figure 51 School Drill.

Figure 52 From Kinder Garden to 12-th Grade School Public Education (K-12) required periodic Earthquake Alarm Drills. Stucture integreity.

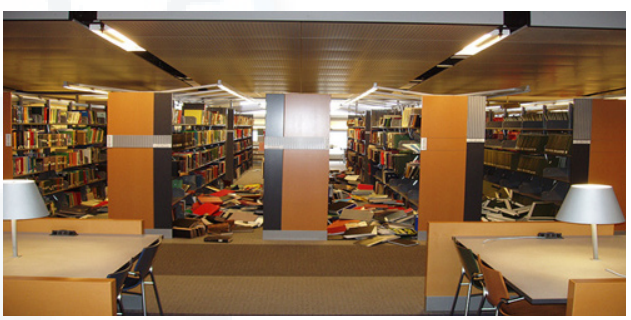

Figure 53 An earthquake in San Diego shook the books off the shelves of a library.

Figure 54 One of the more famous photos from the magnitude-6.9 1989 Loma Prieta temblor, a California Highway Patrol Officer surveys the damage after the top deck of the Bay Bridge fell onto the lower deck, smashing cars. Remarkably, only one driver died. The US NASA CALTECH leads Satellite system Figure 6. Bay Rapid Transit (BRT) Railway System crossing San Francisco (SF) Bay requires structure check after Richet scale 2; SF City Building Code Enforcement Law; Federal and Academic collaboration, established the "ShakeAlart," at UC Berkeley Lab, (cf. Richard Allen, Nature V. 502, pp.29-31, 2013)v.

Figure 55 NASA/Caltech established Global Earthquake Satellite System (GESS).

BSS by physics source pixel sequentially (at Min Free-Helmholtz Energy (MFE) NL Regularized LCNN Matlab Code) Sources Separation (BSS) de-mixing of time series.

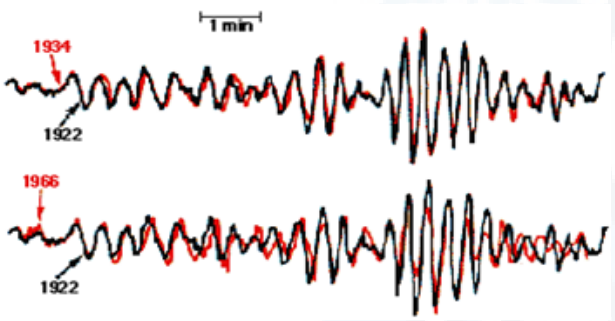

Figure 56 (a) (b) *Significant earthquakes have occurred on the Parkfield section of the San Andreas Fault at fairly regular 22 years intervals - 1857, 1881, 1901, 1922, 1934, 1966, and 2004.The next significant earthquake was anticipated to take place within the period 1988 to 1993.*

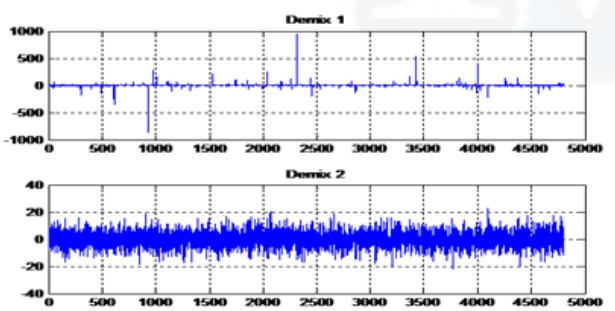

Figure 57 Blind Sources Separation (BSS) of seismic wave's time series yields the Earthquake among clutter and noise sources.

Furthermore, we can map bipolar wave x, y, t to positive signal as the functional of $u(x,y)$ and $v(x,y)$

$$f[x,y,t] \cong g[u(x,y),v(x,y),\tau]\cdot h[u(x,y),v(x,y),\tau]$$

$$\frac{\delta[W]}{\delta\tau} = \frac{\delta H}{\delta[W]},$$

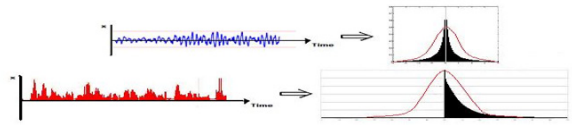

Figure 58 Positive signal processing enjoys a narrow variance for a higher order 4th cumulate known as Kurtosis in a transform domain to achieve a joint-density factorization as Independent Component Analysis (ICA) in terms of unknown ANN learning matrix [W].

Consequently, we recommend augmenting every Smartphone with Inertia Motion Unit (IMU) that is matured through every safety airbags in every car. Also, we need a Smartphone Smart Sensor Web (S^3W) at mini-super computers at cell towers with smart algorithm (known as Computational Intelligence CI not AI) that can apply the thermodynamics equilibrium theory at the minimum Helmholtz free energy to solve Blind Source Separation (BSS) of the seismic waves complex time series from hundreds Smartphone at different time of arrival in seconds.

The Smartphone Nowcast proof of principle is based on the gravitational vibrations due to the up-rising molted rock having a lower density and thus a lower gravitational attraction. The phenomena has produced the low frequency seismic tremor vibration that is well detectable to 4-feet animals on the ground as they have never been reported on suffering a massive casualty in all large scale earthquakes. Likewise, the potential of Nowcast can be detected by a distributed sensor network made of miniaturized car-seat low-cost inertial motion units (IMU) detecting the increasing low frequency tremor vibrations over a distributed terrestrial towers and transmitted by inexpensive cellular phone transceivers. A method of forecasting naturally-occurring phenomena, comprising: taking localized measurements of the earth's gravitational force change; interpreting trends in the measurements; relating the trends to a naturally-occurring phenomenon of interest; predicting a likelihood of occurrence of the phenomenon of interest based on the relationship; and reporting on the likelihood of occurrence to interested parties.

Explicitly, we wish to measure the aforementioned Smartphone and satellite gravity/gyroscope potential data to a set of distributed ***Inertial Motion Units (IMUs)*** embedded as small proofing mass in ***Micro Electric Mechanical System (MEMS)***, used in every ***car airbags*** and some *unmanned aerial vehicles*. A single ***IMU/MEMS*** device works in Smartphone can detect in situ gravitational perturbation of the Earth mantel convection. The gravitational perturbation affects the orbital dynamics of proofing mass of ***IMU*** causing the radial imbalance displacement, which in turns squeezing the neighborhood deformable ***piezoelectric materials*** in contact with the proofing mass generates the electric read-out currents feeding an onboard mini-super-computer.

Here is a value-added contribution that the Author with his 17 Phd. students contributed to modern **Computational Intelligence (CI)** known as **Artificial Neural Network (ANN)** supporting **Natural Intelligence (NI)** unsupervised learning capability based on (1) isothermal equilibrium brain and (2) power of pairs sensors and self-reference processing. The goal of NI is to gain about 15 seconds of next imminent large Earthquake. This Nowcast capability is not based on the antiquity rule-based **Artificial Intelligence (AI)** that requires another rule to break the early rules. Breaking rule takes the courage, judgment and intelligence. This

is USPTO IP right of Bind De-mixing of seismic wave, in order to build a sensitive and robust **Smartphone Smart Sensor Web (SSSW, or S³W)**. After our past fiasco in the Earthquake saddens history and experience, we give a popular science introduction and methodology gives in this dummy book. The consumer shall not pay this NI technology directly, but the Smartphone manufactures must honor several US PTO patents right.

Smartphone support everywhere and always on Next Gen Internet that support Massively Parallel and Distributed (MPD) Natural Intelligence (NI) Architecture for Smartphone Nowcast Next Big One.

The timing and re-group of roaming Smartphone are key parameters to be solved. Otherwise, we can adopt a dynamic reconfigurable Artificial Neural Network (ANN) taking advantage of unsupervised learning de-clutter and de-noise.

We formulated a not rule-based Artificial Intelligence (AI). This is CI based on Thermodynamics equilibrium theory in terms of Boltzmann entropy definition of at min. Helmholtz free energy Min. H= E- T_oS. (T_o =37°C for homosapiens). CI employed Thermodynamics potential driving the learning theory using massive parallel and distributed (MPD) embodiment of Artificial Neural Network (ANN) architecture that each neuron is a Smartphone. The cell tower could be programmed at mini-supercomputer at every cell towers. It solves Smartphone time of arrival signal uncertainty. Then the co-registration seismic wave intensities form a vector components of Input data X(t). One can employ a MPD Smartphone using a very small proof mass, to increase the sensitivity and reduce the power consumption.

Theorem (3): ANN unsupervised learning algorithm considered the vector matrix theory $\vec{X}=[A?]\vec{S}$ from which a learning [W] matrix solving $\frac{\delta H}{\delta[W]}=-\frac{\delta[W]}{\delta t}$; Thus, utilization of ANN inverse $[W?]\vec{X}=\vec{S}$ the uprising thrust hit the pot cover periodically generating large earthquakes with the magic cycle **24 years**.

The cause and periodicity for large earthquake at 10 rose to power 6 magnitude and beyond.

The basic idea of plate tectonics is as follows: Due to the irreversible thermodynamic in the interior of the earth, the outer shell of the earth was fractured into several plates—likes mountain-top rocks into ocean beach sands. These 30 fragmented plates, among 13 major plates floating on the earth's mantle, move relatively to each other.

There are six possible modes of plate motion:

a. Upward movement creating mountains.

b. Downward movement creating oceans or basins.

c. Under thrusting motion creating oceanic trenches

d. Land separation creating sea floor spreading.

e. Land sliding causing geological instability, and

f. Relative plate movements creating stresses along the plate boundaries, which cause earthquakes.

From scientific point of view, the tectonic plate theory has two fundamental problems: First, why was the outer-crusted shell of the Earth fractured into several plates? A **wake up call** is **1976 Tangshan Earthquake** in China occurred within the Eurasian Plate, not in the plate boundary. As such, numerous more seismic wave observation stations must be built everywhere that is simply not sensible. Thus, **Smartphone Nowcast the next big one** becomes more and more important.

Benefit of early warming is clear, where each Smartphone is ANNS neurons and they will be adjust the learning weight matrix so that the thermodynamic equilibrium to be reached.

Application could be everywhere always on. For example, infamous Japan Tsunami, propagating to Indonesia causing major calamity in our Century. Also, man-made trembling of New York World Trade Center Twin Tower when the steel cords were melting down by jet fuels leading to the catastrophic collapses. In this review paper, we recommend such a fusion of Smartphone Smart Sensor Web (*SSSW*), including (1) terrestrial ground stations, (2) mobile Smartphones, and (3) low-lying Satellites Net (e.g. legendary *Iridium 66* system).

We suggest further build a Seismic Wave board on the *International Future Space Station (IFSS)* with a *longer antenna baseline* for increasing the low frequency Earthquake seismic wave detection. Then, the set of vector time series of distributed sampling masses currents may be taken to solve, without the need of knowing nonlinear impulse response function, the *Blind Sources Separation (BSS)* for the Earth underlying unknown gravity sources. This algorithm is a smart unsupervised learning, which is either based on an Independent Component Analysis (*ICA)* of *Higher Order Statistics (HOS)* beyond 2nd order variance for spatiotemporal invariant system [US PTO 7,366,564], or the *minimum free energy equilibrium physics* for spatiotemporal variant systems beyond a local singularity [US PTO 7,355,182]. These two classes of *BSS algorithms* may happen in the crust stress singularity for local earthquake and tsunami and other non-singularity of smooth inner core magnetic *North-South poles fluctuations,* and *pole reversals over decades*.

We estimate that *Size, Weight, and Power as well as Cost (SWaP&C)* with respect to the Smartphone and IFSS scanning swap duty cycle. It seems satisfy the International Space Station Cargo constraints. The advantage of IFSS can go beyond land measurements by the *local in-situ seismic observations* stations *beyond California "Clashes among Tectonics Plates*," mechanism, also cover vast amount of ocean 7 Seas and the central tectonic plate e.g. China Sichuan (due to India-Eurasia plate collision adjustment). When IFSS passed the ground, the ground truth can be used to calibrate on the IFSS. One may hope that one day the combined space and terrestrial system can accurately model Earth mantle convection stress, driven by colder and heavier molten rock pushing downward the underneath lighter and hotter molten rock rising upward, namely *Cooking Pot Plate Earthquake Model.*

Figure 15 Japan artist brush painting Tsunami over Fuji Mountain about 869 AD Tsunami due to Earthquake deposits reached 2 to 3 km inland and up to 4 m above the present shoreline. The Next Big One could refer to a big **Earthquake,** whereas it would happen in the sea generating a huge wave called **Tsunami**. Those are culturally frightening words Earthquake and Tsunami reminding of us thousands deaths, as reflected in a classical brush painting in Japan. The following picture indeed says more than a thousand of words.

Health Care: The Next Big One[$] (NBO) could refer to numerous calamities in our society. It could happen all the way from home-front safety to homeland security. Thus, "**Smartphone Nowcast**" capability is a powerful technology integration that could help large scope of Apps—from sensing to communication. Smartphone magnify the ***Next Gen Internet*** with "always –on (7 days per week, 24 hours per day, and 265 days per year) and everywhere" capability in the World. **Smartphone Nowcast** can help *Home Alone Seniors (HAS)* among **78 million aging** (beyond 70 years old) baby-bombers born after WWII in the US alone. One of them might suffer **Heart Attacks, Strokes (HAS), and Cancers** due to overly secreted stress hormones: ***adrenaline and cortisone***. When a ***Next Gen Smartphone*** is equipped with sensitive ***Inertia Motion Unit (IMU)*** and a full ***electromagnetic (EM)*** spectrum Cameras (***EO_IR_RF***), we can help every law enforcements, and War fighter soldiers. It can supplement the so-called Critical Perimeter Surveillance to confirmed second look with Infrared filtered Smartphone day camera. This is physiologically based on nonlinear synergistic coupling between infrared emission and microwave heating. When Smartphone could relatively easily broaden beyond traditional communication L-band transceiver at 1 GHz at 1 foot (30 cm) wavelength to slightly higher microwave oven frequency at 2.4 GHz at 12 cm wavelength, it can used as the radiation source to warm up the stress hormones (bio-molecules adrenaline and cortisone at much higher resonant frequency). Furthermore, we can confirm by taking the second look by means of Smartphone infrared-filtering camera to confirm indeed the home alone senior (HAS) have too active warm physiology to begin with.

(2) **Earthquake Nowcast is the topic of the Book.** Besides the new augmented MEMS/IMU, we need Robust **Natural Intelligence** (**NI**) the traditional rule-based **Artificial Intelligence (AI),** initiated by Marvin Minsky at MIT,that requires another rule to break the rule, etc. the intelligence becomes diminishing. Traditional Computational Intelligence could no longer support the **Massively Parallel and Distributed (MPD) roaming Smartphone Earthquake Nowcast Strategy, without the lock steps and synchronous processing.** Rather we need emulate those roaming animals with instincts on the Earth gained by fittest survival evolution principle called the **Natural Intelligence (NI)** not **AI.**

We wish to formulate mathematically, in common sense **Math 101,** to answer where **NI** comes from these facts. We sought after a few precious seconds ahead big Earthquake Nowcast, to help human seeking cover for the safety. **To increase the sensitivity of detecting the major seismic waves,** we recommend using terrestrial MPD Smartphone sensors. Moreover, it seems to make sense the proving mass ball of **Inertial Motion Unit (IMU)** suspended in a piezoelectric amorphous crystal should be as small as possible. Knowing that engineering has nothing to do with the Truth, but consistent approximations, we wish to substantiate such an intuition. In turns of Kepler model of planet Earth, we have to prove the independent of the 13 major plus 30 fragmented tectonic plates, as well as the independence of the proofing mass ball used in piezoelectric IMU adopted in every different models of Smartphone. This reason behind the invariance of test mass is important because the direct source of local Earth mass change is due to thermal expansion of the Earth inner crust cooking enormous heat of Earth iron core isotope decay according to Noble Laureate Enrico Fermi prediction of neutron decay into proton, electron and neutrino to preserve the angular momentum:

$$Fe_{26}^{57} \rightarrow Fe_{26}^{56} + p^{+} + e^{-} + \upsilon \; + \; heat.$$

Furthermore to increase the sensitivity and robustness Earthquake Nowcast, we investigate the following important theorems related to Kepler.

Theorem of cooking pot model of earthquake: Earthquake cycle does not depend on the Earth surface tectonic plates mass; nor the proofing mass ball of IMU, rather the orbital calculation made first by Kepler and then Sir Isaac Newton. As such, we can take the advantage to increase the sensitivity by reducing the proofing mass of Smartphone by using a miniaturized IMU embodied in Micro-Electro-Mechanic System (MEMS).

Theorem of Rayleigh-Benard convective instability: We need further introduce the Rayleigh-Benard convective instability to estimate the periodicity of 2 dozen years for major Earthquakes.

Chapter 3.3: Natural Intelligence for Smartphone Nowcast

An ANN system for unsupervised learning solves Blind Sources Separation (BSS), where every node is a Smartphone.

NI: Isothermal Brain Processing Vector Time Series

Massively Parallel and Distributed (MPD) Architecture of Processors, emulating Brain Style Artificial Neural Network (ANN) based on billions neurons billions of housekeeping servant glea cells. This NI ability has been inferred in the imagination of Science-Fi "Terminator III."

The animal instinct may be based on the observation about *homeostasis.* The layer-by-layer *associative memory* of Hippocampus, supporting higher Intelligent Quotient (IQ). Moreover, each tip of Hippocampus has a bull horn-like Amygdala for our emotional-IQ. Both IQ & e-IQ might contribute to the intuitive and instinct feeling.

Fact#1: Warm Blood Homeostasis: It can maintain a steady kinetic transports of squeezing the red blood cells through blood vessel capillary bed. A steady transport of oxygen molecules attached with iron molecules in the red blood hemoglobin cells, i.e. decided in a majority rules democratic voting at the homeostasis condition. The Physiologically speaking, the fact of matter is the optimum elasticity of red blood cell hemoglobin to squeeze through the narrow opening of blood capillary vessels, not un-like a hen giving daily eggs. All sensors processing are **MPD** at isothermal bath of **brains**.

Theorem: A higher core body temperature is not necessary more Natural intelligent (NI).

While we are at 37°C (evolutionally, an optimum elasticity to squeeze the blood hemoglobin through capillary vessels), chicken are at 40°C (perhaps to hatch the egg better).

We eat Chicken, not vice versa. ***Q.E. D***

Figure 59 Hen has higher body core temperature at $40^{o}C$ higher than homosapiens at $37^{o}C$ for easy to hatch baby chick.

The computation platform takes the advantage of modern NI unsupervised learning capability of an asynchronous and reconfigurable *Artificial Neural Network (ANN),* where each node is a Smartphone in a layer by layer of arbitrary sizes. They can measure local in-situ Shake-Alert and recorded in real time at mini-super computers *at Smartphone* Cellphone Towers. This might help avoiding natural and man-made calamity just few seconds ahead of a major event.

Fact #2: Power of Pair sensors & actuators.

Why do animal always have pair's sensors: two eyes, two ears, nose having two nostrils, toque with left-right similar sensing, and two hands as tactile sensors for grabbing for the better *self-reference* unsupervised learning matched filtering.

Fact #3: Missing halves of brain. When Einstein passed away, he donated his brain for the biological studies. It turned out to be 10 billion's neurons, and 10 billion glea cells, as if there were one neuron per Star of the Universe. In other words, there were missing house-keeping 10 billion's servant glea cells in early studies. Each glea cell serves each neuron master to keep brain in isothermal equilibrium at fixed temperature 37 degree.

Beach white sands (Australia) versus Mountain top rocks

Figure 60 Which scenery has a larger degree of uniformity entropy?

Quiz: Which has larger entropy? Sands or Rocks?

Obviously, the beach white sand is more homogeneous degree of uniformity than mountain top rocks. One upon a time, eon ago, they might share the same molecular structure and species, now they have different molecular binging energy, namely the information that is dear to paleontologist hearts.

Answer: Beach white sand has obviously more degree of uniformity, versus the original before eroded at mountain top rocks that have stronger variation of molecular *binding energy* known *archeologically* to the *paleontologist* as the information.

$S_{sand} > S_{rock} > 0$; ***the Bolzmann heat death***

$Info_{sand} < Info_{rock}$; **In the beginning of the world**

Claudius Shannon gave an information theory, because Bell telephone system was exploring the fiber-optical technology for telephone communication. The bigger is the pipe, the more is the bits capacity. On the other hand, the big is the bit space; the larger is the uniformity defined originally as the entropy by Boltzmann. Thus, it seems that the entropy measure the capacity related to the entropy. This erroneous notion was captured by his disciple Claudius Weave, in his re-edited his teacher Shannon book: "An Information Theory," proclaimed to be "The Information Theory." This new title might give Engineers, as if the Entropy related to the Information. In the sense of voting, a *uniform* voting record has larger *entropy* having no information revealed to the candidate. Thus, the **entropy** is not the information, rather the negative of information, a **dis-information**.

The following is Blind Sources Separation of time series into two sources, one could be the Earthquake event, and the other is the clutter noise. Affirmative answer to Smartphone Nowcast modern technology has been given "Now-Cast of natural resource and calamity warning, Harold Szu, USPTO 8392122 B2, Apr. 29, 2008:" For example, when the Smartphone will be augmented with *Inertial Motion Unit (IMU)* in miniaturized *Micro Electro-Mechanic System (MEMS)* taken from the matured technology of automobile seat airbags, that can be helping Nowcast after the sensitivity adjustment of inertial proofing mass and computational intelligence of unsupervised learning Artificial Neural Netowrk (ANN) Blind.

What is the molecular "**Entropy S**" that Ludwig Boltzmann introduced and die for (by committed suicide to protect Henri Poincare time reversible Newtonian dynamics). Entropy is a measure of the "**Degree of Uniformity**."

Figure 61 (a) Ludwig Boltzmann, (b) James Clark Maxwell, (c) Henri Poincare.

Modern Physics:

His disciple Prof. Paul Ehrenfest has resolved the paradox between the quantum mechanics and classical mechanics. He followed the total energy Hamilton H-dynamics, extending Lagrange L-dynamics:

$$H \equiv \sum_i p_i \frac{dq_i}{dt} - L(q_i, \frac{dq_i}{dt}, t)$$

$$\frac{dq_i}{dt} = \frac{\partial H}{\partial p_i}; \frac{dp_i}{dt} = -\frac{\partial H}{\partial q_i}; \frac{\partial H}{\partial t} = -\frac{\partial L}{\partial t}$$

Classical Poisson bracket is defined:

$$\frac{dH}{dt} = \sum_i \left\{ \frac{\partial H}{\partial q_i}\frac{dq_i}{dt} + \frac{\partial H}{\partial p_i}\frac{dp_i}{dt} \right\} + \frac{\partial H}{\partial t}$$

Quantum mechanics takes into account that the common sense of microscopic measurement at molecular level. The measurement will disturb the results and the order sequence will give the different uncertainty of $i\hbar$ of the order of magnitude of Planck constant $\hbar \equiv h/2\pi$. In other words, the measurement by the position operator $\boldsymbol{r}$ versus the measurement by the momentum operator $\boldsymbol{P} \equiv -i\hbar\nabla$ so that ∇ operates on wave component $\boldsymbol{P}\exp\left[i(k\cdot r - \omega t)\right] = p\exp\left[i(k\cdot r - \omega t)\right]$ bring down the Einstein momentum $p = \hbar k$ and their different sequence (momentum operator first and position operator $\boldsymbol{r}$ second, vice versa generate the uncertainty quantity) measure how much the measurement disturb the microscopic quantity. Ehrenfest relationship replaced the Hamiltonian dynamics in terms of Poisson curvy bracket with commutator square bracket.

"But don't you see what this implies? It means that there is a fourth degree of freedom for the electron. It means that the electron has a spin (s=1/2) that it rotates," proclaimed George E. Uhlenbeck while Samuel A. Goudsmit discussed with him in the spring of 1925 about the splitting of Zeeman effect, when an electron beams emerges from a black-body oven under an inhomogeneous magnetic field gradient, known as the hyperfine structure of spectral lines missing the central line, only 2 lines spin up and spin down.

$$2s+1=2\ ;s=\frac{1}{2}$$

"Fortune favors the prepared mind;" "Science knows no country, because knowledge belongs to humanity, and is the torch which illuminates the world." French microbiologist Louis Pasteur discovered the principles of vaccination, microbial fermentation and pasteurization.

Max Dresden, a thesis student George Uhlenbeck, said, "*I am very troubled*." He paused for dramatic effect. "*Ludwig Boltzmann committed suicide (in his debate with Henri Poincare about the irreversible heat death versus time reversible Newtonian equation). His student Paul Ehrenfest committed suicide* (after terminating his son suffering with Down syndrome during Nazi days). *Ehrenfest's student, George Uhlenbeck, was my advisor. If Uhlenbeck commits suicide, I'm next*." said Prof. Dresden. Fortunately, the curse, if any, was broken as Prof. Uhlenbeck lived a fully life with his son Oke and wife Alisa 88 years old died on Oct. 31, 1988, Boulder, Colorado. (Uhlenbeck born Dec. 6, 1900, Jakarta, Indonesia father is dutch business man; returned home for college education under Prof. Paul Ehrenfest: Leiden University). Prof. Max Dresden died of cancer in 1997.

$$[Q,R]\equiv QR-RQ=i\hbar\{q,r\}\equiv i\hbar\{\frac{\partial H}{\partial q}\frac{dr}{dt}+\frac{\partial H}{\partial r}\frac{dq}{dt}\}$$

George E. Uhlenbeck, a thesis student of Paul Ehrenfest, continued the foundation of thermodynamics and statistical mechanics.

Figure 62 Paul Ehrenfest unified the quantum mechanics and classical mechanics and George E. Uhlenbeck and Samuel Goudsmit discovered half spin quantum number of electron beam split under magnetic field gradient.

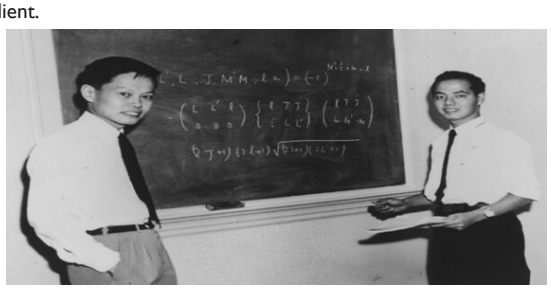

Figure 63 Noble Laureates Physicists: Franck C. N. Yang, and T.D. Lee working Fermi lab.

They discovered the parity violation of TCP invariance (Time reversible & Charge-conjugate and Parity mirror symmetry) about Fermi neutron decay weak interaction.

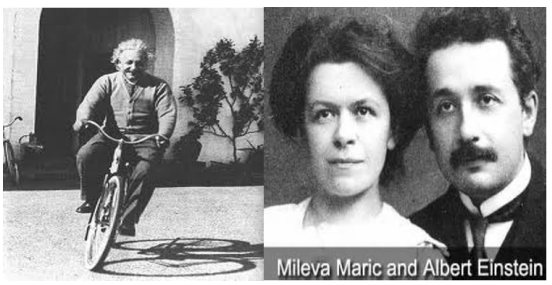

Figure 64 Albert Einstein and Mileva Maric worked on the photoelectric effect, Brownian diffusion motion, and the special relativity in 4 dimensional space Lorentz transform at constant speed of light.

Knowing Poincare and Boltzmann time reversal invariant argument, Einstein wrote down his celebrated Brownian motion diffusion equation in the 1st order in time and second order space curvature.

The smoke comes from chimney initially as a linear trajectory $r=r_o+vt$ subsequently thermal diffusion takes over. The trajectory becomes square root trajectory.

Figure 65 Why smokes involve straight linear trajectory from the chimney and then becomes a curvy square root of time trajectory?

This observation can be understood from Einstein Brownian motion of displacement. In Space travel age, the re-entry vehicle with Astronauts will suffer the different degree of atmosphere friction force generating heat when passing through the outer space vacuum to dilute atmosphere of rarefied gases. We must estimate the dissipation heat so generated for better protection of astronauts during the re-entry burning off vehicle skin layers.

$$\frac{\partial G}{\partial t}=D\frac{\partial^2 G}{\partial x^2}$$

Gaussian distribution:

$$G=\exp(-\frac{x^2}{Dt})$$

$$\left\langle x^2\right\rangle=Dt$$

$$r.m.s.=\sqrt{\left\langle x^2\right\rangle}=\sqrt{Dt}$$

$$<\vec{x}(\tau)\cdot\vec{x}(\tau+t>\cong D_o t\ ;$$

Einstein Theorem of Thermal Fluctuation $\frac{3}{2}k_BT$ and Dissipation viscosity η :

$$\frac{3}{2}\frac{k_BT}{\eta}=D_o$$

Harold Szu thesis (1971 Rockefeller University) answered the question Einstein theorem of Fluctuation, left-hand side, and

dissipation, right hand side, is true for all mean free path (mfp) density during the re-entry vehicle entering the atmosphere of various mfp density.

We took Boltzmann integro-differential transport equation as a kinetic model to compute the kinetic transport within two infinite parallel plates using the Maxwell boundary condition of an arbitrary accommodation probability $0< \gamma < 1$ for the collision re-emission in thermal equilibrium with the plate temperature.

Figure 66 Prof. C. S. Wu working at NIST Low temperature physics of parity violation of TD Lee and C N Yang.

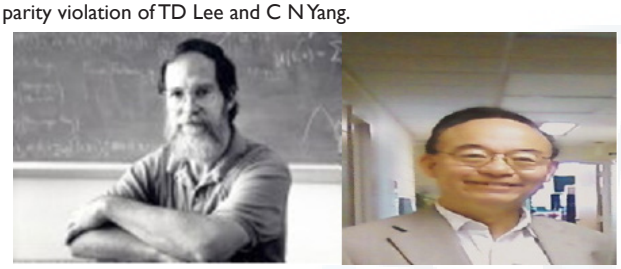

Figure 67 Ronald F. Fox (Physics, GIT, 1969, 9 decedents) formulated the stochastic version of Boltzmann differential and integral transport equation. Harold H. Szu (Naval & Army Fed Labs, 1971, 17 decedents) applied it and augmented with a stochastic wall conditions to prove the Einstein fluctuation-dissipation relation is true for all mean free path density. Both are Ph. D. thesis students of Prof. George E. Uhlenbeck at the Rockefeller University, NYC, NY circa 1970 in Sichuan province. Unfortunately, Chinese authority ignored the NASA warning, Sichuan earthquake, the following is Blind Sources Separation of time series into two sources, one could be the Earthquake event, and the other is the clutter noise. Affirmative answer to Smartphone Nowcast modern technology has been given "Now-Cast of natural resource and calamity warning, Harold Szu, USPTO 8392122 B2, Apr. 29, 2008:" For example, when the Smartphone will be augmented with Inertial Motion Unit (IMU) in miniaturized Micro Electro-Mechanic System (MEMS) taken from the matured technology of automobile seat airbags, that can be helping Nowcast after the sensitivity adjustment of inertial proofing mass. and computational intelligence of unsupervised learning Artificial Neural Netowrk (ANN) Blind Sources Separation (BSS) de-mixing of time series.

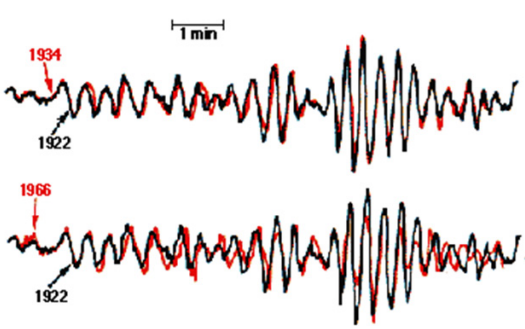

Figure 68 (a) (b) Significant earthquakes have occurred on the Parkfield section of the San Andreas Fault at fairly regular 22 years intervals - 1857, 1881, 1901, 1922, 1934, 1966, and 2004. The next significant earthquake was anticipated to take place within the period 1988 to 1993.

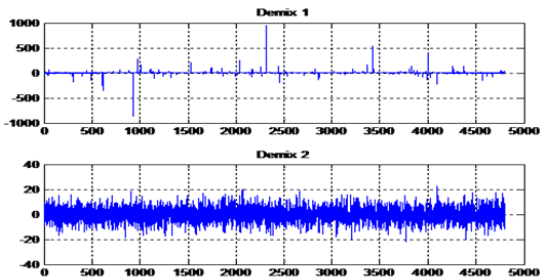

Figure 69 Blind Sources Separation (BSS) of seismic wave's time series yields the Earthquake among clutter and noise sources.

Furthermore, we can map bipolar wave x, y, t to positive signal as the functional of $u(x,y)$ and $v(x,y)$

$$f[x,y,t] \cong g[u(x,y),v(x,y),\tau]\cdot h[u(x,y),v(x,y),\tau]$$

$$\frac{\delta[W]}{\delta\tau} = \frac{\delta H}{\delta[W]},$$

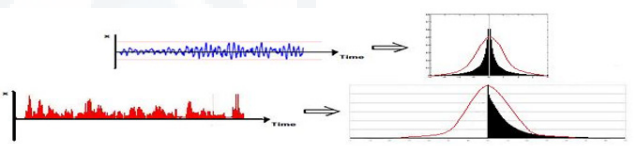

Figure 70 Positive signal processing enjoys a narrow variance for a higher order 4th cumulate known as Kurtosis in a transform domain to achieve a joint-density factorization as Independent Component Analysis (ICA) in terms of unknown ANN learning matrix [W].

Historical Wiener Least Mean Square Matched Filtering, Kalman adaptive matched filtering, ANN, and to the *Independent Component Analysis (ICA)* based on either statistical higher order moment Kurtosis, or the thermodynamics equilibrium physics at the minimum Helmholtz free energy.

The 2nd law of thermodynamic of open dynamic system such as human brain must be operated at the Min. Free-Helmholtz Energy (MFE) as the isothermal equilibrium cost function: min. $H \equiv E - T_o S$ for unsupervised learning that could be associated with input vector time series & output feature extraction pairs. We derived such an *Artificial Neural Network (ANN) learning Hebbian rule* operated at the isothermal equilibrium. The *ANN* algorithm was known as the space-variant regularized *Lagrange Constraint Neural Network (LCNN)* to solve *Blind Sparse Sources Separation (BSSS)*.

Introduction-I

Almost all animals, roaming on the Earth that can learn the experience, seemed to have equipped: (1) warm blood brains, for steady kinetic transports for house-keeping glea cells operations, and (2) power of pair's sensors gathering vector time series $\overline{X}_{S_i}(t)$ for self-reference unsupervised learning. Likewise, Human have vector time series sensors (eyes, ears, nostril holes & olfactory balls, tessellated taste buds tongue, hands, legs) and the brains are kept at isothermal equilibrium at $T_o = 37^o C$. These are necessary but not sufficient conditions for intelligent beings (Higher temperature did not necessarily imply a smarter learning,

chicken brain was kept 40^oC, but lacking hands & tools was not necessarily smarter than us).

Almost all image processing at distant sensing deals with Equivalent Planck Source's (EPS's) of arbitrary emissivity. Solving inverse Blinded BSSS problem requires thermodynamic learning rules.

It turned out that physics dealt with efficient measurement sciences that took into consideration of robust and repeated results, of which mathematical linear programming adopted in CRT&D compressive sensing[1–3] turned out to be a linear order approximation of our thermodynamics MFE cost function:

$$\min . H = E - T_o S \,, \tag{1}$$

The MFE liked an efficient car engine having the internal combust energy E and the exhaust entropy S operated at optimum engine temperature T_o.

Eq. (1) included CRT&D linear programming for a special case when the nega-entropy, –S, was convex hull L1 minimization

$-T_o S \approx T_o \sum_i^k < \log s_i >_{S_i}$,where the class entropy must be real positive $-\log s_i \geq 0; s_i \leq 1$; and the internal energy E is analytic state function in the Taylor series expansion of which the first order error slope follows the linear order error:

$$\mu_j\left(\vec{s}^{(o)}\right) \equiv \left.\frac{\partial E}{\partial s_j}\right]_{\vec{s}=\vec{s}^{(o)}} \approx \left(s_j - s_j^{(o)}\right), \tag{2a}$$

becoming the LMS L2 similarity.

$$E = E_o + \sum_{i=1}^{k} \frac{\partial E}{\partial s_i}\left(s_i - s_i^{(o)}\right) = E_o + \sum_{i=1}^{k}\left(s_i - s_i^{(o)}\right)\left(s_i - s_i^{(o)}\right) = E_o + \left\|s_i - s_i^{(o)}\right\|^2 \tag{2b}$$

In this review paper, we have generalized the CS Eq. (2) self-consistently with Nonlinear 2nd order Lagrange Constraints Neural Network (LCNN).

Planck law

Planck's law described a quantized set of *electromagnetic (em)* waves that oscillated within a back-body resonator cavity, realizing the vanishing *em*-amplitudes at a constant wall temperature T_K. Macroscopically, the resonator supported positive integer numbers of harmonic wavelengths like a violin string vibrating at the fundamental frequency ν and the constant speed c_o : $\left\{\lambda = \frac{c_o}{n\nu} \mid n = I_+\right\}$. Use was made of *Einstein* n-photon energy: $E \Rightarrow E_n = nh\nu$ to compute *Maxwell-Boltzmann* probability: $\exp\left(-\frac{E}{K_B T_K}\right) \equiv z^n$, resulted in a geometric series of $z \equiv \exp\left(-\frac{h\nu}{K_B T_K}\right)$:

$$z^1 + z^2 + z^3 + \ldots = z\left(1 + z + z^2 + ..\right) = \frac{z}{1-z} = \frac{1}{z^{-1} - 1} \tag{1}$$

where the fluctuating vacuum state $n = 0$ was intentionally excluded to result in z^{-1} other than z in Eq. (1) [cf. Remark 6].

Multiplying the density of states $\frac{2h\nu^3}{c_o^2}$, *Planck* derived rigorously and reproduced early laws:

$$I_\nu(T_K) = \frac{2h\nu^3}{c_o^2}\frac{1}{\exp\left(+\frac{h\nu}{K_B T_K}\right) - 1} = \frac{2h\nu^3}{c_o^2}\exp\left(-\frac{h\nu}{K_B T_K}\right); h\nu \gg K_B T_K; \quad \text{Q.E.D.} \tag{2}$$

$$Wien\,law\left\{2\nu^2 K_B T_K; h\nu \ll K_B T_K \;; Rayleigh - Jeans\,Law\left(UV\,catastrophe\,Ehrenfest\right)\right.,$$

where *Planck*'s constant $h = 4.1 \times 10^{-15} eV\,\sec; K_B T_K = \frac{1}{40} eV$ *at room* $T_K = 300$ and thus *Boltzmann* $K_B \approx 0.1 meV$.

Image processing by equivalent Planck sources (EPR's):

An apparent brightness temperature may be characterized by the peak frequency ν_o in terms of frequency dependent emissivity $0 < \varepsilon_{\nu_o} \leq 1$,

$$I_{\nu_o}\left(T_{B_{\nu_o}}\right) \equiv \varepsilon_{\nu_o} I_{\nu_o}\left(T_K\right) \tag{3}$$

Since Planck source has a unit emissivity, then an arbitrary emissive source is associated with *EPS*.

$$T_{B_{\nu_o}} \cong \varepsilon_{\nu_o} T_K \tag{4}$$

Proof:

By definition Eq(3), use was made of Planck's law Eq(2) for $0 < \varepsilon_{\nu_o} \leq 1$:

$$\varepsilon_{\nu_o}\left(\exp\left(\frac{h\nu_o}{K_B T_{B_{\nu_o}}}\right) - 1\right) = \left(\exp\left(\frac{h\nu_o}{K_B T_K}\right) - 1\right);$$

$$\frac{T_{B_{\nu_o}} K_B}{h\nu_o} = \frac{1}{Log\left[1 + \frac{\exp\left(\frac{h\nu_o}{K_B T_K}\right) - 1}{\varepsilon_{\nu_o}}\right]}$$

Figure 71 plotted the apparent brightness temperature $T_{B_{\nu_o}}$ against the black body Kelvin temperature T_K at the peak emissivity ε_{ν_o} in 10% increments. **Q.E.D.**

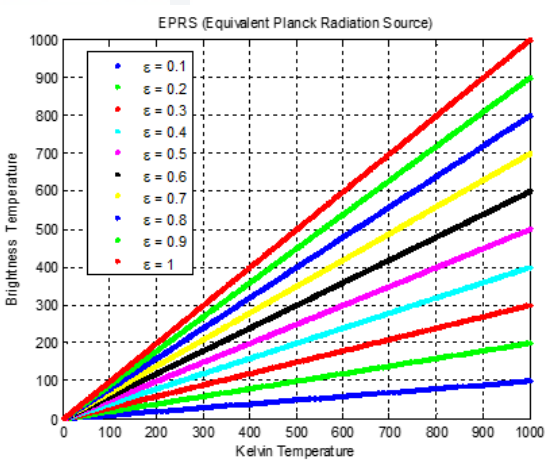

Figure 71 Defining EPS, we plotted the Brightness temperature $T_{B_{\nu_o}}$ versus the Kelvin Temperature T_K. Setting unit $h\nu_o / K_B = 1$, we plot: $y = \frac{1}{Log\left(1 + \frac{1}{\varepsilon_{\nu_o}}\left(\exp\left(\frac{1}{x}\right) - 1\right)\right)}$ from 1 to 1000, as we step emissivity $\varepsilon_{\nu_o} \leq 1$ in 0.1 increments.

Mixing matrix:

We measured infrared (IR) triplets $\vec{X}_s$ $(3\sim 5\mu m, 8\sim 10\mu m \, and \, 10\sim 12\mu m)$ spectral vector per pixel. We derived the complex object unknown mixture of discrete heat sources, associated with discrete temperature $S \Rightarrow S_j \Rightarrow \vec{S}; j = 1,2,3$. Typically, we had illuminating source S_1 , object body hot spot source S_2 , and other sensor coolant source S_3 , etc. in terms of Boltzmann entropy probability normalization $1 = S_1 + S_2 + S_3$. The mixing matrix mapped j-temperature sources to spectral i-components:

$$\vec{X}_{s_i} = \left[A_{i,j}\right]\vec{S} = S_1\vec{a}(T_1) + S_2\vec{b}(T_2) + S_3\vec{c}(T_3) \quad (5)$$

The *EPS* temperature sources of mixing matrix [A] are usually not known for the generation of ground spectral data. The *IR triplets* per pixel as transposed (*Tr*) row vector $\vec{X}^{Tr} \equiv (X_1 \quad X_2 \quad X_3)$ were measured at the center of each band value 4 μm, 9 μm, and 11 μm in Figure 72. The mixing matrix had three column vectors $\vec{a}(T_1), \vec{b}(T_2), \vec{c}(T_3)$ corresponding to three EPS associated equivalent brightness temperature $(\vec{a}(330^o K), \vec{b}(265^o K); \vec{c}(200^o K)$ shown in Figure 73. Each source S_j might have different percentage values for each pixel $\vec{S}^{Tr} = (S_1, S_2, S_3) = (30\%, 50\%, 20\%)$:

$$\begin{bmatrix} X_1 \\ X_2 \\ X_3 \end{bmatrix} = \begin{bmatrix} a_1 & b_1 & c_1 \\ a_2 & b_2 & c_2 \\ a_3 & b_3 & c_3 \end{bmatrix} \begin{bmatrix} S_1 \\ S_2 \\ S_3 \end{bmatrix} = 10^{-5} \begin{pmatrix} 67.46 & 4.65 & 0.05 \\ 502.82 & 152.39 & 21.41 \\ 449.86 & 168.13 & 33.61 \end{pmatrix} \begin{bmatrix} S_1 \\ S_2 \\ S_3 \end{bmatrix}$$

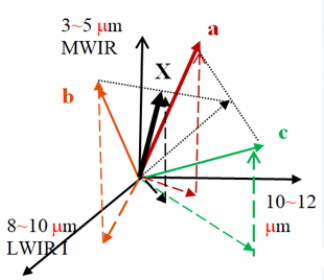

Figure 72

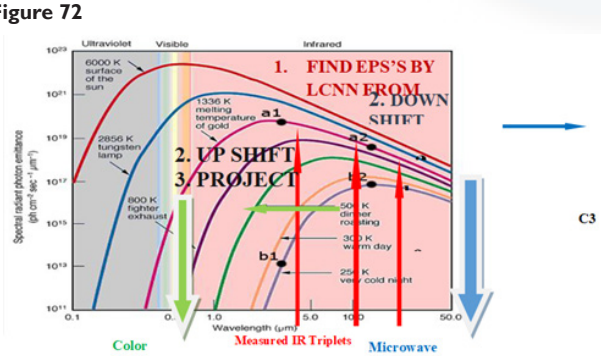

Figure 73 Compressive Sensing by means of Equivalent Planck Source's (EPS's): These virtual upper-down spectral extrapolations were possible because the peak wavelength associated one and only one Kelvin Temperature in a single monotonic curve, where the left-shoulders are up-left-shifted to a shorter sub-micron wavelength toward X-rays. Wilhelm Wien's displacement law $\sim T^4$ followed due to monotonic single peaks per Kelvin temperature, according to the dimensionality analysis of the integrated Eq(2a).

Mathematically, Blinded EPS Separation (BSS) is challenging because the mixing matrix [*A*], Eq(5) mapping the temperature sources to the spectral band values, was unknown for remote sensing, and the inverse weight matrix is usually ill-conditioned:

$$\vec{S}_j = \left[W_{j,i}\right]\vec{X}_{s_i} \;, where \left[W_{j,i}\right] = \left[A_{i,j}\right]^{-1} \quad (6)$$

The following Theorem 2, to be proved in paper, met the challenge.

Thermodynamic learning rule

The key enabler of our new approach is resolving the Mexican Standoff slowdown, or in critical slow down during thermodynamic phase transition phenomena.

Lemma: Because of the unsupervised learning, the energy cost function is unknown for image processing at remote sensing. The first order Taylor series becomes 2nd order in the smallness, requiring the second order Taylor series expansion, curvature C^k , to determine the Lagrange error slope vector μ_α together with the estimation error convergence self-consistently.

$$E \cong E^{(o)} + \mu_\alpha\left(\left[W_{\alpha,\beta}\right]X_\beta - S_\alpha^{(o)}\right) + \frac{1}{2}C^k\left|\left[W_{i,\beta}\right]X_\beta - S_i^{(o)}\right|^2 \Rightarrow O(0)^2 \; ; (7)$$

Critical slowdown phenomena:

When the state function is known, then the 1st order Taylor series derivative is of the 1st order of smallness. However, when the state function is unknown, Lagrange knew the critical slowdown phenomena in thermodynamic phase transition because the state function is unknown requiring other expansion to determine it, then the 1st order may become the 2nd order in smallness. For example in BSS, the minimum of Helmholtz free energy $min.H = \boldsymbol{E} - T_o\boldsymbol{S}$, which is expanded in Taylor series with respect to unknown number of heat sources in terms of associated class entropy per a single pixel $\boldsymbol{S} \Rightarrow \left\{\boldsymbol{S}_i \leftrightarrow \vec{\boldsymbol{S}} = [W]\vec{\boldsymbol{X}}_s\right\}$. We applied the 1st order Taylor series of MFE of the unknown cost function $\boldsymbol{E}$

$$\left(\frac{\partial E}{\partial S_\alpha}\right)\left(S_\alpha - S_\alpha^{(o)}\right) \equiv \mu_\alpha c_\alpha\left(\vec{S}\right) \Rightarrow O(0)^2, \quad (9)$$

where the inner product involving with the 2nd order smallness is difficult to determine the iteration involving doubly both the data and the slope of data. Simultaneously, the *unknown Lagrange energy slope vector* flattens near the minimum bottom with a zero slope.

$$\mu_\alpha\left(\vec{s}^{(o)}\right) \equiv \frac{\partial E}{\partial s_\alpha^{(o)}} \Rightarrow O(0)$$

together with the weighted learning of the ***s***-spectral vector measurement data $\vec{\boldsymbol{X}}_s$ generating an learning error vector

$$c_i\left(\vec{\boldsymbol{s}}^{(o)}\right) \equiv \left(\boldsymbol{s}_i - \boldsymbol{s}_i^{(o)}\right) = \left[W_{\alpha,\beta}\right]\boldsymbol{X}_\beta - \boldsymbol{s}_\alpha^{(o)} \Rightarrow O(0)$$

Consequently, the 1st order of MFE involves 2nd order smallness in the product that becomes too small to determine whether it is the cause or the consequence about which one of the product to take the next step approaching the zero. Such double loops of iterations will suffer a slow convergence, known in unsupervised learning of artificial neural network (ANN) community in a nicked name called Mexican standoff in a wild western Hollywood movie. Taylor expansion of the *MFE* Eq(6) involved unknown internal energy *E* defines the linear slop as the

Lagrange vector constraint of error slope $\vec{\mu}_j$ and the second order of smallness curvature as the Karush-like penalty function:

$$E = E_o + \sum_{i=1}^{K} \frac{\partial E}{\partial \boldsymbol{s}_i^{(o)}}(\boldsymbol{s}_i - \boldsymbol{s}_i^{(o)}) + \frac{1}{2}\frac{\partial^2 E}{\partial \boldsymbol{s}_\alpha^{(o)} \partial \boldsymbol{s}_\beta^{(o)}}\left(\boldsymbol{s}_\alpha - s_\alpha^{(o)}\right)\left(\boldsymbol{s}_\beta - \boldsymbol{s}_\beta^{(o)}\right)$$

$$\cong E_o + \grave{\imath}\,\acute{a}\left(\vec{\boldsymbol{s}}^{(o)}\right)\left(\boldsymbol{s}_\alpha - \boldsymbol{s}_\alpha^{(o)}\right) + \frac{1}{2}C^k \mid \vec{\boldsymbol{s}} - \vec{\boldsymbol{s}}^{(o)} \mid^2,$$

$$\frac{\partial^2 E}{\partial s_i^{(o)} \partial s_j^{(o)}} \cong C^k \delta_{i,j};\ C^k = \beta_o C^{k-1};\ \beta_0 > 0; k = 1,2,3,etc. \quad (10)$$

Theorem 1: Hebb learning rule of neural network weight matrix:

Given measured ***s***-spectral band vector per pixel location, $\vec{\boldsymbol{X}}_s$: we solve unknown heat sources $\vec{\boldsymbol{S}} = [W]\vec{\boldsymbol{X}}_s$ by Artificial Neural Network unsupervised leaning weight matrix update.

$$\vec{S} = [A]^{-1}\vec{X} \equiv [W]\vec{X}. \quad (11a)$$

$$[W_{i,j}]^{k+1} = [W_{i,j}]^k - \frac{1}{C^k}\frac{\langle \vec{\mu}_i^k \vec{X}_j \rangle}{\langle [\vec{X}\vec{X}^T] \rangle} \quad (11b)$$

Proof:

$$H^{(2)} = E_o + \frac{\partial E}{\partial \boldsymbol{s}_\alpha^{(o)}}\left(\boldsymbol{s}_\alpha - \boldsymbol{s}_\alpha^{(o)}\right) + \frac{1}{2}\frac{\partial^2 E}{\partial \boldsymbol{s}_\alpha^{(o)} \partial \boldsymbol{s}_\beta^{(o)}}\left(\boldsymbol{s}_\alpha - \boldsymbol{s}_\alpha^{(o)}\right)\left(\boldsymbol{s}_\beta - \boldsymbol{s}_\beta^{(o)}\right) + T_o K_B \sum_{i=1}^{k} \boldsymbol{s}_i \log \boldsymbol{s}_i + (\mu_o - T_o K_B)(\sum_{i=1}^{k} \boldsymbol{s}_i - 1)$$

We may consistently vary $H^{(2)}$ w.r.t. Artificial Neural Network learning weight matrix:

$$\frac{\delta H^{(2)}}{\delta W_{j,i}} = \mu_j X_i + C^k \left\{ [W_{j,\alpha}] X_\alpha - s_j \right\} X_i = 0$$

We assumed the Ergodic hypothesis that the temporal average of high frequency turbulent fluctuations was equivalent to the equilibrium ensemble average with the nearest neighbor 3x3 average, denoted with the angular brackets. This was consistent with our fundamental assumption of space-variant blind de-convolution due to space-variant impulse response function, justified as the varying resolution issue observed only at 3x3 macro-pixel level.

$$\langle \vec{\mu}\vec{X}^T \rangle + C^k [W] \langle \vec{X}\vec{X}^T \rangle - C^k \langle \vec{s}\vec{X}^T \rangle = 0;$$

$$[W]^{k+1} = \left\{ \langle \vec{s}\vec{X}^T \rangle - \frac{1}{C^k} \langle \vec{\mu}^k \vec{X} \rangle \right\} < [\vec{X}\vec{X}^T] >^{-1}, \quad (12)$$

Use is further made of the definition of weight matrix: $\vec{s} = [W]\vec{X}$, we can simply the first term of Eq(9) and derived the learning rule Eq(8).

$$[W_{i,j}]^{k+1} = [W_{i,j}]^k - \frac{1}{C^k}\frac{\langle \vec{\mu}_i^k \vec{X}_j \rangle}{\langle [\vec{X}\vec{X}^T] \rangle}$$ **Q.E.D.**

Remarks (Everything that you might ask; but did not)**:**

1. Hebb Product Rule;
2. Helmholtz MFE;
3. Boltzmann Entropy;
4. Grey-Body Planck Law;
5. Quantum Statistics;
6. Vacuum Fluctuation:

1. **Hebb Product Rule:** Donald Hebb discovered from neurobiological synaptic junction learning rule is similar to a pipeline flow, that is proportional to how much goes in and how much comes out the pipeline known as Hebb product learning rule:

$$W_{i,j} \propto \vec{X}_i \vec{\mu}_j$$

We demanded a proper normalization $\frac{\langle \vec{\mu}_i^k \vec{X}_j \rangle}{\langle [\vec{X}\vec{X}^T] \rangle} \to 1$, if $\vec{\mu}_i^k \sim \vec{X}_i$.

What is thermodynamic learning rule? It's systematic guessing the most probable inverse source solution by directly computing for the maximum probability. By systematic trials and errors, we can de-mix the local mixtures by MFE principle. There is a finite number of ways that the positive sum of positive photon counts can be. Among them, we choose the lowest energy cases: e.g. giving Beethoven first 3 notes: " 5, 5, 1…." : We split the sum 5 = (0+5; 1+4; 2+3; 3+2; 4+1; 5+0) in the unit of energy at temperature K_BT=1/40eV for T=300°; and find hidden sources tones 2=3 and 3+2 occurring twice that have the highest canonical probability 2 exp(-2/K_BT)exp(-3/K_BT). In MFE, we might wish to rule out the rare *high energy* cases: 0+5 and 1+4, in favor with lower energy but *higher chances* in equilibrium: twice 2+3; unless other summations involve also these specific pixels. Given a set of vector measurements of multiple spectral bands, we applied the thermodynamic equilibrium theory to find hidden object sources at MFE by LCNN.

2. **Helmholtz MFE:** Helmholtz assumed such an open dynamic sub-system within the heat reservoir closed system where Boltzmann heat death at maximum entropy was assumed.

$$\Delta H_{object} \equiv \Delta E_{object} - T_0 \Delta S_{object} \le 0;\ \min . H \equiv E - T_o S$$

Proof:

Let S_{Total} denote the total entropy of a closed system. Then S_{Total} is the sum of entropy of reservoir and object,

$$S_{Total} = S_{\mathrm{Re}\,servoir} + S_{object}$$

If the object takes ΔE_{object} energy from its surroundings, the entropy change of $S_{Reservoir}$ will be $\Delta S_{Reservoir} = -\Delta E_{object} / T_0$, and the total entropy change is

$$\Delta S_{Total} = \Delta S_{Reservoir} + \Delta S_{object} = -\frac{\Delta E_{object}}{T_0} + \Delta S_{object} = -\frac{\Delta E_{object} - T_0 \Delta S_{object}}{T_0} = -\frac{\Delta H_{object}}{T_0} \quad (14)$$

where $\Delta H_{object} \equiv \Delta E_{object} - T_0 \Delta S_{object}$ is the change of the object's Helmholtz free energy which is an analytic state function defined by $H = E - T_o S$. Note that $\Delta S_{Total} > 0$ since the total entropy of a closed system is always increasing, and $\Delta H_{object} \le 0$ given a positive T_0. **Q.E.D.**

3. **Boltzmann Entropy:** Ludwig Boltzmann inscribed on his tomb headstone the entropy formula (cf. a picture of his Math Genealogy)

$$S = \boldsymbol{K_B}\, Log\ \boldsymbol{W};$$

where W was the aforementioned phase space trajectory volume, representing all the possibility that an identical macroscopic system can be prepared and realized; and $\boldsymbol{K_B}$ the Boltzmann constant 0.1 meV. To be explicit for remote sensing, we considered 3 kinds of identical ideties; *R* denotes the number of red balls/molecules/photons, likewise *G* & *B* in a closed

system. Thus, the chance of realizing total N balls is $N!$ divided by identical colors $R!G!B!$, because of the over-counting of permutation of identical particles.

$$W = \frac{N!}{R!G!B!}.$$

Sterling approximation of logarithmic factorial was valid when $N > 10$.

$$Log\, N! \cong N\, Log\, N - N\ ;\ N/N = R/N + G/N + B/N; 1 = S_1 + S_2 + S_3$$

Then, Boltzmann discrete entropy formula follows:

$$S = -K_B \sum_{i=1}^{K} S_i Log\, S_i - \text{const.}\left(\sum_{i=1}^{K} S_i - 1\right);$$

$$const. = \frac{\mu_o}{T_o} - K_B$$

where the minus sign was derived due to $Log\, S_i \le 0$ for $S_i \le 1$ and the Lagrange scalar constraint of the probability norm $\sum_{i=1}^{K} S_i - 1 = 0$ was chosen to be $\left(\frac{\mu_o}{T_o} - K_B\right)$ that insured the normalization and a simple slope: $\frac{\partial S}{\partial S_i} = -K_B\left(1 + \sum_{i=1}^{K} \log S_i\right) - \left(\frac{\mu_o}{T_o} - K_B\right) = -K_B \log S_i - \frac{\mu_o}{T_o}$ Q.E.D.

The maximum entropy in a closed system corresponds to the minimum free energy in open sub-systems

4. **Grey-Body Planck Law:** Planck's law is a triumph of modern quantum physics during 1900~1919. Max Planck received the Nobel Prize in Physics in 1918. A remarkable result that we exploited theoretically in this paper was that the spectral irradiance $I_\nu(T_K)$, leaking out of a small hole of the black body cavity opaque walls kept at a constant temperature, was peaked at a single wavelength monotonically $\lambda_o = \frac{c_o}{\nu_o}$ that uniquely determine the associated Kelvin temperature T_K once and only once in Figure 73. We were not the first one either. Astronomers applied the apparent measured brightness temperature T_B related by the unique peak spectrum value to an equivalent black body Kelvin temperature T_K. It turned out roughly $T_B \sim \varepsilon T_K$. Cosmic Background Radiation is not a blackbody for a large expanding universe having no outside, yet the estimation of an approximated reflectivity $\gamma \sim 0.1$ suggests by the conservation of energy, the equivalent emissivity is about $\varepsilon \sim 0.9$. Nevertheless, The universe was cooled down after the Big Bang happened at 13B years ago, the universe reached 3000K~0.25 eV, which is the time of hydrogen atoms were formed with 13.6 eV ionization energy (5% light mater, 27% dark mater, 68% dark energy). Thus, the background light having not enough energy became de-coupled from the hydrogen matter, and the universe became transparent and the remnant of Cosmic Microwave Background Radiation (CMBR) can be observed and may be called the "time of last (inelastic) scattering." The decoupled photons from matter are continuously cooled down 1000 times at now 2.7 °K ~0.23meV. Robert Dicke, George Gamow, Ralph Alpher, and Robert Herman conjectured that CMBR was the inflation Big Bang theory. 1978 Nobel Laureates Arno Penzias and David Wilson applied Dicke radiometry of 15 meter horn antenna to measure the peak at $\lambda_o = 7.35$ cm at $T_B \sim 2.73^o K \sim 0.9x3^0 K$. Subsequently, NASA's Cosmic Background Explorer (COBE) satellite using differential microwave instruments confirmed an anisotropic CMBR (George Smoot & John Mather, Nobel Prize 2006).

5. **Quantum Statistics**: G.E. Uhlenbeck & S. Goudsmidt discovered in 1910 in the Stern & Gerlach experiment an electron beam split under an inhomogeneous magnetic field into 2 beans: spin up or spin down: that the spin fine structure constant $2s + 1 = 2$ that implies the e-spin quantum number s=1/2. It suggested the e-wave function with the phase factor $e^{i(n-1)\pi} = (-1)^{n-1}$ generates alternation signs in the Fermi-Dirac distribution function $z - z^2 + z^3 - z^4 + \ldots = z(1 - z + z^2 - z^3 + \ldots) = \frac{Z}{1+Z} = \frac{1}{Z^{-1}+1} = \frac{1}{\exp\left(+\frac{E}{K_B T}\right)+1} \le 1$ for odd integer electron spin Fermion the Pauli's exclusion principle, a pigeon, a cell, and leading to a finite Fermi surface as the Band gap phenomena in the semiconductors.

Bose-Einstein condensation of integer spin Boson is due to the friendship principle that the condensed ground state becomes divergent $\frac{1}{\exp\left(+\frac{E}{K_B T}\right)-1} \to \infty$, where $E / K_B T \to 0$. BCS theory of superconductor of electron spin ½ was due to the lattice vibration of bounding two Fermions together called Cooper pairs, electrons or positron becoming a spin-1 Boson. Paul Chu et al. discovered higher temperature superconductor made of ceramic $Y_1 Ba_2 Cu_3 O_x$ material whose lattice defects, positron holes, enjoyed a larger internal pressure due to a larger replaced Ba_2 molecule, which bounded two Fermions together, by phonon exchange energy, into a spin-1 Boson and sustained a disruptive thermal noise $\gtrsim 77^o K$.

6. **Vacuum Fluctuation:** Paul Ehrenfest wrote the corresponding principle between classical mechanics and quantum mechanics. Poison Bracket was related to Heisenberg uncertainty principle commutator between position $\hat{P}$ and momentum $\hat{Q}$ operators. It represented the effects of two different sequences of measurements. It helped us quantized the Hamiltonian $\hat{H}$ of simple harmonic oscillator in the quantum field theory in terms of 2nd quantization operators $\hat{a}^\dagger : \hat{H} = \hat{P}^2 + \hat{Q}^2 = \left(\hat{P} + i\hat{Q}\right)\left(\hat{P} - i\hat{Q}\right) = \hat{a}^\dagger \hat{a}$ that computes the vacuum fluctuation due to the commutator uncertainty principle generating the non-zero vacuum energy $\hat{H}\left|0\right> = \frac{1}{2} h\nu \left|0\right>$. This zero-point vacuum fluctuation existed everywhere helped Higgs following Anderson phase transition model: $\hat{\phi}^4 \approx \hat{\phi} - \phi_+)^2 (\hat{\phi} - \phi_-)^2$ (having a lower potential well at symmetric ground state $|\phi_+>$ associated with a non-zero order parameter) condensing the energy into the mass $m = E / c_o^2$. CERN experiments seemed to have verified the Higgs boson phase transition mechanism.

Nonlinearly regularized Lagrange constraint neural network (LCNN)

The Mexican standoff will be regularized by **Karush, Kuhn-Tucker (KKT) 2nd order** penalty by steepening an isotropic

sphere. CRT&D CS assumed Lagrange slope to be estimation error itself, and no longer is an unknown. However, when the cost function is unknown, we have demonstrated the double iteration at the linear order is at 2nd order smallness, and therefore cannot consistently determine at the 1st order LCNN. We identified the penalty as the 2nd order Taylor series of MFE generating a linearly decoupled closed set of 3 equations for solving sources from spectral vector data, as a fast LANCELOT algorithm, called regulated LCNN (Szu, Miao, Qi, SPIE 2007). Given input s-spectral vector data X_s per pixel we give double iteration superscript index $k = I_+ \equiv \{1,2,3,etc.\}$.

Theorem 2: NL Regularized Lagrange Constraint Neural Network (LCNN) is a fast LANCELOT algorithm of nonlinear optimization. Given lemma on ANN learning matrix $\left[W_{j,i}\right]^k$ and EPS sources estimation error vector j-component c_j together, we determine the Lagrange error energy slope j-component μ_j^k iteration.

Hebb rule: $$\left[W_{i,j}\right]^{k+1} = \left[W_{i,j}\right]^k - \frac{1}{C^k}\frac{\left\langle \vec{\mu}_i^k \vec{X}_j \right\rangle}{\left\langle \left[\vec{X}\vec{X}^T\right] \right\rangle}; \quad (17)$$

Lagrange error slope rule: $$\vec{\mu}_j^{k+1} = \vec{\mu}_j^k + C^k \left\{ \left[W_{j,\alpha}^{k+1}\right] \vec{X}_\alpha - \vec{S}_j^{k+1} \right\}; \quad (18)$$

Unknown sources:

$$T_o K_B \log \vec{S}_j^{k+1} + C^k \vec{S}_j^{k+1} = C^k \left[W_{j,\alpha}^{k}\right] \vec{X}_\alpha + \vec{\mu}_j^{k} - \mu_0^k \quad (19)$$

Curvature Penalty: $C^k = \beta_o C^{k-1}; \beta_0 > 0; k = 1,2,3,etc.$

Proof:

The tradeoff between minimum energy and maximum entropy for the most probable configuration requires the 1st and 2nd order Taylor series expansions:

$$H^{(1)} = E_o + \frac{\partial E}{\partial s_\alpha^{(o)}}\left(s_\alpha - s_\alpha^{(o)}\right) + T_o K_B \sum_{i=1}^{k} s_i \log s_i + (\mu_o - T_o K_B)\left(\sum_{i=1}^{k} s_i - 1\right) \quad (20a)$$

$$H^{(2)} = E_o + \frac{\partial E}{\partial s_\alpha^{(o)}}\left(s_\alpha - s_\alpha^{(o)}\right) + \frac{1}{2}\frac{\partial^2 E}{\partial s_\alpha^{(o)} \partial s_\beta^{(o)}}\left(s_\alpha - s_\alpha^{(o)}\right)\left(s_\beta - s_\beta^{(o)}\right) + T_o K_B \sum_{i=1}^{k} s_i \log s_i + (\mu_o - T_o K_B)\left(\sum_{i=1}^{k} s_i - 1\right) \quad (20b)$$

We take variation calculus to set flattening extremes to be zero:

$$\delta E^{(1)} = \frac{\delta E^{(1)}}{\delta s_\beta^{(o)}} c_\beta\left(\vec{s}^{(o)}\right) \equiv \mu_\beta \left\{ \left[W_{\beta,\alpha}\right] X_\alpha - s_\beta^{(o)} \right\} \quad (20c)$$

$$\delta H^{(1)} = \frac{\delta H^{(1)}}{\delta s_j} = -\mu_\beta \frac{\delta c_\beta}{\delta s_j} + T_o K_B \log s_j + \mu_o \quad (20d)$$

$$\delta H^{(2)} = \frac{\delta H^{(2)}}{\ddot{a} s_j} = -(\mu_\beta + C^k \left\{ W_{\hat{a},\acute{a}} X_\alpha - s_\beta \right\} \frac{\delta c_\beta}{\ddot{a} s_j} + T_o K_B \log s_j + \mu_o \quad (20e)$$

where use is made of isotropic curvature in an increasing constant penalty term for k+1 iteration: $C^{k+1} = \beta_o C^k; \beta_o \approx 4$, and the simple component selection: $\frac{\delta c_i}{\delta s_j} = -\delta_{i,j}$.

From the variation of 2nd order (17c):

$$\delta H^{(2)} = 0: \; T_o K_B \log s_j + C^k s_j = C^k \left[W_{j,\alpha}\right] X_\alpha + \mu_j - \mu_0 \quad (21a)$$

From the variation of 1st order (17b):

$$\delta H^{(1)} = 0: \boldsymbol{\mu}_j + T_o K_B \log \mathbf{s}_j + \mu_o = 0 \quad (21b)$$

We obtain the consistency condition, after cancelling the entropy related common terms: $T_o K_B \log s_j + \mu_o$, the next iteration of the 1st order Lagrange error energy slope $\boldsymbol{\mu}_j^{k+1}$ is determined by the 2nd order variation of MFE:

$$\mu_j^{k+1} = \mu_j^k + C^k c_j^{k+1}; \quad c_j^{k+1} = \left[W_{j,\alpha}^{k+1}\right] X_\alpha - s_j^{k+1} \quad (21c)$$

This linear decoupled Lagrange error slope equation is historically called LANCELOT in FORTRAN massive database optimization. The blind sources estimation error provided the next gradient descent of Lagrange energy error slope vector μ_j^k .

De-mixing weight matrix Eq(18) was proved in Theorem 5. **Q.E.D.**

Pseudo code of LCNN, for 3-source model

Given multispectral data vector $x = (x_1 x_2 x_3)^T$ at a single pixel,

Initialize $\mu^0 = [000]^T, C^0 = 1, \beta_o = 4, and\, W = A^{(-1)}.$

Set iteration index k = 1, and maximum iteration number ITM

while $k \le ITM$

Calculate sources s^{k+1} subject to $0 \le s \le 1$ by solving **Eq(21a)**:

$$T_0 K_B \ln\left(s^{k+1}\right) + C^k s^{k+1} = C^k W^k x + m^k - m^k{}_0$$

If s^{k+1} converges, return. Otherwise continue;

Update de-mixing matrix **Eq(17)**:

$$W^{k+1} = W^k - (1/C^k) < m^k x^T > / < xx^T >$$

Update **Eq(21c)**:

$$m^{k+1} = m^k + C^k (W^{k+1} x - s^{k+1})$$

Update $C^{k+1} = \beta_o C^k$

$k \leftarrow k +$ 1 end

Conclusion

This thermodynamics learning rule may have open up a new era of dealing spectral image processing by thermodynamics. Various applications have been developed and reported in different journals. It might allow us to consider virtually crossing full electromagnetic spectrum. Compressive modeling and simulation based on NL LCNN will be published in Optical Engineering (Krapels, Cha, Espinola, Szu). IR triplets seeing through hot fire and cold dusts will be published in IEEE Tran IT (Cha, Abbott, Szu). Thermodynamics physics laws and modern applications will be published in Journal Modern Physics (Szu, Willey, Cha, Espinola, Krapels). Lots more will be waiting with your participations with MATLAB source code in Appendix A **BSS by Physics Source Approach pixel sequentially**, a benchmarked result showed there; in Appendix B **BSS by Engineering Filter Approach pixel parallelism**.

We also review the past accomplishment of Satellite gravity measurements without BSS, and convince potential sponsors the value about our design by concentrating on a matured hardware technology with smart BSS software.

Brain Information Theory: Szu applied, instead of the artificial minimum error energy, the physics equilibrium principle at the minimum isothermal free energy of $H = E - T_0 P;$ to be the basis of unsupervised learning. This is because of the following biological observation. All warm blood animals roaming on the earth have constant brain temperatures, and taken the advantage

of pairs of input sensory. Assuming furthermore the brain energy is analytic in the input vector time series and output feature vector time series, Szu has derived the sigmoid logic, and unsupervised Hebbian learning rule. This is called the Lagrange Constraint Neural Network (LCNN), US PTO 7,366,564.

Modern unsupervised learning algorithms:

Fast ICA: Prediction by replacing LMS with the higher order statistics (HOS) such as the 4th order cumulate Kurtosis sought after the stationary departure from Gaussian random distribution

$$\begin{pmatrix} s_1 \\ s_2 \end{pmatrix} = \begin{bmatrix} w_{11} & w_{21} \\ w_{12} & w_{22} \end{bmatrix} \begin{pmatrix} x_1 \\ x_2 \end{pmatrix} \tag{17}$$

$$dw_m / dt = d\kappa_4(s)/dw_m = 0$$

$$\kappa_4(s) = < s^4 > -3 < s^2 >^2 \tag{18}$$

where the form was due to infinite identical distribution (i.i.d.). Gaussian reduction was that

$$< s_1 s_2 s_3 s_4 >_G = < s_1 s_2 >_G < s_3 s_4 >_G < s_1 s_3 >_G < s_2 s_4 >_G + < s_1 s_4 >_G < s_2 s_3 >_G .$$

When all s_i were *i.i.d.*, then $\kappa_4(s) = < s^4 > -3 < s^2 >^2 = 0$ if Gaussian. The direct fixed-point solution was a cubic root that required no desired output in the weight adjustment. This algorithm could de-mix two spoken language without knowing the mixing matrix, since each person may have a different Kurtosis value K>0 called super-Gaussian as one subtract the positive 4th power of the waveform with a narrower than Gaussian amplitudes. On the other hand, the multi-modal histogram of images gives positive values of the Kurtosis, called sub-Gaussian. Thus, the classical auto-regression had evolved to the unsupervised learning by *HOS*.

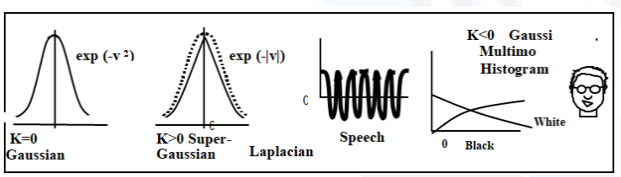

Figure 74 Higher order statistics (HOS) the 4th Cumulant Kurtosis K.

Independent component analysis ICA:

One assumes a linear instantaneous mixing vector time series

$$X(t) = s_1(t)a_1 + s_2(t)a_1 \equiv [A]S(t), \text{ where}$$

$$S(t) = (s_1, s_2)^T \text{ and } [a_1, a_2] \equiv [A]. \tag{19}$$

Thus, ANN sought after a weighted sum: $V(t) = [W]X(t) \approx s([W]X(t))$ that outputs nothing but the disinformation/garbage defined the identity correlation matrix [I]:

$$< V(t)\, V(t)^T >_G = [I] \approx [W][A] < S(t)\, S^T(t) > [A]^T [W]^T \tag{20}$$

which implied $[W][A] \approx [I]$ because independent $< V(t) V(t)^T > \approx < S(t) S^T(t) > \approx [I]$ had a nontrivial higher order statistics (HOS). Thus, the internal knowledge [W] was discovered as $[A]^{-1}$, called ICA.

$$\partial [W] / \partial t = \partial S(s_1, s_2) / \partial [W] \tag{21}$$

For the complicated joint density function (*j-pdf*) for multiple-variables correlation function, e.g. $\rho(x_1, x_2)$ this might be accomplished by finding a matrix $[W]$ which transformed the jointly measured data (x_1, x_2) to the independent sources (s_1, s_2) defined by the factorization of *j-pdf* of *unit-norm & zero-mean, defined by* $\rho_2(s_1, s_2) = \rho_1(s_1)\rho_2(s_2)$;

$$\begin{pmatrix} s_1 \\ s_2 \end{pmatrix} = [demixing\ W\ ?] \begin{pmatrix} x_1 \\ x_2 \end{pmatrix}; \quad \begin{pmatrix} x_1 \\ x_2 \end{pmatrix} = [mixing\ A\ ?] \begin{pmatrix} s_1 \\ s_2 \end{pmatrix} ? \tag{29 a,b}$$

so that sources correlation vanished

$$< s_1 s_2 > \equiv \iint s_1 s_2 \rho_2(s_1, s_2) ds_1 ds_2 = \iint s_1 s_2 \rho_1(s_1)\rho_1(s_2) ds_1 ds_2 = < s_1 >< s_2 > = 0 . \tag{30}$$

Then, one could find each *pdf in each independent variable s*, and then, an inverse transform could lead back to the *j-pdf* $\rho(x_1, x_2)$. P. Comon coined the name of Independent Component Analysis (ICA), similar to but general than the Principle Component Analysis (PCA) when the HOS were the second order. A popular contrast function achieving the factorization used by Bell and Sejnowski in 1996 to derive an ANN learning algorithm that was the closed system equilibrium at the maximum entropy. To follow the differential learning theory, we replaced the sum of discrete Shannon entropy formula by the continuous probability density function (pdf) $s_i = f(y_i)dy_i$. After taking the limit *over the discrete index i*, the sum became the integral

$$Max\ S(y) = -Max \grave{o} f(y) Logf(y)\, dy = -Max < Logf(y) > \tag{31}$$

Using the normalization condition $1 = \int f(y)\, dy = \int g(x)\, dx$ and Jacobbian strong condition: $f(y) = g(x) / |dy / dx|$, one computed explicitly the sigmoid transfer function of a single neuron:

$$y = s(x) = \left[1 + \exp\left(-(wx - w_o)\right)\right]^{-1} \tag{32}$$

Therefore, single neuron learning algorithm was by maximizing the entropy S yielded the weight w

$$dw / dt = \partial S(y) / \partial w \tag{33}$$

$$dw / dt \cong \partial Log |dy / dx| / \partial w$$

$$= | dy / dx |^{-1} \partial |dy / dx| / \partial w$$

$$= w^{-1}(2y - 1)\, x \tag{34}$$

where use was made of $dy / dx = wy(1-y)$; $dy / dw = xy(1-y)$; and $\partial |dy / dx| / \partial w = y(1-y) + w(dy / dw - 2ydy / dw)$. If one appended to one neuron the index j, Bell & Sejnowski derived in 1996 for N neurons a matrix vector algorithm

$$[\partial S / \partial W_{ij}] = [W_{ij}^T]^{-1} - (2y_i - 1)x_j^T \tag{35}$$

Since the matrix inverse involving too many computations about a cubic order of the matrix size, Amari-Yang-Cichocki considered such a non-local and non-biological learning to invert the Hebbian matrix, and they introduced the natural gradient based on local memory, rather than the steepest gradient ascent. Thus, a faster convergence algorithm without the inverse matrix:

$$(\partial S / \partial W)) [W]^T [W] = \left\{ \left[W^T\right]^{-1} - (2y - 1)\, x^T \right\} [W]^T [W]$$

$$new\ [W] = \left\{ [I] - (2y - 1)\, u^T \right\} old\ [W] \tag{36}$$

This was the so-called Infomax algorithm seeking the joint-pixel-density-factorization coined by Comon as the Independent

Component Analysis (ICA), which was furthermore improved by Amari et al. using the natural gradient for a faster convergence, similar to early Jutten-Herault's neighborhood inhibitory BSS algorithm presented at the Snow Bird Conference in 1986, Finland group.

This paper highlights the synergetic detection of the Earth's gravity and stress fields. We have shown that satellite gravity data can be used to calculate the stress distribution in the Earth for earthquake studies and Earth resources survey. Particular emphasis is laid on recent progress and results of stress calculations from which the origin and precursor of the 5/12/2008 Sichuan earthquake in China can be scientifically addressed. This space geodynamic approach for study the origin of earthquakes is unique in that it can pinpoint the triggering stresses for large intraplate earthquakes without ambiguities of geological structures, fault geometries, and other tectonic properties. Also, it is distinct from the probabilistic earthquake occurrence models in the literature, which are based on statistics of available earthquake data.

Satellites can seek gravity signals for remote sensing the mantle convection generated stress concentrations in the Earth. The images of these stress concentrations are defined as geological tumors. A geological tumor is benign if the stress concentrated region does not consist of fault or crack systems. However, the geological tumor is malignant if the stress concentrated region contains faults or cracks. Fracture of rocks in the malignant geological tumor due to stress concentration is the cause of earthquakes. Otherwise, the crusted region with even and smooth stress distribution can be considered as geologically stable. In 2006, satellite gravity scanning of the stresses in the crust under China discovered that stresses were centralized in the region of (31N, 103E) in Sichuan. The strength of this stress concentration approached the facture point of rocks. Therefore the Dragon Gate Fault system in this region may break up due to stress concentration. Thus, the stress concentration image detected in 2006 by satellites was a precursor to the May 12, 2008 Wenchuan Earthquake in Sichuan. Since the satellite detected geological tumor under Sichuan is malignant so that the three cities of Wenchuan, Beichuan and Chinchuan above the Dragon Gate Fault System could be completely destroyed. In addition, stresses have concentrated sharply under the crust along the Gold Sand River. Future construction of Dams along this river should be of great concern. Also, it is noted here that the image of the geological tumor under the Pacific Ocean has already extended to the east coast of Taiwan. We should be prepared to prevent the 2008 Sichuan earthquake to be repeated in Taiwan.

The even and smooth stress distribution in the crust along the lower Yangtze River indicates that the engineering site of the Three Gorges Dam is geologically stable, safe, and sound. It seems reasonable to claim that the 2008 Sichuan Earthquake has verified our Gravity-Stress theory for crustal deformation. Finally, satellite detection of the tensional stress belts under the crust may provide basic principles for earth resources survey in the west part of China. Global real-time system is possible under United Nations Auspicious.

What is Smartphone Nowcast technology?

Besides usual engineer's design considerations for Size, Weight and Power, Cost (SWaPC), Smartphone technologists shall consider miniaturized silicon piezoelectric material. This technology has already used in every car safety airbag detonation mechanism. The device can convert proving mass stress-strain to the electricity in every Inertial Motion Unit (IMU) embodying Micro Electric-Mechanic System (MEMS). Smartphone lab will take into account of the robustness versus the sensitivity trade-off according to earthquake magnitudes and frequencies statistics compared against car accident frequency (cf. earthquake dispersion spectrum, cf. USGA archival data).

BSS by physics source pixel sequentially (at min. Free-Helmholtz energy (MFE) NL regularized LCNN Mat lab code)

----------**Excursion**----------

BSS by Physics pixel sequentially

(Min. Free-Helmholtz energy (MFE) NL regularized LCNN mat lab code)

Pseudo code of LCNN, for 3-source model

Given multispectral data vector $x = (x_1, x_2, x_3)^T$ at a single pixel,

Initialize $m^0 = [000]^T, C^0 = 1, \beta_0 = 4,$ and $W = A^{-1}$.

Set iteration index $k = 1$, and maximum iteration number ITM

while $k \le ITM$

Calculate sources s^{k+1} subject to $0 \le s \le 1$ by solving **Eq (21a)**:

$T0KB \ln(s^{k+1}) + C^k s^{k+1} = C^k W^k x + m^k - m^k 0$

If s^{k+1} converges, return. Otherwise continue;

Update de-mixing matrix **Eq (17)**: $W^{k+1} = W^k - (1/C^k)\langle m^k x^T \rangle / \langle xx^T \rangle$

Update **Eq (21c)**:

$m^{k+1} = m^k + C^k (W^{k+1} x - s^{k+1})$

Update $C^{k+1} = \beta_0 C^k$

$k \leftarrow k + 1$ End

Appendix B: BSS by engineering filter approach: pixel parallelism (at maximum output entropy).

Bell, Sejnowski, Amari & Oja (BSAO) have systematically formulated an *unsupervised learning of ANN algorithm for unknown but identical for space-invariant mixing* by varying the unknown de-mixing weight matrix $\left[W_{i,j}\right]$ until nothing but the Max Entropy entropy $S(y_i)$ of the output $y_i = \left[W_{i,\alpha}\right]x_\alpha$, where $x_j = \left[A_{j,\alpha}?\right]s_\alpha?$, and the repeated Greek indices represent the summation. ANN model used a monotonically sigmoid-squashed threshold output

$$y_i = \sigma(x_i) \equiv \{1+\exp\left(-\left[W_{i,\alpha}\right]x_\alpha\right)\}^{-1}.$$

that is nonlinear analytic solution of Riccati equation $\frac{dy}{dx} = y(y-1)$, for asymptotically binary logic $y = 0 or 1$ for no or yes. Since a single neuron learning rule turns out to be massively parallel to N neurons in tensor index notion, for simplicity, we derived for a single neuron to point out why the engineering filter does not follow Hebb's synaptic weight updates. A bona fide unsupervised learning did not have a desirable specific output entropy $S(y)$ became maximized, the de-mixing filtering $\left[W_{i,j}\right]$ becoming the inverse of unknown mixing matrix $\left[A_{j,\alpha}\right]$. Thus, the filter weight adjustment is defined as:

$$\frac{\delta w}{\delta t} = \frac{\partial S(y)}{\partial w},$$

$$S(y) = -\int f(y)\log f(y)\,dy \Rightarrow$$

$$\delta w = \frac{\partial H(y)}{\partial w}\delta t = \{|w|^{-1} + (1-2y)x\}\delta t.$$

Derivation: From the normalized probability definitions:

$$\int f(y)dy = \int g(x)dx = 1;\ f(y) = \frac{g(x)}{\left|\frac{dy}{dx}\right|};\ H(y) \equiv -<\log f(y)>_f,$$

we expressed the output pdf in terms of the input pdf with changing Jacobian variables. We exchanged the orders of operation of the ensemble average brackets and the derivatives to compute

$$\frac{\partial H(y)}{\partial w} = \frac{\partial <\log\left|\frac{dy}{dx}\right|>_f}{\partial w} \cong \left|\frac{dy}{dx}\right|^{-1}\frac{\partial\left|\frac{dy}{dx}\right|}{\partial w};$$

Since Riccati equation was satisfied by the sigmoid:

$y = [1+\exp(-wx)]^{-1}$; $\frac{dy}{d(wx)} = y(1-y)$. we readily derived by chain rule the following results

$$\frac{dy}{dx} = wy(1-y); \frac{dy}{dw} = xy(1-y).$$

Substituting these results into Max Ent learning rule, Bell-Sejnowski Eq (9):

$$\frac{\partial H(y)}{\partial w} = \left[W\right]^{-1} - (2y-1)x \quad \textbf{Q.E.D.}$$

The first term computing the inverse matrix $|w|^{-1}$ is not scalable with increasing N nodes, while the second term satisfied the Hebbian product rule between bipolar output 2y-1 and input x. S. Amari et al. at RIKEN assumed the identity $\left[\delta_{i,k}\right] = \left[W_{i,j}\right]\left[W_{j,k}\right]^{-1}$ and multiplied the identity through both sides of original non-biological algorithm

$$\frac{dH}{dW_{i,j}}\left[\delta_{i,k}\right] = \{\left[\delta_{i,j}\right] - (2\vec{y}-1)\vec{y}^T]\}[W_{i,j}]^{-1},$$

where use was made of $y_i = \left[W_{i,\alpha}\right]x_\alpha$ to change the input x_j to the synaptic gap by its weighted output y_i.

Amari et al. derived a natural gradient ascend as the final BSAO algorithm in information geometry,

$$\frac{dH}{dW_{i,j}}\left[W_{i,j}\right] = \{\left[\delta_{i,j}\right] - (2\vec{y}-1)\vec{y}^T]\},$$

which was not in the original gradient direction $\frac{dH}{dW_{i,j}}$ and enjoyed a faster update without the inverse .

Fast ICA: Erkki Oja began his ANN learning of nonlinear PCA for pattern recognition in his Ph D study 1982.

$$\left\langle \vec{x}\vec{x}^T\right\rangle \hat{e} = \lambda\hat{e};$$

$$w' - w = \vec{x}\sigma\left(\vec{x}^T\vec{w}\right) \cong \left\langle \vec{x}\vec{x}^T\right\rangle\vec{w};$$

$$\frac{d\vec{w}}{dt} = \left\langle \vec{x}\vec{x}^T\right\rangle\vec{w} \cong \sigma\left(\vec{x}^T\vec{w}\right)\vec{x} \cong \frac{dK(u_i)}{du_i}\frac{du_i}{dw_i} \equiv k\left(\vec{x}^T\vec{w}\right)\vec{x};$$

where Oja changed the unary logic to bipolar hyperbolic tangent logic $v_i = \sigma(u_i) \approx u_i - \frac{2}{3}u_i^3 \cong \frac{dK(u_i)}{du_i};\ u_i = w_{i,\alpha}x_\alpha$.

By derivation we obtain therefore the **BSAO** unsupervised learning collectively in a termination condition: It becomes similar to a Kurtosis slope, which suggested to Oja a new contrast function K. The following is the geometric basis of a stopping criterion of unsupervised learning. Taylor expansion of the normalization, and set $|\vec{w}|^2 = 1$:

$$|\vec{w}'|^{-1} = [(\vec{w} + \int \vec{x}k\left(\vec{w}^T\vec{x}\right))^T\left(\vec{w} + \in \vec{x}k\left(\vec{w}^T\vec{x}\right)\right)]^{-\frac{1}{2}}$$

$$= 1 - \frac{\in}{2}k\left(\vec{w}^T\vec{x}\right)(\vec{x}^T\vec{w} + \vec{w}^T\vec{x}) + O\left(\in^2\right).$$

$$\vec{w}'' \equiv \vec{w}'\,|\,\vec{w}'|^{-1}$$

$$= \left(\vec{w} + \in \vec{x}k\left(\vec{w}^T\vec{x}\right)\right)\left(1 - \frac{\in}{2}k\left(\vec{w}^T\vec{x}\right)(\vec{x}^T\vec{w} + \vec{w}^T\vec{x})\right)$$

$$\Delta\vec{w}'' = \vec{w}'' - \vec{w} = \in\left[\delta_{\alpha,\beta} - w''_\alpha\, w''^T{}_\beta\right]\vec{x}_\alpha\frac{dK(u_\beta)}{d\vec{w}''_i}$$

ICA algorithm is let the joint probability density function be factorized equally according to Max Entropy requirement of white noise. Unfortunately, such a filter approach cannot work for the remote sensing imageries, because the atmospheric turbulence changes spatially rather quickly due to of a large pixel foot print about tenth squared kilometers (Landsat 30 km^2 per pixel). If one were insisting to apply ICA to mix together all spatial (x,y) ***s***-spectral vectors data $\vec{X}_s(x,y,t)$ in parallel, the assumption of spatial invariant mixing matrix will produce inaccurate sources at the **maximum entropy (Max Ent)**. Spatial invariant assumption will not work for a close-up dual infrared spectral band image for

screening for cancers, because of the localization of cancer has a strongly space-variant physiology with and without the cancer. Solving the inverse of space-variant impulse response Green's function or optical point spread function (psf) we need new MFE approach to BSS. To improve it, we have explored space invariant imaging (in terms of 3x3 macro-pixels) for macro-pixel joint density factorization ICA method; (Du, Kopriva, Szu, by Non-negative Matrix Factorization IEEE 2005; & by JADE & Fast ICA Op Eng. 2006). Then, the comparison experience help us reformulated in 2007 a nonlinear LCNN, ala KKT penalty, to regularize the linear LCNN for assuming space-invariant result within 3x3 nearest-neighbor macro-pixels per tumor cluster cells, but space-varying among macro-pixels with or without tumor.[4] In remote sensing, the Mexican standoff product challenge was overcome by the 2nd order energy expansion curvature known as KKT nonlinear optimization penalty. Typical 80 spectral band images among 158 Airborne Visible/Infrared Imaging Spectrometer (AVIRIS) (Kopriva, Szu, Fast ICA, SPIE ICA etc.2002) and corresponding BSS out of applying LCNN to 158 channels data sources maps where blue color means no class, i.e. low probability while red color means high probability.

The time-frequency-joint representation (tfjr) of seismic waves, music, radar and quantum mechanics

To read further the seismic wave and ray phenomena, we provide an excursion with Fourier transform and related reference in Radar and Quantum Mechanics as 2nd order time-frequency-joint representation (TFJR). Sound is different from light being a longitudinal wave, i.e. propagation direction is along the amplitude vibration direction (as the light is transversal wave). Music is sound, and musicians have systematically recorded the discrete *time and frequency joint representation* in music score written in Piano scale fashion.

Figure 75 Music Score, Joseph Fourier, and Heat Diffusion.

Joseph Fourier 1768-1830 (age 62) (tailor son, orphan at age 9, educated at Convent of St. Mark, military math lectureship, Loyal Advisor to Napoleon Egypt exhibition, Succeeded Joseph-Louis Lagrange Professorship at the École Polytechnique; French Academician), Discover of Earth Green House Effect (Annales de Chimie et de Physique 27(1824): pp.136–67); His name is one of the 72 names inscribed on the Eiffel Tower.

Fourier circa 1800 associated the marker on a spinning wheel with angular displacement in degrees $\theta = \omega t = 2\pi\nu t$ that is associated with wave height in amplitude a or b in time in terms of sinusoidal wave functions of two types: odd sine and even cosine:

$$a\sin(-\theta) = -a\sin(\theta); b\cos(-\theta) = b\cos(\theta)$$

Consequently, Joseph Fourier defined using:

$i \equiv \exp\left(\frac{i\pi}{2}\right)$, in $\frac{2\pi}{4} = \frac{\pi}{2}$ in 4-periodicity defined as:

$i \equiv \sqrt{-1}; i^2 = -1; i^3 = -i; and\ i^4 = 1$ back to the positive 1. Fourier took another invariant representation of Euler's number e, namely a number approximately equal to 2.718281828, such that it is its own mapping If $= e^x$; then $\frac{dy}{dx} = e^x = y$.

Thus, the standard Taylor expansion can lead to the Fourier integral transform (for continuous time and frequency representation) $= 2\pi\nu t = \omega t$:

$$\exp(i\theta) = 1 + i\theta + \frac{1}{2}(i\theta)^2 + \frac{1}{3x2}(i\theta)^3 + \ldots = \cos(\theta) + i\sin(\theta)$$

where the real part is the even function and imaginary part is the odd function. During the end of WWII UK & US/NRL engineers inspired by bat eco-location ability at night, and developed Radar in foggy mist ocean weather condition. They tested device independently for air defense. It's an application of group wave interference effect. If we wish the width of the group wave is to be small to increase the accuracy of distance measurement, we must increase the group frequency spread to beat one another outside the width of the distance measure. Similarly, Modern day quantum mechanics uncertainty relationship turns out is precisely the same as the De Broglie group wave phenomena. A precision measurement of a particle requires electron microscope high-energy photon that will impart recoil momentum to the particle generating the uncertainty of momentum or position. The uncertainty of wave package is of the order of magnitude of Plank constant measured in blackbody radiation spectral

$h = 6.6310^{-34}\,\mathrm{m}^2\,\frac{kg}{sec}$; or, $4.1410^{-15}\,eV\,sec$.

Eugene Wigner wished to develop the mathematical representation to represent the group wave package known as the Wigner distribution function. Similarly, Woodward wished to develop a consistent review in Radar known as the Woodward Ambiguity Function; both are given in a succinct review, cf. "The mutual time-frequency content of two signals," H. Szu, J. Caulfield, Proc. IEEE V.72 (1984), pp. 902-908). Highlights are given as follows:

We introduce their mean time t_o and Fourier conjugate variable Doppler frequency μ

$$t_o = \frac{t_1 + t_2}{2}; \mu = \nu_1 - \nu_2$$

As well as the mean frequency ν_o and the Fourier conjugate variable delay time τ

$$\nu_o = \frac{\nu_1 + \nu_2}{2}; \tau = t_1 - t_2$$

Now we can compute the transform 4-D $\{(t,\nu)_1;(t,\nu)_2\}$ to new pairs of coordinates $\{(t_o,\mu);(\tau,\nu_o)\}$. It turns out the coordinate transform Jacobian is unity. $dt_1\,dt_2 = \mathcal{J}\left|\frac{dt_1\,dt_2}{d\tau_1 d\tau_1}\right| d\tau_1 d\tau_1$.

We can consistently define Radar Woodward Ambiguity Function $A(\mu,\tau)$ and Wigner distribution function $W(\nu_o,t_o)$ in Quantum Mechanics. While in Radar Woodward measured the group wave travels along the mean time t_o analyze the Doppler frequency shift μ; in quantum mechanics Wigner measured the other pair wave package traveling along the interference difference time τ and analyze the Fourier conjugate mean frequency ν_o.

We define a lower case letter $s_j(t_j)$ to be the group wave signal and the corresponding pair of Fourier transform denoted in uppercase letter $S_j(\nu_j), j = 1,2$,

$$S_j(\nu_j) \equiv FT_{t,\mu}\left[s_j(t_j)\right] = \int_{-\infty}^{\infty} s_j(t)\,\exp(-i2\pi\nu_j t)\,dt\;;$$

and vice versa the inverse

$$s_j(t_j) \equiv FT_{\upsilon,t}{}^{-1}\left[S_j(\nu_j)\right] = \int_{-\infty}^{\infty} S_j(\nu)\,\exp(i2\pi\nu t_j)\,d\nu$$

Because the Paul Dirac delta function in tfjr domain

$$\delta(t-t') = \int_{-\infty}^{\infty} d\nu\,\exp(i2\pi\nu(t-t'))\;;$$

$$\delta(\nu+\nu') = \int_{-\infty}^{\infty} dt\,\exp(i2\pi t(\nu+\nu'))$$

WAF: $A(\mu,\tau) \equiv FT_{t_o,\mu}\, s^*\left(t-\frac{\tau}{2}\right)s\left(t+\frac{\tau}{2}\right)$

WDF: $W(\nu_o,t_o) \equiv FT_{\tau,\upsilon_o}\, s^*\left(t_o-\frac{\tau}{2}\right)s\left(t+\frac{\tau}{2}\right)$

Consequently, $W(\nu_o,t_o) = FT_{\mu,-t_o}\,F_{\tau,\upsilon_o}\,A(\mu,\tau)$

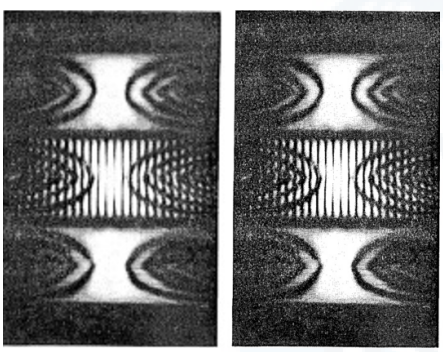

Figure 76 Woodward Ambiguity Function of an ideal rectangular function, when WAF is turned 90° becomes Wigner Distribution Function.

Chapter 4: Earth resource exploration; orbital perturbation dynamics

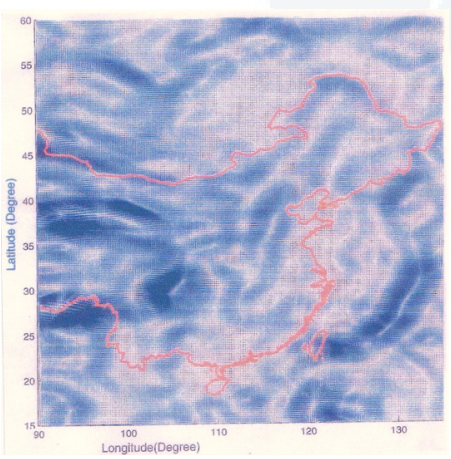

Figure 77 Stresses were concentrated at (31N,103E) under Sichuan.

For the past 4 decades, models of mantle convection have made remarkable advances. However, the global seismotectonic stresses in Earth's interior due to mantle convection are yet to be determined. The problem is that no one has been able to come up with a satisfactory scenario that must characterize the deformation stresses in Earth which can cause earthquakes and create tectonic features. The fundamental problem of the deformation of the Earth involves stress conditions on the base of the crust caused by mantle convection. Convection-generated stresses can be inferred from satellite gravity models. The new gravitation model EGM96 has improved spherical harmonics of the model to degree and order of 360. In order to provide insights into the origin of earthquakes and prove the existence of the mesospheric plates which range in depth from 100 km to 300 km, Liu et al. (2003) have developed a global stress pattern from satellite gravity models as shown in Fig.1, in which the length of the arrows represents the magnitude of the stress strength. For the sake of completeness, we have taken literally from the book literature for the solid crux dynamics A quantitative calculation indicates that the gravitational torque on the mantle from the liquid core may be sufficient to explain the accelerations and decelerations in the Earth's rotation on the 1000 year timescale. The corresponding torque by the mantle on the core may also explain the westward drift of the magnetic field of 0.2° per year. Gravitational core-mantle coupling would stochastically affect the rate of change of the Earth's tilt by just a few per cent. Its contribution to polar wander would only be about 0.5% the presently observed rate of 10 centimeters per year. [Rubincam,. D.P., Gravitational core-mantle coupling and the acceleration of the Earth, *J Geophys Res*, 108, B7, 2338, doi: 1029/2002JB002132, 2003]. Satellite detected stress concentrations are particularly intense in the ring of fire around the Pacific as indicated by strong convergence of arrows. These are the Western U.S., the Andes and the associated ocean trenches, off the Tonga and Japan trenches and near the East Indies. An important aspect of these stress belts relative to earthquakes is the implication for seismic hazard assessment. It has been found that the satellite detected stress belts around the Pacific and the statistically significant prediction of the Circum-Pacific seismic belts are in good agreement. These research results indicate that satellites could detect the triggering stresses of the large earthquakes in the ring of fire around the Pacific and over the world. The stress fields thus derived also have possible applications in earthquake prediction studies. The US/China joint earthquake prediction program beginning in 1981 has presented a thorough study of the relationship between gravity variations and seismotectonic stress changes under the *Beijing-Tianjin-Tangshan-Zhangjiakou (BTTZ)* region in China. It has been proposed to seek gravity signals for probing seismotectonic stress changes under the *BTTZ* region.

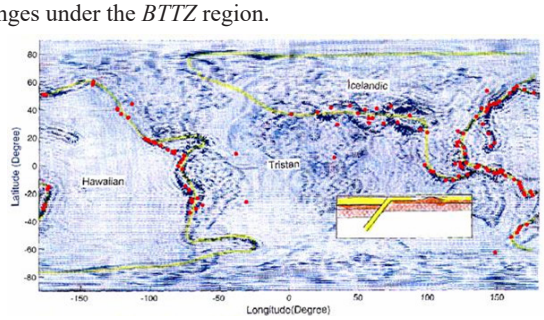

Figure 78 This equatorial equidistant seismotectonic stress map as inferred from satellite gravity signals up to the 150 harmonic degree shows approximate boundaries of the Hawaiian, Tristan and Icelandic mesoplates (200 km below Earth's surface). Formation of the three mesoplates has provided a framework for resolving a decades-old controversy (Pilger 2003) and explaining these destructive tectonic stresses as the origin of the 131 Ms > 7.0 earthquakes during 1977 to 2000.

Figure seems to suggest a stress origin of shaping our world. Large earthquakes are shown to be restricted in the global belts of stress concentration. It is confirmed that the boundaries of the Hawaiian, Tristan and Icelandic mesoplates as defined by Pilger (2003) are subjected to large stress concentration.

Numerical schemes have been programmed for solving equations 2-10. The harmonic coefficients $C_{n,m}$ and $S_{n,m}$ in the gravity field have been significantly improved in 2006. For 13 < n <150, this set of satellite gravity data is accurate enough to compute the stress distributions in the Earth.

The gravitational harmonic coefficients $C_{n,m}$ and $S_{n,m}$ were introduced into equations 2,3,9 and 10 to compute the magnitude and direction of the resulting stresses. In order to calculate the global and regional convection patterns and stress fields, we have discretely digitized the surface of the Earth into 1,296,000,000 grid points with each grid point carrying 250,000 orbital parameters. This was a huge and complicated computation project. Six of the 500 computed maps are shown Figure 49.

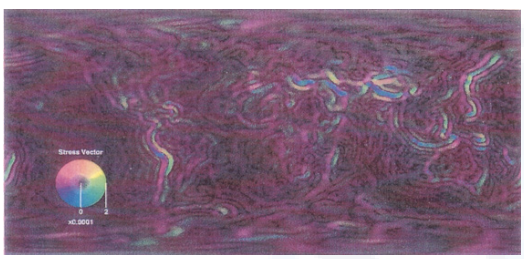

Figure 79 Global Mantle Convection Pattern (20 Km under the surface of the Earth).

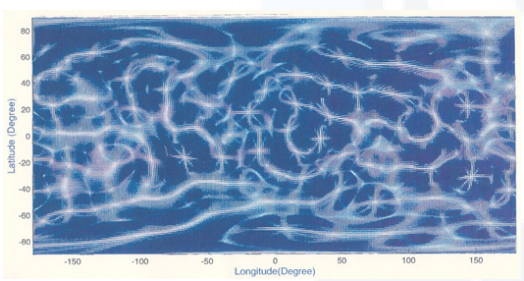

Figure 80 Global Stress Distribution (40 Km below the surface of the Earth).

MANTLE CONVECTION GENERATED STRESSES IN THE EARTH

Given a set of harmonic coefficients, $C_{n,m}$ and $S_{n,m}$ determined from satellite measurements of gravity field, the relationship between the mantle convection pattern and the gravity field may be described by:[1–4, 8–24]

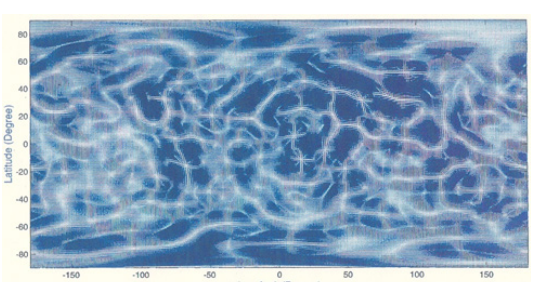

Figure 81 Stress Distribution (30 Km below the surface of the Earth).

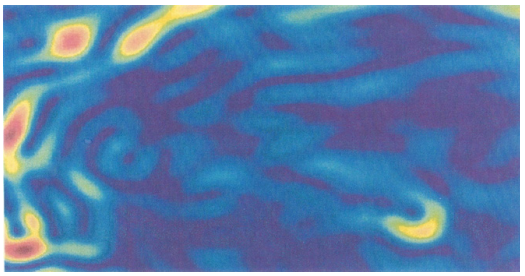

Figure 82 Reginal Mantle Convection Pattern (20 Km below the surface of the Pacific Ocean; the yellow spot in the lower right corner indicates the up welling mantle flow under Hawaii).

The Space approach can measure a far-field measurement of low frequency seismic waves in a longer antenna, especially flying over the oceans.

Similarly, seldom animal remains discovered in China flooded upstream of the 3 Gorgy Dam, concerned UN.

European has stress accumulated under the crust of Belgium Liege in **1983.** All infrastructures has been ruined but killed no human, due to orderly evacuation.

Unpredictability chaotic dynamics:

NASA satellite discovered the stress accumulation under Sichuan Beichuan.

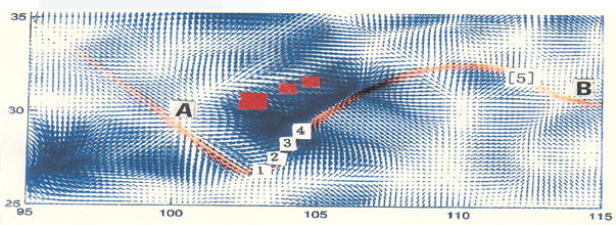

Figure 83 Stress distributions under a section (AB) of the Yangtze River. [I]. Four big dams are proposed to be built on the upper section of the Yangtze River (Gold Sand River): 1. Wutungtei, 2. Beihotun, 3. Shelotau, and 4. Shongchabou. [II]. In the lower section of the Yangtze River, 5 indicates the engineering site of the Three Gorge Dan.

Figure 84 Satellite revealed the over stress China central plate.

China's 3 Gorge Dan Hopeh Province Quake at Richet Scale 8.2 of 3:42 am, July 28, 1976 claimed 750,000 lives. 1976+magic means & variance+ central plate delay 8=2008. On May 12, 2008, China Sichuan Earthquake 2008 at Richet scale 7.8 and 88,000 lives perished.

Note: stress concentration image also appeared near east of Taiwan under the Pacific Ocean). Nevertheless, we know it was due to readjustment of the collision between India and Eurasia plates, with 33,000 pre-quakes and post-quakes.

At *3:42 am*, millions of people in northeastern China's *Hopeh Province* were awakened by a loud roar. An Richet *scale 8.2 earthquake* shook the ground violently on that rainy Wednesday morning. The quake's epicenter was in a highly populated area: Tangshan, a coal-mining city with about a million residents. Buildings crumbled so quickly they appeared to be "made of cards," a survivor later reported. Coal tunnels beneath Tangshan collapsed, burying miners working the night shift. Pits created by the collapsing mines swallowed up a train and a hospital.

Beijing, the capital of China, and Tianjin, another major Chinese city, were also damaged by the quake. Across the nearby countryside, dams collapsed, railroad tracks were wrecked, and trees were uprooted. Just 15 hours following the first earthquake, another major quake struck. Fortunately, most people who had survived the first quake were camping in fields and on streets, where they were safe from further building collapses. It is believed that *750,000 people* died in China's great quake of *July 28th, 1976*. As with any disaster of this magnitude, it is difficult to know the true number of casualties.

Figure 85 The earliest known deadliest quake in history shook China in 1556, taking about 830,000 lives.

China, the world's most populous country, has suffered some of the greatest natural disasters, including floods, famines, and earthquakes. *The deadliest known quake in history shook China in 1556, taking about 830,000 lives.* Four hundred twenty years later, on the morning of *July 28th, 1976,* China was rocked by a quake that.

Looking now back four years:

Chem-bio contamination:

The Tsunami flooded the cooling system of Fukushima #1 Nuclear Reactor and melted down the reactor with nuclear iodine isotope leakage into ocean causing children thyroid cancer cases over decades. Japan could no longer enjoy the sashimi raw fish because the fish has been contaminated with nuclear radiation, Japan and Korean developed kilometer deep ocean fish farm.

It initiated primarily by the tsunami of the Tōhoku earthquake on *11 March 2011*. The damage caused by the *tsunami produced equipment failures*, and without this equipment a *loss-of-coolant* accident followed with *nuclear meltdowns*. (The decay heat in the Unit 4 spent fuel pool had the capacity to boil about 70 tons of water per day (12 gallons per minute). The *releases of radioactive materials* began on *March 12*. It is the largest nuclear disaster since the *Chernobyl disaster of 1986* and the second disaster (after Chernobyl) to measure *Level 7* on the *International Nuclear Event Scale*, releasing an estimated 10 to 30% of the radiation of the Chernobyl accident.

Japan's Great *Kantō* Earthquake of Sept. 1, 1923 claimed 150,000 lives.

Figure 86 Kantō Earthquake of Sept. 1, 1923.

On *September 1, 1923*, at two minutes before noon, a tremendous quake shook Japan's *Sagami Bay region, near the cities of Tokyo and Yokohama*.

Many people in Japan had been cooking their noontime meal when Great *Kantō earthquake* struck. As buildings in Tokyo and Yokohama toppled, stoves overturned. *Fires ignited and grew so large that they generated their own winds*, created what are called firestorms. In Tokyo, more than 40,000 people sought safety in an open park known as the Military Clothing Depot. Nearby buildings caught fire, launching a firestorm that swept through the crowd like a flaming hurricane at *150 miles per hour*. At that one location, at least *38,000 perished*. To make disaster even worse, the quake caused the ground in the Sagami Bay region to rise in some places and fall in others. The movement of the land the area of the bay triggered *30-foot tsunamis* that flooded Japanese cities and towns.

Fires, toppling buildings, and tsunamis claimed up to *150,000 lives*. Roughly half of Tokyo and most of Yokohama were destroyed by the Great Earthquake of 1923. Because of the extensive damage to Tokyo's telephone and telegraph wires, the city turned to an unusual means of communication. For a week after the earthquake, messages were sent out of Tokyo by *400 specifically trained carrier pigeons*.

Chapter 5: Earthquake physics sources; why periodic?

Amazing earthquake facts

Figure 87 Earthquakes in Alaska

- Alaska has more earthquakes than any other state.
- Alaska has a magnitude 7 quake almost every year.
- *Alaska* experiences a magnitude 8 quake on the average of every 14 years.
- The most violent earthquake ever recorded in the United States took place in *Anchorage, Alaska* in March 1964. It measured 8.4 on the Richter scale. More than 100 people died.
- Sand, mud, and water sometimes bubble up during earthquakes, gushing water and soil like miniature mud volcanoes.
- An Earthquake can cause secondary effect such as fire in San Francisco in 5:12 am, April 18, 1906 and an avalanche or a landslide causing snow, rocks and mud to crash down from a mountain.
- The 2004 Indian Ocean earthquake released enough energy to power all the homes and business in the United States for three days.
- A weaker earthquake can cause more damage and death than a stronger earthquake if its epicenters is in or close to large cities.
- Following an 8.1 magnitude earthquake in New Madrid, Missouri in 1811, aftershocks continued for more than a year.
- A typical Earthquake lasts under a minute.
- The Appalachian Mountains in the United States were formed millions of years ago by thrust fault activity.
- In Northern California 1989, Loma Prieta Earthquake interrupted the World Series which was being played in nearby San Francisco. Still, when scientists placed a *Radio Seismic Wave Sensor* near the *Loma Prieta epicenter* even though BART trains were not running when the Napa quake hit at about 3:30 a.m., the transit agency received a 10-second warning from *ShakeAlert* (UC Berkeley).
- While seismic waves can travel at hundreds or thousands of miles per hour, a well-placed sensor, e.g. *Smartphone*, can send a warning even faster, giving people a few crucial moments to take cover and providing the potential for automated reaction from critical infrastructure equipment like transit trains, hospitals and fire departments.
- A joint effort between Universities and USGS is to create a *Unified West Coast Early-Warning System*.
- Scientists predict that during the next 30 years, Californians have a 65 percent chance of experiencing an earthquake of magnitude 7 or greater.
- Seismologist's best information about future earthquakes comes from studying the patterns of past earthquakes.
- The safest buildings can bend back and forth without breaking from an earthquake.
- The Transamerica Pyramid in San Francisco was designed to be twice as strong as building codes require. Its shape and structure help make it earthquake resistant.
- The moon has quakes too.
- The interior of Antarctica has icequakes, but these quakes happen on the ice sheet and not the land itself.

South American Peru's earthquake of 3:23 pm, May 31, 1970 claimed 120,000 lives.

Figure 88 Land slide in Peru May 31, 1970,

- At 3:23 pm., on May 31, 1970, an earthquake jolted the South American country of Peru. Enormous damage occurred in Peru's coastal department of *Ancash*. In the city of *Huaraz*, as many as *20,000 people* died in the crumbling buildings. Chimbote and other towns in the area were also greatly damaged or destroyed. The quake's focus was *15 miles off the coast of Peru, far below the Pacific Ocean seafloor*. Due to the great depth of its point of origin, the quake did not disturb the seabed, so no major tsunamis occurred. But while it produced no killers from the ocean depths, the quake triggered some deadly events from the heights of Peru.
- The quake shook loose a huge mass of material from *Huascaran*, the 22,205-foot *mountain* that is Peru's highest peak, unleashing a combination *avalanche-landslide*. Millions of tons of snow, ice, rocks, and mud shot down the mountain's slopes at speeds sometimes exceeding *150 miles per hour*. In *Yungay, 20,000 people were buried alive*. Elsewhere the half-mile-wide mass of debris flattened villages and farms like a giant bulldozer. When it finally ended, the Peruvian quake and accompanying landslide-avalanche had claimed nearly *80,000 lives* and had destroyed the homes of nearly a million people. It was the deadliest natural disaster ever to strike North or South America.

Mississippi River Earthquakes at New Madrid, Missouri, Magnitude 8.1, February 7, 1811-1812.

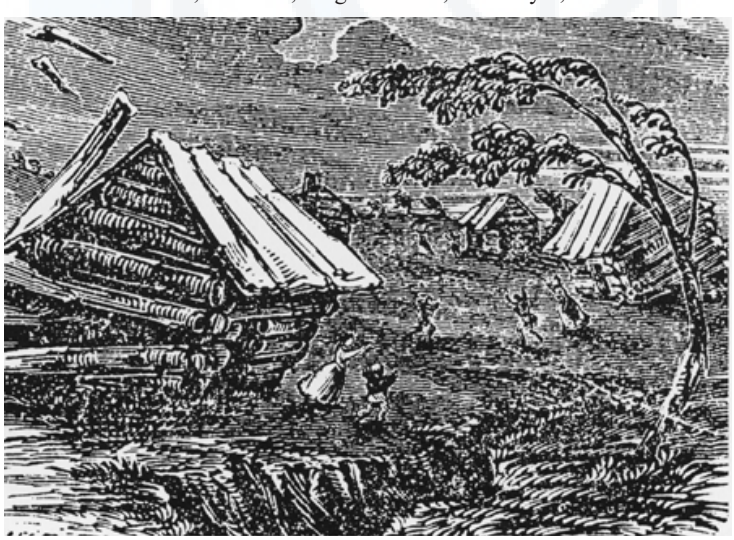

Figure 89 Mississippi River Earthquakes at New Madrid, Missouri of Magnitude 8.1, February 7, 1811-1812

- A huge quake jolted *New Madrid, Missouri*, located on the *Mississippi River*. Many of the town's one thousand residents fled their shaking cabins and ran outdoors, where the quaking ground tossed them about. Scientists later estimated this quake's *magnitude at 8.1*, making it the most powerful earthquake ever to strike the nation's midsection.
- Over the next two months many more quakes, a few of them almost as powerful as the first one, shook the New Madrid region. Few buildings within 250 miles of New Madrid remained intact. The quakes reshaped the land. In places the ground was lifted. In other places it sank. Water filled the sunken areas, creating swamps and lakes, including *Reelfoot Lake* in the *northwest Tennessee*.
- The town of new Madrid was among the places covered by water. It was later rebuilt more than a mile from its former location, which now lies beneath the Mississippi River. The quakes also uprooted forests, triggered landslides, and shook bluffs into the Mississippi River. More quakes just a few months later, on *February 7, 1812*, temporarily changed the contour of the Mississippi River's bed. As a result, portions of the mighty river flowed backward for several hours.

European earthquake

Figure 90 Lisbon Earthquake, 9:30 am, Nov. 1, 1755 claimed 60,000 lives

- The earthquake, which seems to have originated on the *Atlantic Ocean seabed about 200 miles from Lisbon*, also triggered a series of *tsunamis*. *Twenty-one foot waves* sank ships and drowned thousands of people in Lisbon. Tsunamis created by the Great Lisbon Earthquake also slammed into coastal regions of Spain and Africa and even reached the islands of the West Indies which is 4,000 miles from Lisbon.
- The shaking Earth, fires, and tsunamis claimed at least *60,000 lives* and destroyed two-thirds of Lisbon. Due to uncertainties about the number of deaths from tsunamis, the toll may have actually been much higher.

How does an earthquake happen?

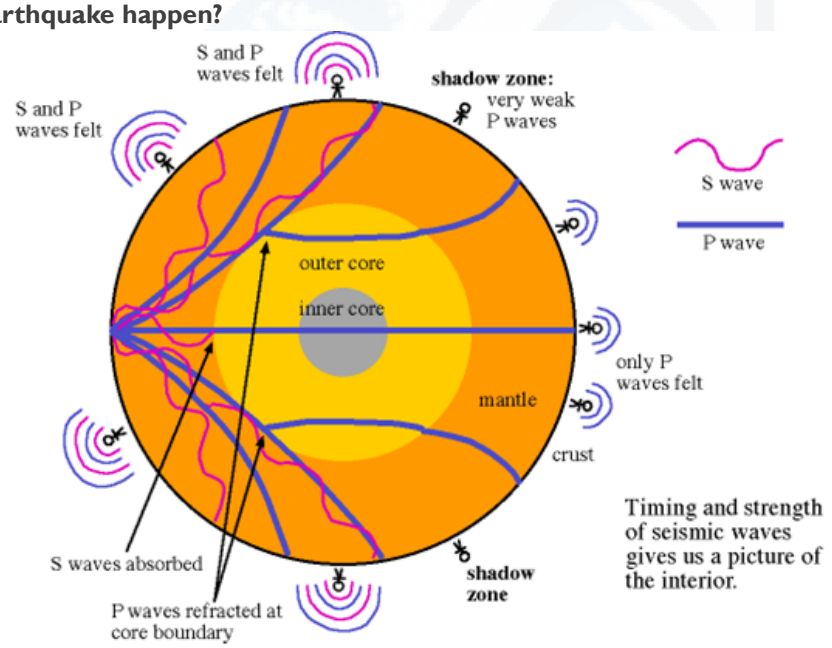

Figure 91 Gravitation waves reveal interior mass density changes (http://oregonstate.edu/instruct/oer/earthquake/04%20chapter%203_color.html)

Figure 92 Belgium Lige 8 November 1983 & Turkey 17 August 1999 Earthquakes.

As a result, the earthquake ruined the city infrastructure but killed no human live except 2.

We considered arbitrarily the Earthquake Calamity having the energy magnitude exceeding 6^{th} to 8^{th} power namely the energy strength from 1 million to 100 million, i.e. by taking the logarithmic of the Earthquake magnitude resulted in the Richter scales 6~8. This calamity is associated with pre-shocks, post-shocks, Tsunami, fires, etc. all rippling tectonic plates re-adjustment effects. We demand modern technology to provide a 97% accurate or reliable Now-Cast with few % False Alarm rate at few minutes (3~10) ahead of the event, in order to save 99% human beings life's.

Earthquake records

Here are pictures of ruins and devastation left over from strong Earthquakes.

Figure 93 From the Loma Preita Earthquake in 1989.A collapsed building destroys a car.

Figure 94 A gigantic Earthquakes in Alaska tore up road back in 2003.

Figure 95 An earthquake in Paso Robles, California caused this building to collapse into rubble.

Figure 96 Places like Hawaii has earthquakes too.This picture shows the aftermath of an office after a Hawaii earthquake.

Figure 97 Falling debris smashed this truck and made it almost unrecognizable.This is the Hanshin Awaji Earthquake in Japan.

Figure 98 Picture of Taiwan School collapsed after earthquake in 1999.

CH NI Nowcast math

Nowcast Mathematics 101:

Why rule based Artificial Intelligence wouldn't do the job?

How to capture Animal Instincts in Natural Intelligence?

The sequential *Kalman* updates mode becomes equivalence to Least Mean Square (LMS) Wiener batch average mode in case of stationary correlation. We may generalize the Wiener Auto-Regression (AR), to Artificial Neural Network (ANN) using the distributive Associative Memory. We have proved a *Lyaponov convergence theorem of ANN*. Furthermore, the *Kalman filter* becomes the *Self Organization Map (SOM) ANN*. *ANN* is generalized to an unsupervised learning by a *Higher Order of Statistics (HOS)*, such as the 4^{th} *Cumulant* called *Kurtosis*. We have proved a loss-less Divide and Conquer Theorem for Constrained Optimization so that we can split the Earth into different regions for monitoring. Then, we have introduced the *independent component analysis (ICA)* for the *blind (under-mantle heat convection) sources separation*.

i. **Wiener auto regression problem statement:** Norbert Wiener introduced the cybernetic targeting strategy for aiming an anti-aircraft gun to shot down an airplane, namely learning from past mistakes after *m* shots bullet-holes located in a time-ordered column vector $X_m(t)$, written conveniently as the transpose of a row vector:

$$X_m(t) = \{x(t),\ x(t-1),\ldots,\ x(t-m+1)\}^T \quad (1)$$

Without knowing a flying bullet aerodynamics medium transfer function, one assumes the next shot $x(t+1)$ can be predicted $u(t+1)$ by means a *stationary*, and thus *shift-invariant*, learning-weighted vector:

$$u(t+1) = w_m(t)^T\, X_m(t) \quad (2)$$

Approach: Minimize the Least Mean Square (LMS) error energy E

$$Min.\ E\ =\ Min.\ <\left(u(t+1)\ -\ x(t+1)\right)^2> \quad (3)$$

AR defined a stationary covariance as a function of the time difference only

$$C_s = < x(t)\ x(t-s) > \quad (4)$$

where by inspection of the outer-product of data vectors $< X_m(t)\ X_m(t)^T >$ was the *nonlocal* property similar to the associative distributive matrix memory. Being a fixed-point algorithm, one could apply a straightforward differentiation giving:

(ii) **Fixed-point Algorithm:**

$$dE / dw_m = \ 2 <\left[w_m{}^T X_m(t) - x(t+1)\right] X_m(t)^T >= 0 \quad (5)$$

Then, a stationary correlation function meant that was a function of the difference of two time points C_s. Thus, weight vector w_m was solved by a symmetric Toeplitz matrix inversion:

$$\begin{bmatrix} C_0 & C_1 & C_2 & \ldots & C_{m-1} \\ C_1 & C_0 & C_1 & \ldots & C_{m-2} \\ C_2 & C_1 & C_0 & \ldots & C_{m-3} \\ \vdots & \vdots & \vdots & \vdots & \vdots \\ C_{m-1} & C_{m-2} & \ldots & C_1 & C_o \end{bmatrix} \begin{bmatrix} w_1 \\ w_2 \\ w_3 \\ \vdots \\ w_m \end{bmatrix} = \begin{bmatrix} C_1 \\ C_2 \\ .C_3 \\ \vdots \\ C_m \end{bmatrix} \quad (6)$$

(iii) **Artificial Neural Nets (ANN)**

To do better than AR with intelligent approach, Minsky developed AI, while Rosenblatt and Widrow were led by biology and filter bank respectively to ANN. A straightforward extension of AR fixed point algorithm led to the ANN learning, which is supervised by $x(t+1)$:

$$dw_m / dt = -\ dE(u,\ x(t+1)) / dw_m \quad (7)$$

A classical ANN introduced an internal degree of threshold freedom for each processing nodes prosaically called the neurons. The linearity is generalized as a sigmoid squash logic function mapping thousands weighted inputs from $\pm\infty$ *to* 0 & 100 *Hz* output firing rates:

$$v(t+1) = \sigma(w_m(t)^T\, X_m(t) \cong w_m(t)^T\, X_m(t) = u(t+1), \quad (8)$$

where the sigmoid function was linear response near the threshold $\theta : y = \sigma(x) \equiv 1/[1+\exp(-(x-] \approx 0.5 + (x - + \ldots$ and monotonic *nonlinear* saturation at o and 1 away from the threshold. This function will be derived exactly for a blind singularity de-mixing from Physics-Physiology Equilibrium Principle (Szu, US PTO 7,366,564 & 7,355,182).

ANN satisfied 4 None Principles: Nonlinear, Non-local, Non-stationary, Non-programming, indicated respectively in Eqs (8,9) which had been piece-wisely implemented similar to AR. The augmented extra ability allowed ANN to solve a NP complete problem and easy generalization to solve a Higher order Statistics (HOS). The biological brain hippocampus had inspired the mathematical model of associative memory that was "read by inner product," defined conveniently by the Dirac bracket $< x \mid y >= const.$, and "write by the outer product." Biologist Donald Hebb observed the learning rule that modified the efficacy of synaptic weight matrix $[W_{x,y}]$ according to the pre-synaptic junction current firing rate x and post-synaptic junction potential value y:

$$write: \sum_{i,j=0,1,2} | x_i >< y_j | = [W_{xy}];\ \ read: Threshold\ \{[W_{xy}] | y_o >\} = | x_o >;$$

Learning was modified the impedance of the communication gaps called synaptic weight matrix $[W_{ij}]$ among neurons as our memory mechanism, and recall was taking the threshold to find out the nearest neighbor. Thus, AiTR became faults tolerant, not by two parallel feature vectors, rather by a sub-volume occupied by the feature vectors of a specific class.

Lyaponov control theorem: Given real scale energy existed for the Newtonian equation of motion:

$$\frac{dx_i}{d\tau} = -\frac{dE}{dx_i} \quad i = 1,2,3,\ldots \quad (9)$$

Proof:

$$\frac{dE}{d\tau} = \sum_{i=1,2,3,\ldots} \frac{\partial E}{\partial x_i}\frac{\partial x_i}{\partial \tau} = -\sum_{i=1,2,3,\ldots} (\frac{\partial E}{\partial x_i})^2 \le 0 \qquad \text{Q.E.D.}$$

where use was used of the fact that any quadratic real value is always positive to prove the convergence.

ANN Convergence Theorem 1: To do better than AR, ANN had generalized AR with a degree of freedom called neuronal sigmoid logic having an internal threshold ϑ_i freedom: While Hopfield modeled an i^{th} neuron *input* dynamics defined by energy E(*v*...); the sigmoid $v_i = \sigma(u_i)$; and the connectivity $u_i = \sum_j w_{ij} v_j - \vartheta_i$, Grossberg modeled an i^{th} neuron *output* dynamics by energy E'(*x*...); the sigmoid $y_i = \sigma(x_i)$; and the connectivity $x_i = \sum_j w_{ij}\ y_j - \vartheta_i$.

$$\frac{du_i}{dt} + \alpha u_i = -\frac{dE}{dv_i};$$

$$\frac{dy_i}{dt} + \alpha y_i = -\frac{dE}{dx_i} \quad (10\ a, b)$$

Proof: In terms of the integrating factor:

$u' \equiv \exp(\alpha t)u;\ E' \equiv \exp(\alpha t)E;\ y' \equiv \exp(\alpha t)y$, both proved independently the Lyaponov convergence with the sigmoid internal freedom:

$$\exp(\alpha t)\frac{dy_i}{dt} + \exp(\alpha t)\alpha y_i \equiv \frac{dy'_i}{dt} = -\frac{dE'}{dx_i};$$

$$\exp(\alpha t)\frac{du_i}{dt} + \exp(\alpha t)\alpha u_i \equiv \frac{du'_i}{dt} = -\frac{dE'}{dv_i}; \quad (11\ a, b)$$

$$\frac{dE'}{dt}=\sum_i \frac{\partial E'}{\partial v_i}\frac{\partial v_i}{\partial u'_i}\frac{\partial u'_i}{\partial t}=-\sum_i (\frac{\partial E'}{\partial v_i})^2\frac{\partial \sigma}{\partial u'_i}<0;$$

$$\frac{dE'}{dt}=\sum_i \frac{\partial E'}{\partial x_i}\frac{\partial x_i}{\partial y'_i}\frac{\partial y'_i}{\partial t}=-\sum_i (\frac{\partial E'}{\partial x_i})^2\frac{\partial \sigma}{\partial y'_i}<0 \qquad (12\ a,b)$$

Q.E.D.

iff the monotonic $\frac{\partial \sigma(x)}{\partial x}\geq 0$

(iv) **Kalman Filter and Self Organization Map:**

One could relate Kalman sequential update of a uniform-weighted average to AR approaching the Wiener matched filter as the N-batch-mode average.

Theorem 3: *Convergent Update Rule*

$$<x>_{n+1}=\ <x>_n+r(x_{n+1}-<x>_n) \qquad (13)$$

where Kalman gain $\rho=(1/n+1)$ for a uniform weight average.

Proof:

$$<x>_{n+1}=\frac{1}{n+1}\sum_{i=1}^{n+1}x_i=\frac{(n+1-1)}{n+1}\frac{1}{(n)}\sum_{i=1}^{n}x_i+\frac{1}{n+1}x_{n+1}=<x>_n+\frac{1}{n+1}(x_{n+1}-<x>_n).\quad Q.E.D.$$

This recursion formula was obviously convergent when new data became no more appreciable difference from the previous average. Such a simple concept enjoyed numerous applications, beside *Kalman filter*, e.g. in *Tuvo Kohonen self-organization map (SOM)* which was populated in A/D vector quantization, recently in the web search community for data visualization, *WEBSOM* for Genome discovery, etc.

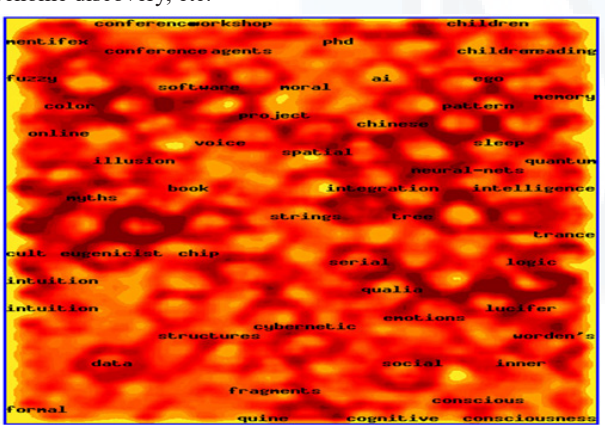

Figure 99 Websom in 2D that could have no cascade of connected homogeneous Websom s_{ij}.

ICA by Engineering Filter Approach: pixel parallelism (at Maximum Output Entropy)

Bell, Sejnowski, Amari & Oja (BSAO) have systematically formulated an *unsupervised learning of ANN algorithm for unknown but identical for space-invariant mixing* by varying the unknown de-mixing weight matrix $[W_{i.j}]$ until nothing but the Max Entropy $S(y_i)$ of the output $y_i=[W_{i,\alpha}]x_\alpha$, where $x_j=[A_{j,\alpha}?]s_\alpha?$, and the repeated Greek indices represent the summation. ANN model used a monotonically sigmoid-squashed threshold output

$y_i=\sigma(x_i)\equiv\{1+\exp(-[W_{i,\alpha}]x_\alpha)\}^{-1}$ that is nonlinear analytic solution of Riccati equation $\frac{dy}{dx}=y(y-1)$, for asymptotically binary logic $y=0 or 1$ for no or yes. Since a single neuron learning rule turns out to be massively parallel to N neurons in tensor index notion, for simplicity, we derived for a single neuron to point out why the engineering filter does not follow Hebb's synaptic weight updates. A bona fide unsupervised learning did not have a desirable specific output entropy S(y) became maximized, the de-mixing filtering $[W_{i,j}]$ becoming the inverse of unknown mixing matrix $[A_{j,\alpha}]$. Thus, the filter weight adjustment is defined as:

$$\frac{\delta w}{\delta t}=\frac{\partial S(y)}{\partial w},$$

$$S(y)=-\int f(y)\log f(y)dy\Rightarrow$$

$$\delta w=\frac{\partial H(y)}{\partial w}\delta t=\{|w|^{-1}+(1-2y)x\}\delta t\ .$$

Derivation: From the normalized probability definitions:

$$\int f(y)dy=\int g(x)dx=1\ ;\ f(y)=\frac{g(x)}{\left|\frac{dy}{dx}\right|}\ ;\ H(y)\equiv-<\log f(y)>_f\ ,$$

We expressed the output pdf in terms of the input pdf with changing Jacobian variables. We exchanged the orders of operation of the ensemble average brackets and the derivatives to compute

$$\frac{\partial H(y)}{\partial w}=\frac{\partial <\log\left|\frac{dy}{dx}\right|>_f}{\partial w}\cong|\frac{dy}{dx}|^{-1}\frac{\partial\left|\frac{dy}{dx}\right|}{\partial w};$$

Since Riccati equation was satisfied by the sigmoid: $y=[1+\exp(-wx)]^{-1}$; $\frac{dy}{d(wx)}=y(1-y)$. we readily derived by chain rule the following results

$$\frac{dy}{dx}=wy(1-y);\frac{dy}{dw}=xy(1-y).$$

Substituting these results into Max Ent learning rule, Bell-Sejnowski Eq(9):

$$\frac{\partial H(y)}{\partial w}=[W]^{-1}-(2y-1)x\quad \textbf{Q.E.D.}$$

The first term computing the inverse matrix $|w|^{-1}$ is not scalable with increasing N nodes, while the second term satisfied the Hebbian product rule between bipolar output 2y-1 and input x. S. Amari et al. at RIKEN assumed the identity $[\delta_{i,k}]=[W_{i,j}][W_{j,k}]^{-1}$ and multiplied the identity through both sides of original non-biological algorithm

$$\frac{dH}{dW_{i,j}}[\delta_{i,k}]=\{[\delta_{i,j}]-(2\vec{y}-1)\vec{y}^T]\}[W_{i,j}]^{-1},$$

where use was made of $y_i=[W_{i,\alpha}]x_\alpha$ to change the input x_j to the synaptic gap by its weighted output y_i.

Amari et al. derived a natural gradient ascend as the final BSAO algorithm in information geometry,

$$\frac{dH}{dW_{i,j}}\left[W_{i,j}\right]=\{\left[\delta_{i,j}\right]-(2\vec{y}-1)\vec{y}^T]\},$$

which was not in the original gradient direction $\frac{dH}{dW_{i,j}}$ and enjoyed a faster update without the inverse.

Fast ICA: Erkki Oja began his ANN learning of nonlinear PCA for pattern recognition in his Ph D study 1982.

$$\left\langle \vec{\tilde{x}}\vec{\tilde{x}}^T\right\rangle \hat{e}=\lambda\hat{e};$$

$$w'-w=\vec{x}\sigma\left(\vec{x}^T\vec{w}\right)\cong\left\langle \vec{x}\vec{x}^T\right\rangle\vec{w};$$

$$\frac{d\vec{w}}{dt}=\left\langle \vec{x}\vec{x}^T\right\rangle\vec{w}\cong\sigma\left(\vec{x}^T\vec{w}\right)\vec{x}\cong\frac{dK\left(u_i\right)}{du_i}\frac{du_i}{dw_i}\equiv k\left(\vec{x}^T\vec{w}\right)\vec{x};$$

where Oja changed the unary logic to bipolar hyperbolic tangent logic $v_i=\sigma\left(u_i\right)\approx u_i-\frac{2}{3}u_i^3\cong\frac{dK\left(u_i\right)}{du_i};\ u_i=w_{i,\alpha}x_\alpha$.

By derivation we obtain therefore the **BSAO** unsupervised learning collectively in a termination condition: It becomes similar to a Kurtosis slope, which suggested to Oja a new contrast function K. The following is the geometric basis of a stopping criterion of unsupervised learning. Taylor expansion of the normalization, and set $|\vec{w}|^2=1$:

$$|\vec{w}'|^{-1}=[(\vec{w}+\int\vec{x}k\left(\vec{w}^T\vec{x}\right))^T\left(\vec{w}+\int\vec{x}k\left(\vec{w}^T\vec{x}\right)\right)]^{-\frac{1}{2}}$$

$$=1-\frac{\in}{2}k\left(\vec{w}^T\vec{x}\right)(\vec{x}^T\vec{w}+\vec{w}^T\vec{x})+O\left(\in^2\right).$$

$$\vec{w}''\equiv\vec{w}'\,|\,\vec{w}'|^{-1}$$

$$=\left(\vec{w}+\in\vec{x}k\left(\vec{w}^T\vec{x}\right)\right)\left(1-\frac{\in}{2}k\left(\vec{w}^T\vec{x}\right)(\vec{x}^T\vec{w}+\vec{w}^T\vec{x})\right)$$

$$\Delta\vec{w}''=\vec{w}''-\vec{w}=\int\left[\delta_{\alpha,\beta}-w''_\alpha\,w''^T{}_\beta\right]\vec{x}_\alpha\frac{dK\left(u_\beta\right)}{d\vec{w}''_i}$$

The ICA algorithm lets the joint probability density function is factorized equally according to Max Entropy requirement of white noise. Unfortunately, such a filter approach cannot work for the remote sensing imageries, because the atmospheric turbulence changes spatially rather quickly due to a large pixel footprint which is about a tenth of a squared kilometers (Landsat 30 km^2 per pixel). If one were insisting to apply ICA to mix together all spatial (x, y) ***s***-spectral vectors data $\vec{X}_s(x,y,t)$ in parallel, the assumption of spatial invariant mixing matrix will produce inaccurate sources at the **maximum entropy (Max Ent)**. Spatial invariant assumption will not work for a close-up dual infrared spectral band image for screening for cancer, because of the localization of cancer has a strongly space-variant physiology with and without the cancer. Solving the inverse of space-variant impulse response Green's function or optical point spread function (psf) we need new MFE approach to BSS. To improve it, we have explored space invariant imaging (in terms of 3x3 macro-pixels) for macro-pixel joint density factorization ICA method; (Du, Kopriva, Szu, by Non-negative Matrix Factorization IEEE 2005; & by JADE & Fast ICA Op Eng. 2006). Then, the comparison experience help us reformulated in 2007 a nonlinear LCNN, ala KKT penalty, to regularize the linear LCNN for assuming space-invariant result within 3x3 nearest-neighbor macro-pixels per tumor cluster cells, but space-varying among macro-pixels with or without tumor.[4] In remote sensing, the Mexican standoff product challenge was overcome by the 2nd order energy expansion curvature known as KKT nonlinear optimization penalty. Typical 80 spectral band images among 158 Airborne Visible/Infrared Imaging Spectrometer (AVIRIS) (Kopriva, Szu, Fast ICA, SPIE ICA etc.2002) and corresponding BSS out of applying LCNN to 158 channels data sources maps where the color blue means no class, i.e. low probability while red means high probability.

Time reversal invariant: $m\frac{d^2x}{d(-t)^2}=m\frac{d^2x}{dt^2};\Leftrightarrow\Delta S>0$ heat death

Ludwig Boltzmann fought against debated heatedly with Mathematician Henri Poincare about the irreversibility of the universe known as the heat death, namely the irreversibility of the entropy of the universe $\Delta\boldsymbol{S}>0$. Poincare insisted the dynamics of physics is time-reversal ($t\rightarrow-t$) invariant of Newtonian equation of motion in the 2nd order acceleration in time $m\frac{d^2x}{d(-t)^2}=m\frac{d^2x}{dt^2}$.

Boltzmann argued the non-zero temperature sustain the incessant collisions among molecules toward the mixing uniformity. As such the degree of uniformity keeps increasing as the measure of entropy. Uniformity could not sustain live. Both arguments are correct on the surface. The resolution of the paradox is:

"The devil, if any, is in the details"

The dynamics is more than the equation, but the "**equation of motion**," that requires the integration of trajectory involving the **initial boundary condition.**

$$\int_o^{t'}Fdt=\int_0^{t'}m\frac{d^2x}{dt^2}dt=m\frac{dx}{dt}\Big]_0^{t'}=mv(t=t')-mv(t=0)$$

The integration involves the irreversible molecular collision mixing toward more mixing uniformity $\Delta S>0$ *heat death*, that can never reproduce identically in repeated experiments. As such, the time reversible invariant could no longer be true in the integration of equation of motion.

On Sept. 5, 1906. Age 62. Boltzmann committed the suicide for his belief in science, as such without name on his tombstone to dishonor his family; but there is the inscription of the famous debate about the entropy S= K ln W cf. Fig 11(a).

$$S=k_B\,Log\,W;or,W=\exp\left(\frac{S}{k_B}\right);\Delta S>0\,heat\,death;$$

to differentiate true sources from clutters and noise. H is isothermal T_0 =contant thermodynamic Helmholtz free energy to be defined in terms of Boltzmann molecular entropy S and the internal energy E to be minimized.

Min. $H=E-T_oS$

A massively parallel collective NI is robust. The mathematics of NI operated at isothermal equilibrium for de-clutter & noise threshold.

The math principle based on the equilibrium that everything will be naturally driven toward the equilibrium at constant temperature to a maximum entropy heat death.

Prof. Ludwig Boltzmann of Vienna laid down the foundation of molecular physics Statistical Mechanics with Maxwell circa 1844.

What's the entropy? It is the degree of uniformity.

The irreversible thermodynamics that an isolated system the total entropy is always increase due to collision mixing toward uniformity.

$\Delta S > 0$,

where the degree of uniformity is called the ***Entropy S:***

$S = k_B Log\ W$ The thermodynamic equilibrium principle is always at the minimum free energy derived by Helmholtz from the Boltzmann entropy formula considering a **sub**system in contact with a heat **res**ervoir

$$W_{res} W_{sub} = \exp\left(\frac{\boldsymbol{T_o S_{res}} + \boldsymbol{T_o S_{sub}}}{k_B \boldsymbol{T_o}}\right) = \exp\left(\frac{-\boldsymbol{E_{sub}} + \boldsymbol{T_o S_{sub}}}{k_B \boldsymbol{T_o}}\right) \equiv \exp\left(-\frac{H_{sub}}{k_B \boldsymbol{T_o}}\right)$$

Since Boltzmann assertion of the heat death is due to non-zero temperature (Neal's 3rd law of thermodynamics) generating a nonstop collisional mixing increasing the degree of uniformity to the heat death: $\Delta S > 0$, then the "negate of the converse" is true: $-\Delta S \le 0$. Use is made of the energy conservation law, the thermal energy of the reservoir $\boldsymbol{T_o S_{sub}}$ is flowed to the internal energy of the subsystem $-\boldsymbol{E_{sub}}$:

$\Delta H_{sub} \equiv E_{sub} - T_o \Delta S_{sub} \le 0$;

$\Delta H \equiv \frac{\Delta H}{\Delta \vec{S}} \Delta \vec{S} = \vec{\mu}\left([W]\vec{X} - \vec{S}\right) \to 0$;

We assume a linear unknown impulse response system of the input vector time series, and the inverse by the unsupervised learning matrix:

Since $\vec{X} = [A]\vec{S}$, then $[W]\vec{X} = \vec{S}$.

The weight matrix [W] defines NI Artificial Neural Network which can be adjusted to reach the thermodynamic equilibrium by minimize the Helmholtz free energy. We derived the Natural Intelligence Hebb learning rule of input and output in bi-linear product between the sensor input vector time series $\vec{X}$ .at neuron nodes and housekeeping output servant glea cells driven by the free energy slope $\vec{\mu} \equiv \left(\frac{\Delta H}{\Delta \vec{S}}\right) : \frac{\Delta H}{\Delta [W]} = \vec{\mu}\vec{X}$,

To be explicit for remote sensing, we considered 3 kinds of identical entities; R denotes the number of red balls/molecules/photons, likewise G & B in a closed system. Thus, the chance of realizing total N balls is $N!$ divided by identical colors $R!G!B!$, because of the over-counting of permutations with identical particles.

$$\boldsymbol{W} = \frac{\boldsymbol{N!}}{\boldsymbol{R!G!B!}} .$$

Sterling approximation of logarithmic factorial was valid when $N > 10$.

$Log\ N! \cong N\ Log\ N - N$; $N/N = R/N + G/N + B/N; 1 = S_1 + S_2 + S_3$

Then, Boltzmann discrete entropy formula follows:

$$S = -K_B \sum_{i=1}^{K} S_i Log\ S_i - const.\ (\sum_{i=1}^{K} S_i - 1);$$

$$const. = \frac{\boldsymbol{i}_o}{T_o} - \boldsymbol{K_B}$$

where the minus sign was derived due to $Log\ S_i \le 0$ for $S_i \le 1$ and the Lagrange scalar constraint of the probability norm $\sum_{i=1}^{K} S_i - 1 = 0$ was chosen to be $\left(\frac{\mu_o}{T_o} - \boldsymbol{K_B}\right)$ that insured the normalization and a simple slope:

$$\frac{\partial S}{\partial S_i} = -\boldsymbol{K_B}\left(1 + \sum_{i=1}^{K} \log S_i\right) - \left(\frac{\mu_o}{T_o} - \boldsymbol{K_B}\right) = -\boldsymbol{K_B} \log S_i - \frac{\mu_o}{T_o}$$ Q.E.D.

The maximum entropy in a closed system corresponds to the minimum free energy in open sub-systems.

Finally, we must know Natural Intelligence (NI), not the rule-based AI to be incorporated in Smartphone. NI is an animal brain-style computing, a hybrid of Algorithm with Architecture in "Algo-tecture, or Archi-rithm," giving a fast and robust Nowcast capability. Every Smartphone, equipped with MEMS/IMU adopted in every airbag, could behave like a Smart neuron, operated at equilibrium thermodynamics at a constant temperature. Synergistically, the temperature helps the hemoglobin with an optimum elasticity squeezing through the narrow channel of capillary, generates a fixed kinetic transport of nutrients among neuron house-keeping 10 billion servant glea cells, one servant cell per a neuron decision cell, the so-called "missing half" of Einstein brain.

When being bombarded by large meteorites upon the earth crust instability, the rounded crust has been further broken apart from the historically dozen major tectonic plates to 15 pieces plus 30 or so minor pieces. Nevertheless, those tectonic plates can still confine those bubbling molten rock underneath, but generating the punctuated earthquakes. Especially, when the up dwelling happens in the middle of the plate, the earthquake could be catastrophic than those smaller adjustments near the boundaries among clashing neighborhood plates. The Earth consists of three components: crust, mantle and core. The crust is a solid thin shell of rocks. Under the crust, there is a mantle of melted rocks. Then the core is a mostly iron fireball, which produces geomagnetic field. In the mantle, temperature and density vary. The mantle currents will create convection stresses under the crust. Mantle current swells up if its temperature is high and density is low. It swells down if its temperature is low and density is high. This is the well-known mantle convection phenomenon. In fact, the mantle convection is the cause of relative tectonic plate displacements and earthquakes.The up swelling mantle currents will cause tensile stresses in the crust. The down swelling mantle convection currents will cause compressive stresses in the crust. The concentrations of these stresses may fracture the fault systems in the crust, and the sudden release of these stress concentrations will initiate earthquakes. Thus, a necessary condition for earthquake occurrence is the energy source building up the stress concentrations in the crust.

While satellite is above the up swelling mantle convection current, it will jump up as gravity decreases due to higher temperature and lower density of the hotter mantle rocks. While satellite is over the down swelling mantle convection current, it will sink towards the Earth as the gravity increases due to lower temperature and higher density of the colder mantle rocks. Thus, satellite orbital variations are directly related to the patterns of mantle convection in the interior of the Earth. In this way, we can trace patterns of mantle convection directly by tracking the changes in satellite orbit, and search for the power origin of earthquakes called blinded source separation (BSS). One discovers the mantle convection as the power origin causing the seismic stresses in the

crust. The satellite detection of stress concentration locations in the crust may provide a necessary condition for prediction.

CH Orbital Dynamics

On the other hand, satellite detection of the convection generated stresses in the interior of the Earth has a history in space and Earth sciences. It has been one of the most important Earth research program since the beginning of the space age. This program is applicable for identification of the forcing mechanisms for uplift, depression, rifting, volcanism, seismicity, plate motion, kimberlitic magnetism, ore formation, and hot spots distribution on the surface of the Earth.[8–24] Specifically, it has been shown that distribution of the 450 principle metal deposits in Africa is restricted in the tensional stress system and all ore deposits are clustered in areas of the uplifted old rocks, indicating that metal deposits of all ages in Africa were exposed by stress induced uplift.(Figure 8). In addition, it has been demonstrated that the compressive and tensional stresses in the global stress concentration belts are the triggering stresses for the 131 Ms>7.0 earthquakes from 1977 to 2000.(Figure 9). Most importantly, the gravity-stress theory in the space program have successfully explained and predicted the origin and precursors of the three interpolate earthquakes, i.e., the 1976 Tangshan earthquake in China, the 1983 Liege Earthquake in Belgium, and the 1993 Latur Earthquake in India.

As for the fundamental problem in the tectonic plate theory, the satellite determined stress field due to mantle convection has provided a scientific explanation for the original fracture of the outer-crusted shell of the Earth. It was predicted in 1974 that the crust under the India Ocean could be fractured.[8] After the 9.2 Sumatra tsunami Earthquake in 2004,the crust under the India Ocean did crack about 1600 Km in length. This was the first natural test, which verified the gravity-stress theory.

The harmonic coefficients $C_{n,m}$ and $S_{n,m}$ of the gravity field in equations 2 and 3 have been significantly improved in 2006 by satellite observations. The harmonics for $13 < n < 360$ may reflect a small-scale mantle flow system. This set of the improved satellite gravity data is accurate enough to identify the locations of stress concentrations in the Earth. In 2006, satellite gravity scanning of the crust under China discovered that stresses had concentrated under the crust of the province of Sichuan. Two stress maps under Sichuan are shown in Figure 23 & 24.

The relation between stress distribution and geological structure is defined as follows: the crusted region with even and smooth stress distribution is geologically stable. However, crusted region with stress concentrations is termed as a geological tumor. The geological tumor is benign if the stress concentrated region does not consist of fault or crack systems. The geological tumor is malignant if the stress concentrated region consists of fault or crack systems. Fracture of rocks in the malignant geological tumor due to stress concentrations is the cause of earthquakes.

Moreover, we show the desirable spherical orbit of a proof mass m is more an accident than a norm and is difficult to maintain under the Earth mass M perturbation $2H^2E/m\gamma^2M^2 = -1$ where H is the invariant angular momentum per unit mass m. As such during the space measurement the covering footprint on the earth along the radius directions may vary in an elliptic orbit from that a circular one. However, the Kepler 2nd law may save us from the variability if we choose fixed time interval integration. This will be important to design the space measurement program.

The complexity of the real world satellite or proofing IMU mass orbit, mainly due to the non-spherical Earth and time-dependent convection of molten rock having heterogeneous layers: solid crust, molten mantle, and fireball magnetic field core. We recommend the complexity may be circumvented by a set of distributed measurements of a set of IMU proofing masses embodied in the MEMS in the Space Station and Satellite. Thus, a local mass perturbation network approach is taken as in-situ calculation.

$$M_o = \int (\rho_{III}(\vec{r}) + \rho_{II}(\vec{r}) + \rho_I(\vec{r}))d\vec{r}\ ;\ \Delta M(t) = \int \tilde{\rho}_{II}(\vec{r},t)d\vec{r}$$

All these are merely suggestive possibility for a network of several IMU/MEMS proofing masses on the Space Station to map out this important potential in the Space demonstrated by the first author and others. Such a distributive network calculation for solving the ill-posed inverse sources problem, called Blind Source Separation (BSS), may require modern mathematics of prediction by a vector time series, which is itemized in Sect 3 for the convenience of geologists and space scientists.

To study the gravitational fluctuation of molten rock at the Earth mantel, we have recapitulated NASA early work on board of the Space Station the IMU/MEMS proofing mass. We wish to point out few important facts by means of the point mass approximation helping the design of new experiments in terms of proofing mass IMU/MEMS at the International Space Station. In our application, the Earth m_1=M, and the satellite or IMU proofing mass m_2 = m. While the m is invariant; but the M varies $M' = M_o + \Delta M$ perturbs consequently $r = r_o + \Delta r$. We will prove several useful design *Theorems*. For example, the proofing mass has nothing to do with its radial orbit, which governs the invariant angular momentum and the mass of the Earth. This is because of the central radius inverse square force law discovered by Isaac Newton

$F = \gamma m_1 m_2 / r^2$, where $\gamma = 6.67x10^{-8}\, gm^{-1}cm^3\sec^{-2}$.

We observe first of all that the invariant proofing mass $m_1 = m$; disappears explicitly from both sides of the Newton equation of motion, and there remains $m_2 = M_\oplus$ of Earth.

$$m\ddot{\vec{r}} = -\gamma \vec{r} m M_\oplus / r^3\ ;\ \ddot{\vec{r}} = -\gamma \vec{r} M_\oplus / r^3$$

Due to the Smartphone and the payload limitation in the Space Station, this fact may work out to our favor of not only increase the sensitivity but also the robustness by using a network approach of MEMS. We find

Theorem 1 any size of proofing mass in the IMU/MEMS can measure the perturbation of the Earth mass

$M' = M_o + \Delta M$.

In the process, we have reproduced

(i) the first Kepler law namely an ellipse orbit and more,

(ii) the second Kepler law: the angular (area) momentum preserving, a

(iii) the third Kepler law that the 3rd power of the semi-major axis is related to the periodicity T: $(a_1/a_2)^3 = (T_1/T_2)^2$ applicable for two proofing masses (or satellites, or nine planets in the solar system).

Following a consistent "dot notation" for time derivative, we begin the spherical coordinate system and compute the first and second derivatives:

$$\dot{\vec{r}} = \dot{r}\hat{1}_r + r\dot{\phi}\hat{1}_\phi;$$

$$\ddot{\vec{r}} = (\ddot{r} - r\dot{\phi}^2)\vec{1}_r + (2\dot{r}\dot{\phi} + r\ddot{\phi})\vec{1}_\phi = -\gamma M/r^2\vec{1}_r \ ;$$

this yields from (ii) the Newtonian equation of motion the angular momentum Kepler 2nd law:

$$r^2\dot{\phi} = \mathrm{H};$$

$$\dot{\phi} = \mathrm{H}/r^2 \ .$$

where the H denotes the angular momentum per unit mass.

Of course, the period of the satellite is governed by (iii) the Kepler 3rd law that is $T_1/T_2 = (a_1/a_2)^{3/2}$ for two proofing masses, or two planets, or two satellites in one dominate mass gravitational field(either Earth or Sun or combined). To demonstrate more details, this conservation law of angular momentum, given (ii) the Kepler 2nd law: sweeping equal area per equal time can help us measure the earth mantle convection dynamics and also the change of the dynamic variable from time to angle

$$d/dt = (d\phi/dt)d/d\phi = \mathrm{H}u^2 d/d\phi,$$

where

$$u \equiv 1/r \ .$$

$$dr/dt = (dr/du)(du/dt) = (-1/u^2)(\mathrm{H}u^2 du/d\phi) = -\mathrm{H}du/d\phi$$

$$d^2r/dt^2 = d(-\mathrm{H}du/d\phi)/dt = -\mathrm{H}^2u^2d^2u/d\phi^2 \ .$$

Setting $w \equiv u - \gamma M/H^2$, we obtain the Kepler equation of motion

$$d^2w/d\phi^2 = -w \ . \ w = A\cos(\varphi - \varphi_0)$$

To show explicitly the Kepler orbits we have $1/r = A\cos(\phi - \phi_o) + \gamma M/\mathrm{H}^2$.

Let $A = \varepsilon\gamma M/\mathrm{H}^2$.

Then $r = (H^2/\gamma M)/(1 + \varepsilon\cos\varphi)$

when compared with a conic orbit $r = a|\varepsilon^2 - 1|/(1 + \varepsilon\cos\phi)$, we have the semi-major axis $a \equiv H^2/\gamma M|\varepsilon^2 - 1|$ that an elliptic orbit if $0 < \varepsilon < 1$; or a desirable circular orbit if $\varepsilon = 0$; or, like a passing comets, unbounded as a parabola if $\varepsilon = 1$; or hyperbola if $\varepsilon > 1$.

The time covered by the radius r in dt time is the infinitesimal triangle $(rd\phi \bullet r)/2$ of which per time is $(r(d\phi/dt) \bullet r)/2 = H/2$, thus, the total time $T \bullet H/2 = \pi ab$ covers the full ellipse of area πab , where $b = a\sqrt{1-\varepsilon^2}$. (iii) Therefore the Kepler 3rd power Law of the total period $T^2 = (4\pi^2/\gamma M)a^3$ drops out from: $T = (2\pi a^2/H)\sqrt{1-\varepsilon^2}$ after the squaring and substituting $a \equiv H^2/\gamma M|\varepsilon^2 - 1|$.

The orbital shape constant ε is determined by the conservation of energy:

$$E = (m/2)(\dot{r}^2 + r^2\dot{\phi}^2) - \gamma mM/r \ .$$

We can choose the x-axis as the closest distance to the Earth, where

$$\dot{r} = 0, \cos\phi = 1, \ or \ \phi = 0 \ .$$

Remembering the orbital equation and conservation of angular momentum, we have

$$E = (m/2)(\gamma^2M^2/H^2)(\varepsilon^2 - 1) = -(1/2)\gamma Mm/a \ .$$

Solving for ε , we have $\varepsilon = \sqrt{1 + (2H^2/m\gamma^2M^2)E}$. In fact, we know when the eccentricity $\varepsilon = 0$ we have an ideal spherical orbit if $(2H^2/m\gamma^2M^2)E = -1$.

Theorem 1: The orbital eccentricity shape ε is independent of the proofing mass.

Proof: We have shown $\varepsilon = \sqrt{1 + 2H^2E/m\gamma^2M^2}$ and the energy $E = -\gamma Mm/2a$, then substituting the energy we have the proofing mass cancelled $\varepsilon = \sqrt{1 - H^2/\gamma Ma}$ .Q.E.D.

Therefore, the shape is locally irrelevant to the proofing mass but the Earth mantle mass change according to the Newton's attraction force law at central radius.

Theorem 2 corollary: The orbital perturbations, generating by the Earth mass

$M = M_o + \Delta M = M_o(1 + \Delta M/M_o)$ being non-relativistic scalar can be only along the radius direction.

Proof: Given the radius dynamics $\ddot{r} = -\gamma M/r^2 + H^2/r^3$, where H is the invariant angular momentum per unit proofing mass. Applying the linear perturbation theory to the orbital $r = r_0 + \Delta r = r_0(1 + \Delta r/r_0)$, and obtain a pair of equations

$$\ddot{r}_o = -\gamma M_o/r_o^2 + H^2/r_o^3 \ ;$$

$$\Delta\ddot{r} = -(\gamma M_o/r_o^2)(\Delta M/M_o - 2\Delta r/r_o) + H^2/r_o^3(-3\Delta r/r_o) \ . \ Q.E.D.$$

Theorem 3: Fixed time interval integration can give orbital-invariant measurement of the dynamics of convection mass perturbation over time.

Proof: Fortunately the Kepler 2nd law, saying that the orbit weeping equal angular area in equal time, suggests a time integration methodology of fixed time-interval for the dynamic mantle convective mass perturbation over time, since an equal coverage of earth surface area in equal time for whatever conic shape of the specific orbit may be. *Q.E.D.*

Moreover, we show the desirable spherical orbit of a proof mass m is more an accident than a norm and is difficult to maintain under the Earth mass M perturbation $2H^2E/m\gamma^2M^2 = -1$ where H is the invariant angular momentum per unit mass m. As such during the space measurement the covering footprint on the earth along the radius directions may vary in an elliptic orbit from that a circular one. However, the Kepler 2nd law may save us from the variability if we choose fixed time interval integration. This will be important to design the space measurement program.

The complexity of the real world satellite or proofing IMU mass orbit, is mainly due to the fact of non-spherical Earth and time-dependent convection of molten rock (having heterogeneous layers: solid crust, molten mantle, and fireball magnetic field core). A set of distributed measurements of a set of IMU proofing

masses embodied in the MEMS can circumvent the complexity in the Space Station and Satellite. Thus, we take a local mass perturbation network approach as in-situ calculation.

$$M_o = \int (\rho_{III}(\vec{r}) + \rho_{II}(\vec{r}) + \rho_I(\vec{r}))d\vec{r} \; ; \; \Delta M(t) = \int \tilde{\rho}_{II}(\vec{r},t)d\vec{r}$$

All these are merely suggestive possibility for a network of several IMU/MEMS proofing masses on the Space Station to map out this important potential in the Space demonstrated by the first author and others.

Orbital Dynamics Could Monitor Natural Underground Mineral Resource. For example, Africa is vast and difficult to cover.

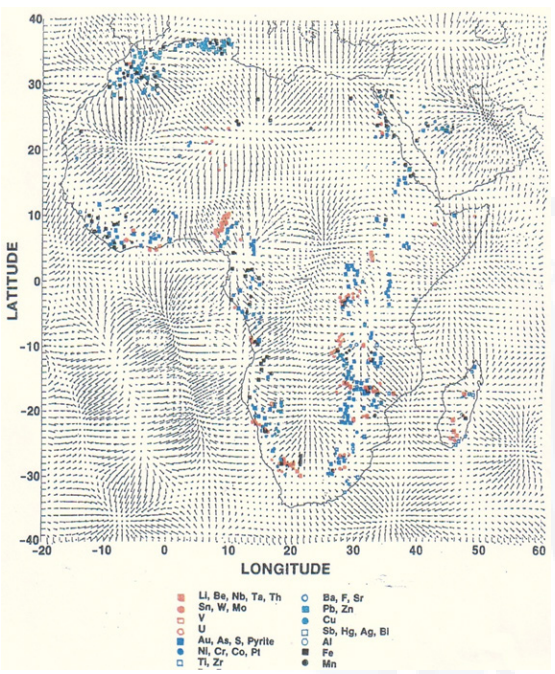

Figure 100 The 450 Principal ore deposits in Africa are clustered and exposed by the tensional stress regimes in the crust.

Appendix A

Facts About the Richter Scale

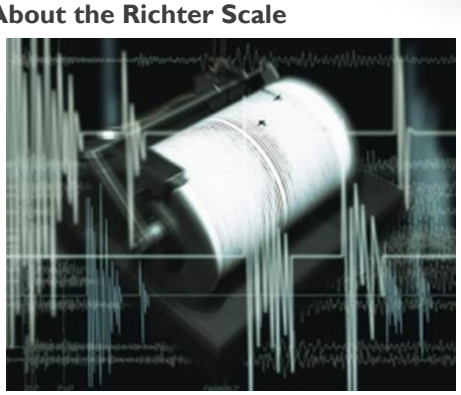

Fig. 55. Richet Scale Instruments

- In 1935, Charles Richter found a way to measure earthquakes using a machine called a seismograph. It draws wiggly lines to show how much motion happens during an earthquake. Richter gave each quake a number with a 1 being very weak and 7 and over being strong. To this day, seismologists still use the Richter scale to measure an earthquakes power.
- The numbers below shows how the magnitude and the intensity of earthquakes are related.
- 1-2. Shaking is rarely felt by people.
- 2-3. Only people at rest feel the shaking, especially if they are on the upper floors of a building.
- 3-4. Many people indoors feel the shaking, but most people do not recognize it as an earthquake.
- 4. Most people indoors and some outdoors notice shaking. Dishes, windows, and doors rattle. Walls creak. Parked cars rock.
- 4-5. Felt by almost everyone. Many sleeping people wake up. Liquid splashes out of glasses. Small objects are knocked over. Some dishes and windows break.
- 5-6. Felt by all. People have trouble walking. Some heavy furniture moves. Dishes break, and pictures fall off walls. No damage to buildings.
- 6. People have trouble standing. Furniture breaks. Plaster and bricks may crack and fall. Noticeable waves on ponds. Church bells ring. Considerable damage to poorly built buildings.
- 6-7. People have trouble driving cars. Walls, chimneys, and tree branches break and fall. Some poorly built buildings may collapse. Tall structures may twist and fall.
- 7. People panic. Underground pipes may break, and well-built buildings are considerably damaged. The ground may crack.
- 7-8. The ground cracks. Water splashes over the banks of rivers and canals. Railroad tracks bend.
- 8. Highways, railroads tracks, bridges and underground pipelines are destroyed. Most buildings collaspe. Large cracks appear in the ground.
- 8 or greater. Destruction of buildings and transportation systems. Almost everything is destroyed. The surface of the ground moves in waves or ripples. The ground is covered with cracks and holes.

Appendix B

WHAT TO DO IN THE EVENT OF AN EARTHQUAKE

Having knowledge beforehand is the "Smartphone Nowcast" best way to prepare for an earthquake. Here are some easy things to remember when you feel an earthquake happening.

- If you are outside, move *away from power lines, trees and buildings*.
- If you are inside, stay *away from windows, mirrors cupboards, and shelves.*
- Take cover *under a sturdy table or desk. Hold on to*
- You can also *stand under a doorway, they are one of the strongest foundations of a house*.
- Be prepared for *possible shaking after the quake*.
- If you are in a *high building, stay out of the elevators and stairways*.
- A family can prepare for an earthquake by having *flashlights, helmets and sturdy shoes, a first aid kit, a fire extinguisher, bottled water, canned food and a can opener.*
- *Stay calm*.
- *Routine store fresh water, safe flash light, no candle and matches, 1st aid medical box,*
- *Smartphone with Nowcast capability*

Appendix C Power point presentation

(BDA ≥ LDA) Nowcast for Earthquake Calamity defining Animals Survival Natural Intelligence (NI ≥AI)

Harold H. Szu, CBA

Research Ordinary Prof, Cath U Am, Wash DC (http://biomedical.cua.edu/faculty-staff/index.cfm); Army Night Vision Ft. Belvoir VA
Fellows IEEE, INNS, AIMBE, OSA, SPIE, & Foreign Academician of RAS
Chair SPIE Conf. (Orlando 1996 to Baltimore 2016) (http://www.ica-wavelet.org);
trained 16 Ph D students (http://www.mathgeneology.org/harold_szu)

Talk Outline: in the spirit of "In God, We Trust; All the Rest, Show Data"

Sect. I. The origin of Earthquakes came from Big Bang energy-mass Condensation by Higgs mechanism to generate the Planet Earth, that made the Earthquakes inevitable;

Sect. II. 3 Models of Earthquakes: (1) Forecast "Continental Drift," (2) Forecast "Tectonic Plates," (3)Now-cast "Cooking Pot Dynamics" characterized iff Singular Stress-Faulty Cracks (SS-FC)(Pat.7,366,564, 4/29/08);

Sect. III. Forecast No Use, because life must go on; Exemplars (III.1) US, (III.2) China, (III.3) Indonesia, (III.4) Italy Pompeii. All point to learn Animal's survival instincts, as basis of NI) ;

Sect. IV. Nowcast with Smartphone to save life just a few minutes ahead;

Sect. V. Nowcast needs (1) Smartphone/IMU (2) BDA Ultra-spectral Remote Sensing, (3) Adaptive Super-Mother Wavelets Pre-processing, (4) Relational Databases Hetero-Assoc Memory (HAM).

Sect. VI. Conclusion:Japan has Smartphone;didn't Nowcast Tsunami Fukushima 3/11/2011 Nuclear Meltdown

Appendix A: "*Nowcast Earthquakes by Smartphone's*" (*Free Down Load*) "Educated Public is the best Consumers."
Appendix B: "Nowcast of natural resource and calamity warning." Harold Szu US PTO 8392122 B2; Pat. No. 7,366,564 (date Apr. 29, 2008 before Sichuan Earthquake May 12-15, 2008) published by Oct. 28, 2010.
Appendix C: H. Szu & H.S. SPIE Conference in Orlando April 2008 (Proc. of SPIE Vol. 7343 2009).

Sect. I Why 10 D. Universe to Planet Earth?

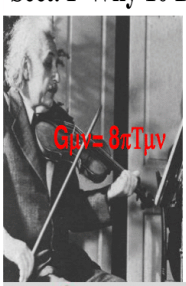

Einstein General Relativity 1916, "info takes time C_o = 3 10^8m/sec". How many d.o.f. in our Universe ? *10D= 4 Lorentz*($\vec{x}$, C_ot) + *4 Maxwell* (2s+2c) + *1 Einstein, special* E=mC_o^2 +*1 Strong Yukawa*, +*1 weak Fermi* = *10 d.o.f.* (cf. "Elegant Universe," by Greene)

Centenial Celebration of Einstein Gravitation Wave

detected by *"Colliding Black Holes"* (cf. Alan Weinstein, Nat'l Ctr. for Supercom Apps, Caltech *AJW, CERN, July 14, 2004*)

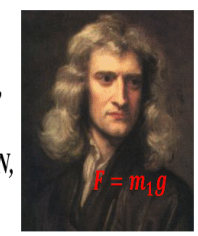

Newton's Theory takes no time Instantaneous action at a distance $g = G\frac{m_2}{R^2_{1,2}}$

GW from Supernova collapse 1/50 yr our galaxy 3/yr Virgo cluster)

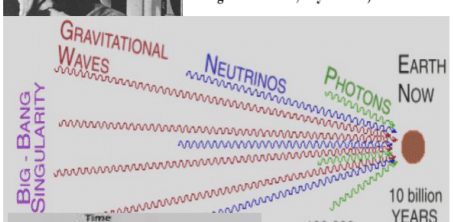

Co-Incident Accounts(CIA) from Livingston New Orleans to Hanford Oregon: by colliding black holes travelled billions light-years. looping around in the geodesic arc with repetition sound 343.2m/sec.

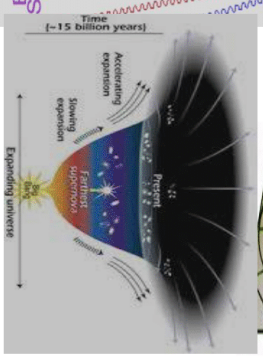

Einstein symphony "bip bip" as black hole object spiral into another until they finally coalesce

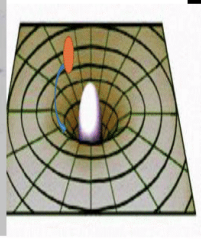

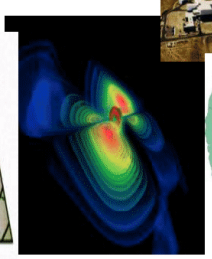

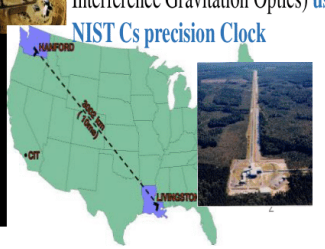

NSF 1995 $360M LIGO(Laser Interference Gravitation Optics) use NIST Cs precision Clock

Expanding Universe after Big Bang generated Gravitation Waves and the curvature warp led to mass condensation cool down to the planet Earth formation:. (1) light matter & (2) dark matter & dark energy (due to Fermi N→ $p^+ + e^- + n$ in 14 min , no neutrons forming no nuclei attracted no electrons with orbital transitions for light production). 2013 Nobel Laureates Peter Ware Higg's boson condensation for spontaneous mass formation (U. Edinburg) by Nambu-type spontaneous symmetry broken (God's particle naming displeased atheist PW Higg)

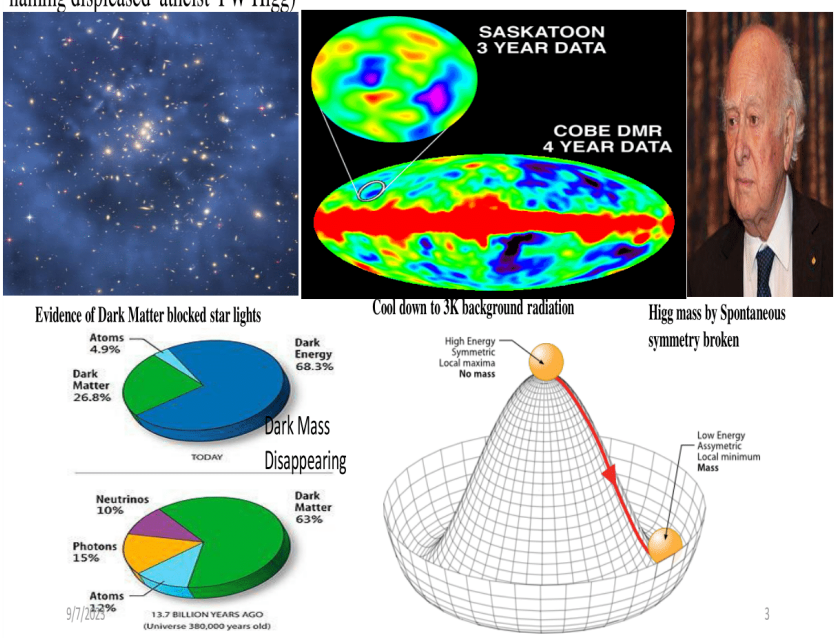

Earthquakes are inevitable because of molten iron core formation mental I. II, III layers, **after the Big Bang Expanding Universe, supported Szu's "cooking pot" Nowcast model with Necessary Conditions: Stress Singularity; Sufficient Conditions: Fault Cracks (Szu, US PTO: Pat.7,366,564, 4/29/08);. Under Ground dynamics**: (1) **convergent** push in; (2) **divergent** out; and (3) **transform slide-pass**. The lateral movement of the plates is at speeds **8.50 cm/yr**. The end of a black hole is (1) colliding another bigger black hole, (2) until big bang GW re-birth.

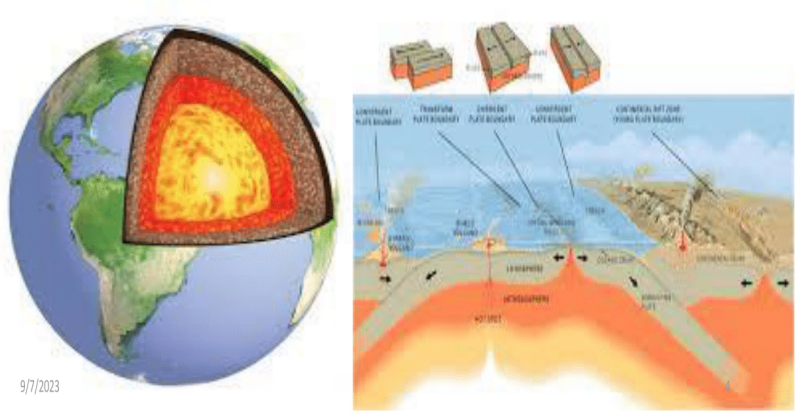

Sect. II. All Forecast Models of Earthquakes are no use if too much ahead as life must be going on; Nowcast tenth minutes ahead can save life:

(1) Continental Drift Model(2) Tectonic plates model ; The map shows 13 major tectonic plates, & 30 fragmented minor plates (http://www.crystalinks.com/platetectonics.html)

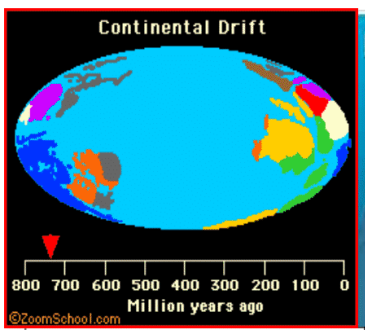

200 million years ago all of the present-day continents combined to form a single supercontinent called Pangea.

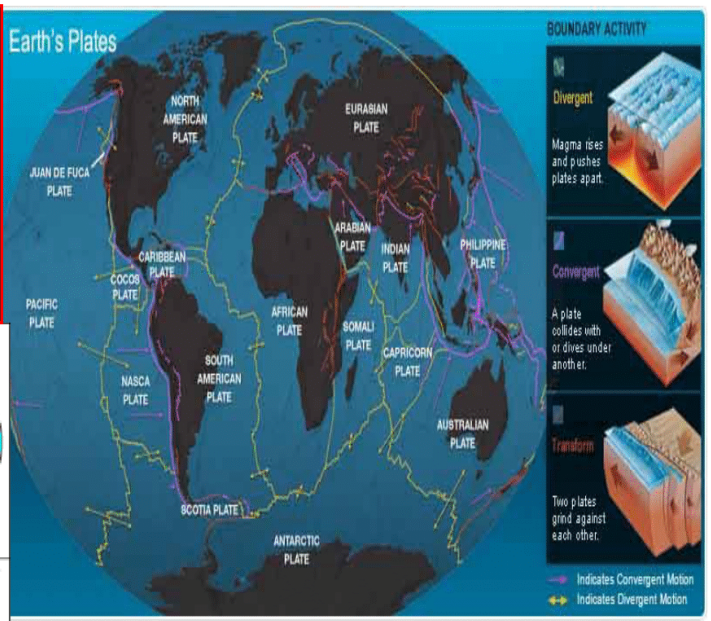

5

Szu's Cooking Pot Dynamic Model of Earthquakes, beside "Continentals Drift" to "Tectonic Plates" forecasted Sichuan May12-15, 2008 one Month ahead; but in vain. The Landsat revealed the necessary condition of stress concentration, and the sufficient conditions of faults or cracks.(Szu & Liu SPIE Aerosense Symposium "ICA, AWT etc. Conf. April 2008, Orlando), SPIE Proc. V.7343, 2009 (attached in Appendix C).and US Patent Disclosure April 2008 (attached in Appendix B). NASA Satellite (Landsat) gravitation measurements on Three Gorges Dams 2006, detected abnormal stress Saddle Point Singularity at (31N, 103E) less gravity at upstream Gold Sand due to upwelling molten rock with less mass density, much more gravity at downstream due to 3 Gorges Dam.

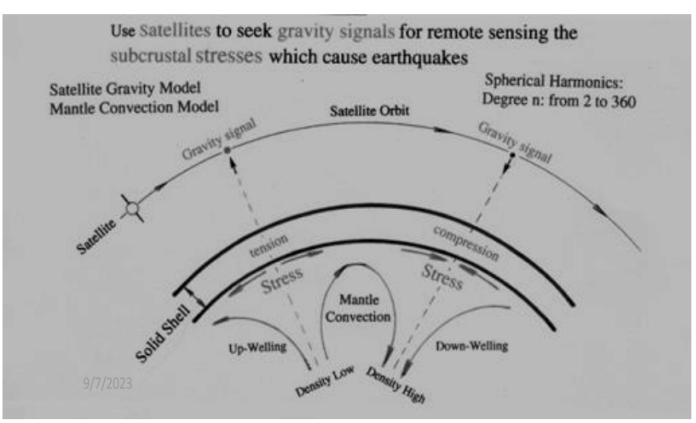

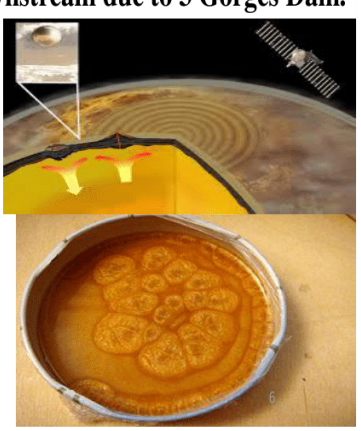

Sect. III Forecast No Use, as life must go on:

Exemplars (III.1) US **San Francisco 5:12 am, April 18, 1906; Fire burned 3 days; claimed 3,000 lives**. Recurrent at 24 years cycles: last one 2004+24-2016=12 years later at 2028

(III.1) San Francisco Test Bed indicating the top tower has better SNR of Seismic waves than the ground floor

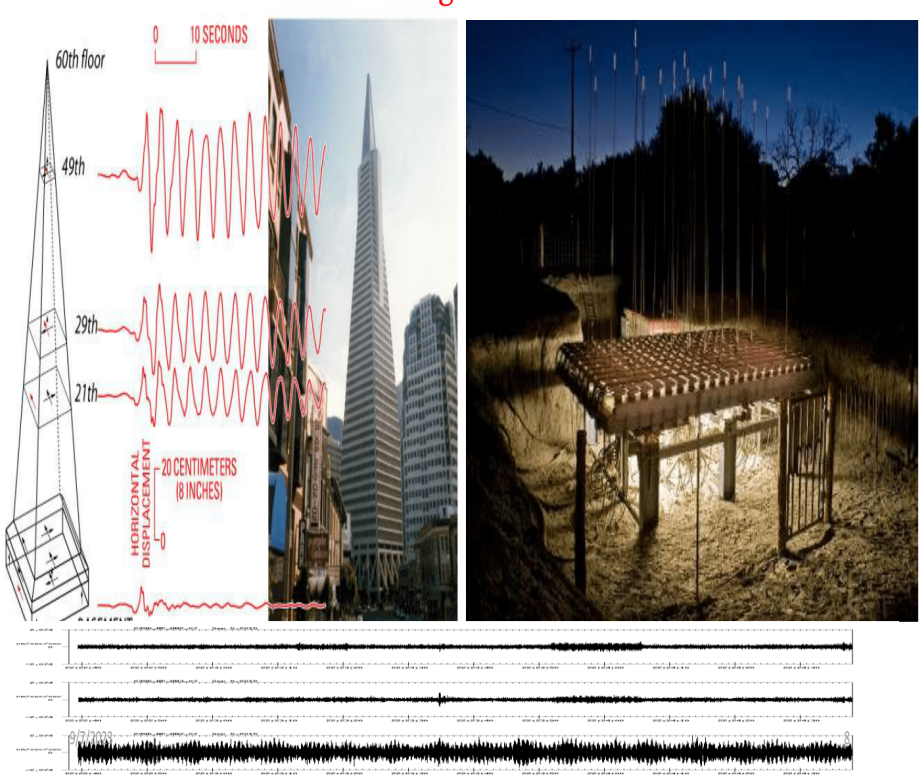

(III.1) San Andreas Fault California looking the North. San Andreas Fault near Parkfield California about 800 miles long suffered periodically large earthquake at Richter scale 5 and beyond. *<1857, 1881, 1901, 1922, 1934, 1966, 2004>=(24 , 7).*

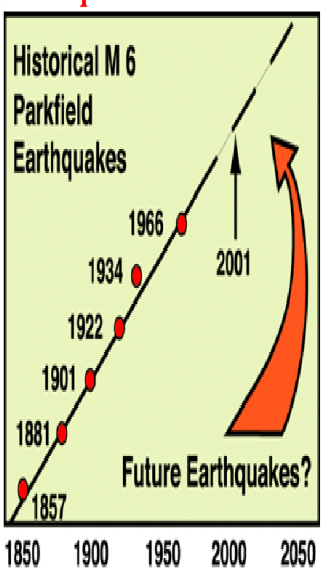

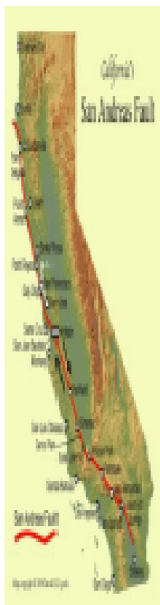

Parkfield San Andreas Fault in 1857, 1881, 1901, 1922, 1934, 1966, and 2004. Recordings of the east-west component of motion made by at DeBilt,Netherlands. 1922 (in black) and 1934 and 1966 at Parkfield (in red) are identical ruptures with some regularity (mean about 22 year) on the fault. (see Bakun and Lindh, 1985 and Bakun and McEvilly, 1979)

(III.2) 8 years ago nightmare, 80,000 deaths on May 12-15, 2008

(III.2) Three Gorges Dam in Yangtze River, China built in 2006. Landsat detection a *Saddle Point Stress Singularity* (31N, 103E) at Dragon Date Fault cracks at Gold Sand River *See-Saw Effect:* Uprising molten rock lighter density against heavy water weight at Three Gorges Dam at (31. N 113E). Earthquakes happened on May 12-15, 2008 at Richet 7.8 with thousands after-shocks in Sichuan Province . We have expressed grave concerns to China.

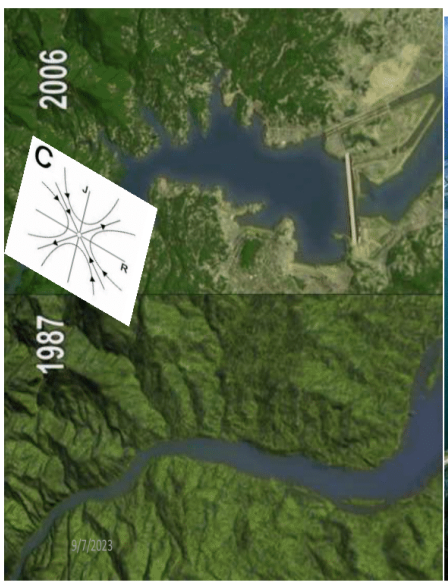

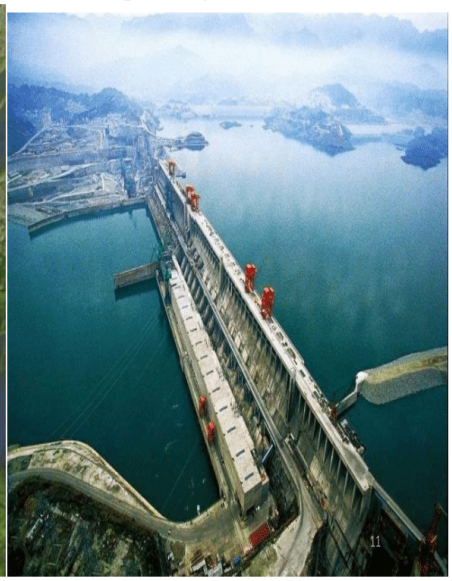

(III.2) Forecast Archival Data **May 12-15 2008** Earthquake Epicenter Wenchuan (31N, 103E) of 7.8 Richet Scale near Dragon Gate Fall of Sichuan. NASA Landsat concerned Three Gorges Dam, measured 2006 the gravitation stress on Landsat (A 2008 Epicenter-B Three Gorges Dam) of the Yangtze River where **dark blue** color represents **less gravity** in May of 2008. We forecasted in April; but 80,000 deaths.

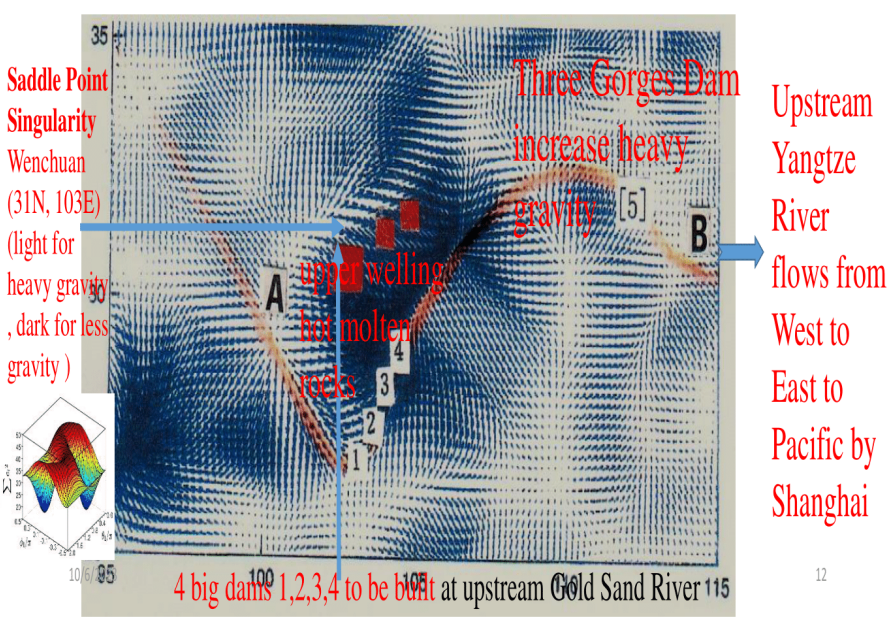

(III.2) Disaster Happened a Month Later May 12-15 2008 Richet 7.8 with 80,000 deaths. within the *central Asian plate* near 3 Gorge Dam on the Yangtze River with 3000 dams on 12-15 May 2008 at Richet scale 7.8 took more than 80,000 human lives in Sichuan Province.

Cities close to the epicenter are flattened; whole mountains collapsed.

(III.3) Gigantic Richter scale 9.2 Tsunami generated by Ocean Earthquake at Indian Ocean 2004 Christmas Earthquake killing 230,000 people e.g. Indian plate was sub-ducted by Burma plate under (Szu & Liu, loc. 2008 SPIE)

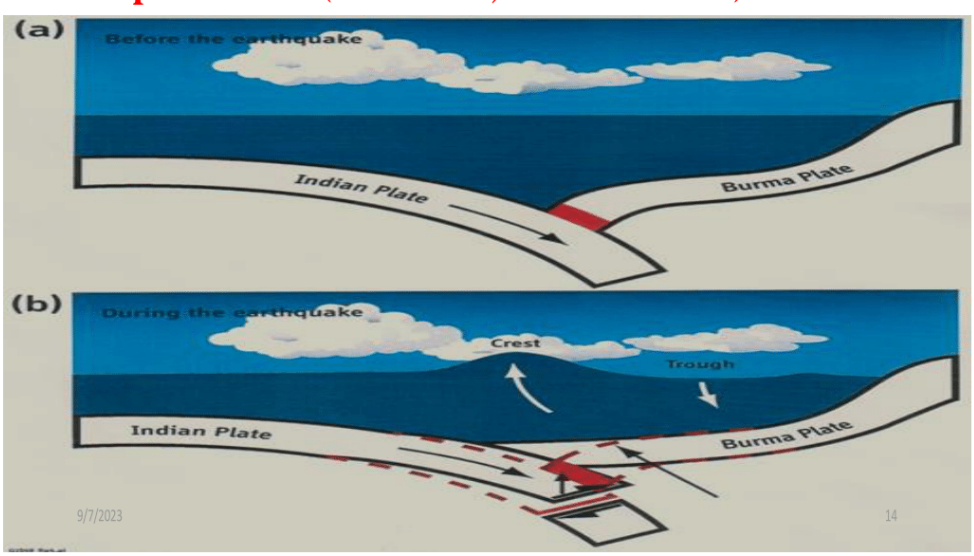

(III.3) More about 2004 Indonesia Christmas Tsunami at Richet 9.2, where the sea floor fractured 1,600 km from Sumatra to Andaman

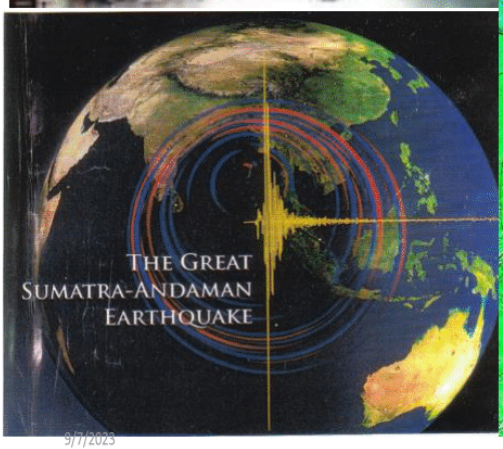

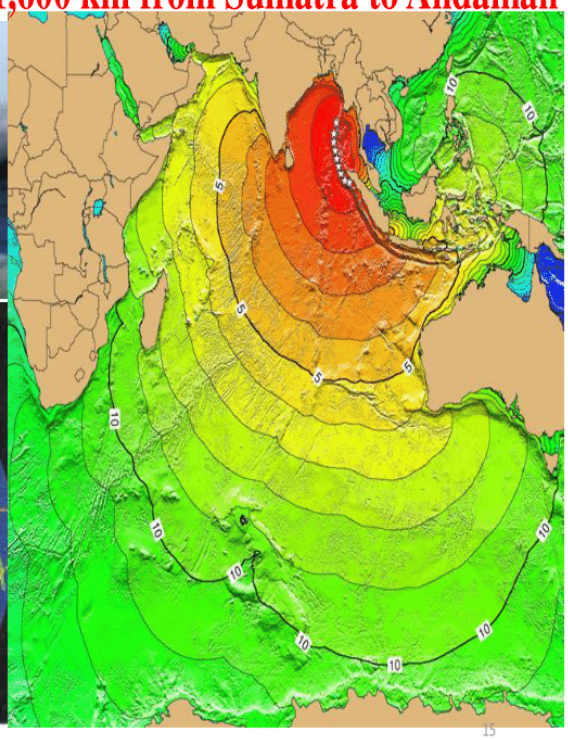

9/7/2023 15

(III.3) Human Aspect 2004 Indonesia Christmas Tsunami wave reached 50 feet high at Richter scale 9.2 killing 230,000 tourist people

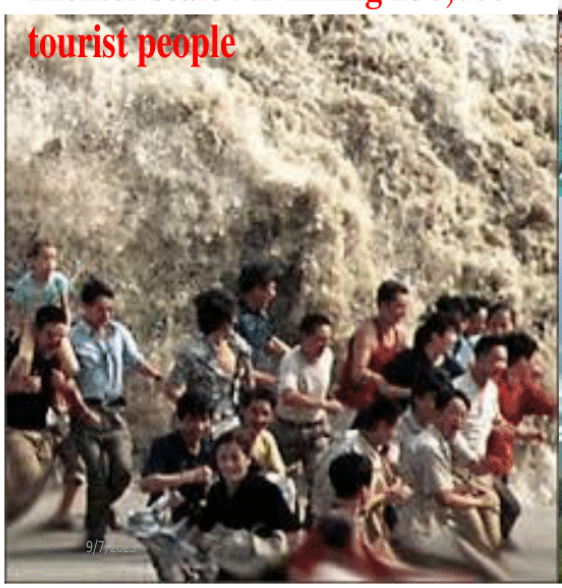

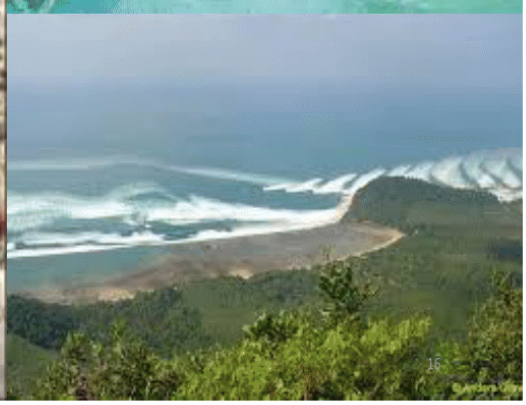

9/7/2023 16

(III.3) After mass of the infamous 2004 Indonesia Christmas Tsunami A village near the coast of Sumatra

(III.4) Evidence of Animal Survival Natural Intelligence

24 August, *AD 79 Mount* Vesuvius Volcano *eruption* was preceded by a *earthquake* 17 years before on February 5, *AD* 62. The whole Pompeii city was buried alive with no survival; archeologists discover no 4 legs wild animals, except 2 legs & domesticated pets under leash. 3 millions waiting for nowcasting the next big one.

(1) Mediterranean Sea Cruise shows a simplified map which indicates Italy Volcano Pompeii located in the Italy city Naples.
(2) Photo of Sunrise over Volcano Pompeii
(3) Photo of animal tied down by a rope was sacrificed.
(4) Homo sapiens sacrificed during the Pompeii Volcano eruption without an early warning.

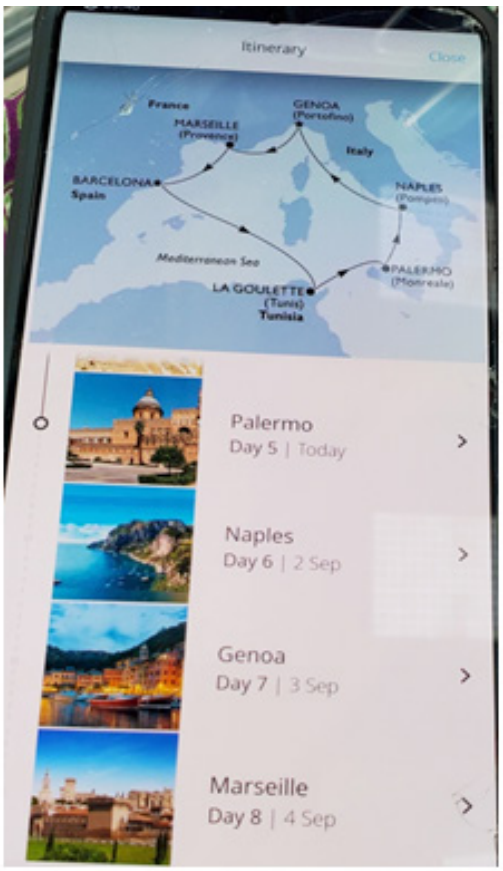
Itinerary
Close
France
MARSEILLE
(Provence)
GENOA
(Portofino)
Italy
BARCELONA
Spain
NAPLES
(Pompeii)
Mediterranean Sea
PALERMO
(Montreale)
LA GOULETTE
(Tunis)
Tunisia
Palermo
Day 5 | Today
Naples
Day 6 | 2 Sep
Genoa
Day 7 | 3 Sep
Marseille
Day 8 | 4 Sep

(1)

(2)

(3)

(4)

Sect. IV Nowcast few moments ahead like animal's survival instinct developed by punctuated selective evolution

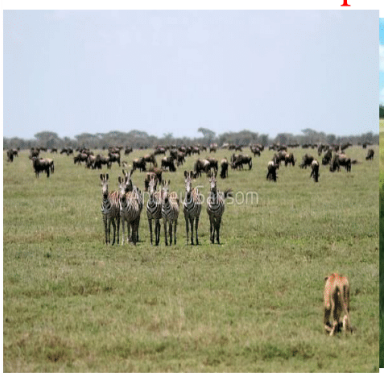

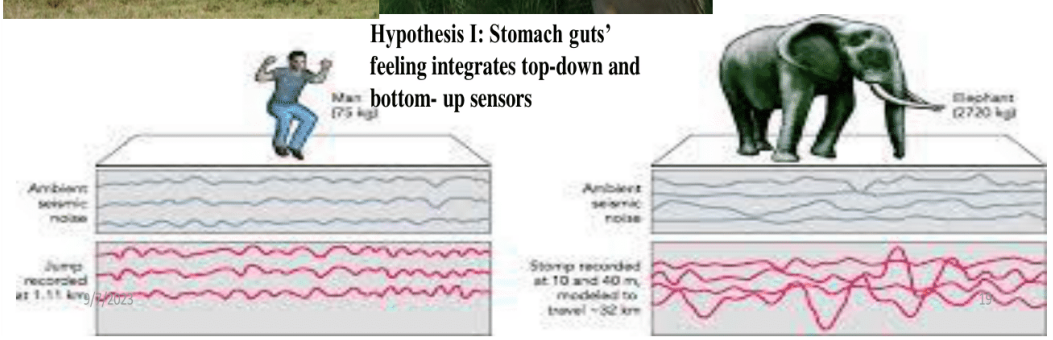

Deep Learning NI Neurophysiology 101: Quiz

How many neurons in our brains?

10 Billions neurons (one per star in the universe)

Not just the size, the number, Dolphin and Whale might have bigger and heavy brain than some of us.

What are the difference ? Why one of the most creative brains of Einstein donated his brain has normal size weight? Not much, except in the house keeping glial cells

How many glial cells we have ? 30 Billions as the silent majority in our brains

What do they do?

Glial cells support the neuronal connectivity at each neuronal local synaptic memory changing the impedance of synaptic gap junction.

Some functions depend on how efficient the house keeping glial cells.

The natural intelligence is not only neurons, but the forgotten silent glial cells; just like the inheritance which is more than Genome but Epi-genome.

Deep Learning by Multiple Layers derived from Boltzmann Entropy to Helmholtz Free Energy to Maxwell Probability to Hebb learning predicting house-keeping glial cells

Given Boltzmann entropy $S_{tot} = k_B\, Log\, W$ on his headstone the irreversible entropy $\Delta S_{tot} > 0$, we have derived statistical mechanics of neuronal dynamics in terms of Helmholtz Minimum Free Energy (MFE), free to do work energy should be small to be most natural guestimate with the highest probability $W = \exp(S_{tot}/k_B) = \exp(S_{tot}T_o/k_BT_o) = \exp(-H_{sub}/k_BT_o)$ where use is made of $S_{tot} = S_{sub} + S_{env}$, and energy conservation $\Delta E_{sub} = -T_o \Delta S_{env}$

Proof: $\Delta H_{sub} = \frac{\Delta H_{sub}}{\Delta \vec{S}_{sub}} \cdot \Delta \vec{S}_{sub} = \vec{\mu}_i\, \Delta \vec{S}_{sub}$

$= \vec{\mu}_i\{\vec{S}_o - \vec{S}\} = \vec{\mu}_i\{\vec{S}_o - [W]\vec{X}(t)\} \rightarrow 0;$

$\frac{\Delta H_{sub}}{\Delta [W_{i,j}]} = \vec{\mu}_i \vec{X}_j = -\frac{\Delta [W_{i,j}]}{\Delta t}$ D. O. Hebb circa 1950 Q.E.D.

Conclusion: Szu recognized Lagrange Parameter $\vec{\mu}_i$ represent a group of biological house keeping Glial (glue in Greek) cells, while pairs of sensors data forming the vector time series $\vec{X}_j$ processing by neuronal synaptic junction weight matrix $[W_{i,j}]$ driven by const. temp brain. This is NI.

Ref: Szu & Hsu single pixel BSS for remotes sensing SPIE 1997, USPTO patent by Szu et al. single pixel BSS 2001; Kuhn Karush Tucker (KKT) Augmented NL Lagrange Methods for Breast Cancer diagnosis by Szu, Miao, Qi "Thermodynamic Free-energy Minimization for Unsupervised Fusion of Dual-color Infrared Breast Images," SPIE Proc. of SPIE Vol. 6247, 2006.

NI Deep learning Donald O. Hebb bilinear I/O product rule circa 1950

to work with another Russian emigré, Leonid Andreyev. Hebb conditioned dogs and became less impressed with Pavlovian techniques. After much soul-searching as to whether he should continue in psychology, he decided in 1934 to burn his boats, borrow money and go to Chicago to continue his doctoral research under Karl S. Lashley.

The elder scientist was to exert a profound influence on Hebb's approach, above all in his emphasis on physiology. Lashley had never doubted that to understand behavior one must first understand the brain. As a lab boy in 1910, he had salvaged slides of a frog brain from the trash heap and tried to find in the neural connections some clue to frog behavior. Lashley performed experiments to detect memory traces in the brain, inventing techniques for making brain lesions and measuring their location and extent. By around 1930 he had become convinced that memories could not be stored in a single region of the brain but must be spread throughout. In 1934, when Hebb went to Chicago, Lashley was concentrating on the study of vision.

A year later Lashley was offered a professorship at Harvard University and managed to take Hebb along. Hebb had to start his research from scratch, and having only enough money for one more year, he sought an experiment that could support a thesis no matter how it came out. He contrived to adapt his interest in the nature-nurture question to Lashley's vision project by investigating the effects of early experience on the development of vision in the rat.

Contrary to the empiricist ideas of his master's thesis, Hebb found that rats reared in complete darkness could distinguish the size and brightness of patterns as accurately as rats reared normally. This finding indicated that the organization of the visual system was innate and independent of environmental cues, a view coinciding with that of the Gestalt school, to which Lashley was sympathetic [see "The Legacy of Gestalt Psychology," by Irvin Rock and Stephen Palmer; SCIENTIFIC AMERICAN, December 1990]. What Hebb did not notice, although the results were included in a paper he published at the time, was that the dark-reared rats took much longer than normal rats to learn to distinguish vertical from horizontal lines. Only many years later, after he had again changed his ideas about the relative importance of innate and learned mechanisms, did he appreciate the significance of this result.

Hebb received his Ph.D. from Harvard in the middle of the Depression, when there were no jobs in physiological psychology to be had. He therefore stayed on for a year as a teaching assistant, a post that enabled him to continue his work with Lashley. In 1937 there was still no improvement in the job market, but Hebb's luck held out. His sister was taking her Ph.D. in physiology at McGill and heard that Wilder Penfield, a surgeon who had just established the Montreal Neurological Institute there, was looking for someone to study the consequences of brain surgery on the behavior of patients. She passed on the information to her brother, and his application for the two-year fellowship was successful. He married again and returned to Montreal. The young man who thought he could run away from his family destiny and become a novelist found himself one of a medical group pioneering the treatment of neurological disorders.

Penfield's specialty was the treatment of focal epilepsy by surgically re-

Appendix D Exact Mathematics Solution

Deep Learning NI needs glial cells (the missing half of Einstein brain)

The silent majority house-keeping glial cells in CNS & PNS

Intelligence needs a holistic mind & body including neurons and glial cells. Although glial cells do not communicate, but they keep neurons well. Glial hold scaffold for brain growth, repairing & rejuvenating brain under Parkinson disease, Alzheimer, PTSD TBI, etc. 6 types of glial cells:

(A) Astrocytes (CNS image A): 1)Star-shaped cells : 1) clean up brain "debris"; 2) transport nutrients to neurons; 3) hold neurons in place; 4) digest dead neurons; 5) regulate extracellular space.
(B) Oligodendroglia (CNS image B): Provide the insulation (myelin) to neurons.;
(C) Microglia (CNS image C spinal cord) : digest dead neurons in spinal;
(D) Satellite Cells(PNS image D) Physical support to neurons;
(E) Ependymal cells (CNS image E)
(F) Schwann Cells (PNS image F in Green): Provide insulation (myelin) to neurons.
(G) UID

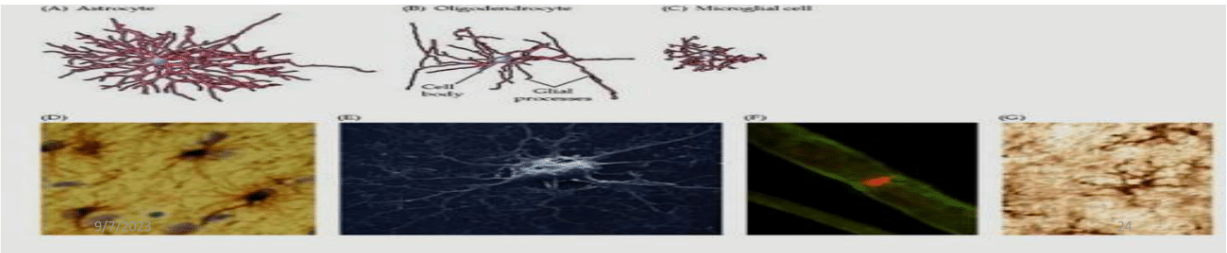

9/7/2023 24

Survival Inspired NI Novelty Detection by Non-Gaussian HOS

Lemma 1: Large Data Analysis (LDA) having a homogeneous date basis (biomedical, epigenetic) that is ready for data mining; Big Data Analysis (BDA) having heterogeneous data bases that might require feature extraction pre-processing data mining at feature space.

Comment: BDA (e.g. IRS, Police, etc.) may require pro-processing to regulate the data set, e.g. Optical Expert System (Szu et. al. IEEE Proc.) *Adaptive wavelets transform* based on *supper-mother theorem (Szu et al. Appl. Opt AWT Special issue)*, before applied LDA data mining at feature space. We shall illustrate AWT with Seismogram data mining for Nowcast Earthquake

Lemma2: Higher temperature is not any smarter: Homosapiens/Human are 37o while birds/Chicken 40o; we ate Chicken, not vice versa. Physiologically, it tuned out that human kept at 37o is to be optimum for human hemoglobin red blood cell squeezing through human capillary bed connecting the arteries and the veins. Q.E.D.

Lemma 3: Higher Order Statistics (HOS) ICA as joint density factorization (jdf) needed for USGS archival databases can provide for CA Parkfield 800 miles San Andreas Fall the <24> mean years. Since the last big Earthquake event at Richet scale 6+ happened at 2004.**HOS for USGS Perspective**: Last big one 2004+<24>=2028; 2028-2016=12 in a dozen years with variance STD= 7, 4-th order cumulant, Kurtosis, quantifies whether the shape of the data distribution matches the Gaussian. Moment and cumulant definitions are given:

$$M(\xi) = < \exp(\xi X) > = \sum_n \frac{1}{n!} < (\xi X)^n > = \sum_n \xi^n \mu_n \frac{1}{n!};$$

$$K(\xi) = \log M(\xi) = \sum_n \xi^n K_n \frac{1}{n!}$$

$$\mu_0 = 1, K_0 = 0;$$

$$K_1 = \mu_1; K_2 = \mu_2 - \mu_1^2;$$

$$skewness\ K_3 = \mu_3 - 3\mu_2\mu_1 + 2\mu_1^3;$$

$$K_4 = \mu_4 - 4\mu_3\mu_1 - 3\mu_2^2 + 12\mu_2\mu_1^2 - 6\mu_1^4 = < X^4 > -3 < X^2 >^2 \text{ by Gaussian reduction to super-G or sub-G}$$

9/7/2023 25

BDA: (1) ID Gap, (2) Fill-in value by feature exaction (3) Implement by LDA/RDB

United Nation: Global Pulse (2012) leveraging BDA for economic development (e.g. BDA Oracle, Apache Spark, HP Intel, IBM, etc)

For Earthquake Nowcast, we use Smartphone embodied the feature extraction by NI SoC with Ears & Eyes-like Wavelets Pre-Processing that *reduced BDA to LDA* followed with brain-like HAM RDA.

Exemplar: Earthquakes from Japan through core revealed a shear waves (low frequency p wave)- (high frequency s wave) inside (solid core p wave) respectively, producing the slowness about 1.5 second upon the arrival at Mw=7.0(*Wookey & Helffrich*, Nature V. 454, no. 7206, pp.873-876, 14 Aug 2008)

Hermitian Hat Wavelet Design for Singularity-Detection in the PARAGUAY River Level Data Analyses, Szu, Hsu, Deane Sa, W. Li, *SPIE Vol. 3078 / April 1997 / Wavelet Apps IV* 96

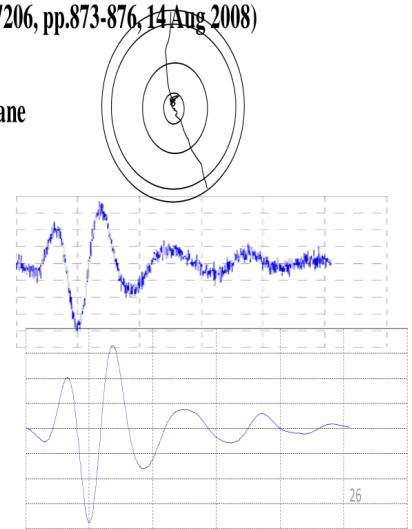

Hermitian Wavelet=
Mexican Hat even & odd Wavelets proved
by the expansion of Seismology Morlet Wavelet

$$\text{Morlet}(t) \equiv \exp(j\omega t)\exp(-t^2)$$
$$\approx (1 + j\omega t + \frac{1}{2}(j\omega t)^2 + \cdots)\exp(-t^2)$$
$$\equiv Mexican_{hat_{even}}(t) + jMexican_{hat_{odd}}(t)$$

9/7/2023 26

Classical ANN Following the Leader Self-Clustering Math 101

Since (1+2)= 3; average is $\frac{1+2}{2} = \frac{3}{2}$; But we learn *recursively* $\frac{1+2+3}{3} = 2$;

$$LHS = \frac{1+2}{2} + \frac{1}{3}\left(3 - \frac{1+2}{2}\right) = \frac{3}{2} + \frac{1}{3}\left(\frac{3}{2}\right) = \frac{3}{2} + \frac{1}{2} = 2 \equiv RHS$$

Wiener Filtering Recusive Learning Vector Quantization Theorem :

$$\textbf{New} \; <\vec{x}>_{n+1} = \textbf{Old} \; <\vec{x}>_n + \textbf{Difference}\; \frac{1}{n+1}\{\vec{x}_{n+1} - <\vec{x}>_n\}$$

$$\textbf{Proof:}\; <\vec{x}>_{n+1} \equiv \frac{1}{n+1}\sum_{i=1}^{n+1}\vec{x}_i \;\; \textbf{split out the new comer} = \frac{1}{n+1}\left(\frac{n}{n}\sum_{i=1}^{n}\vec{x}_i\right) + \frac{1}{n+1}\vec{x}_{n+1}$$

$$= \textbf{re-arranged}\; \frac{(n+1)-1}{n+1}\left(\frac{1}{n}\sum_{i=1}^{n}\vec{x}_i\right) + \frac{1}{n+1}\vec{x}_{n+1} = <\vec{x}>_n + \frac{1}{n+1}\{\vec{x}_{n+1} - <\vec{x}>_n\}\; \text{Q.E.D.}$$

"Following leaders"(Teuvo Kohonen SOM NI 102, and) split new comers into different classes by direction cosine :

$$\textbf{New} <\vec{x}>_{n+m+2} = \textbf{Old} \; <\vec{x}>_n + \textbf{difference}\frac{1}{n+1}\{\vec{x}_{n+1} - <\vec{x}>_n\}$$
$$+ \; \textbf{Old} <\vec{y}>_m + \textbf{difference}\; \frac{1}{m+1}\{\vec{y}_{m+1} - <\vec{y}>_m\}$$
$$\textbf{direction cosine}\; \frac{<\vec{x}>_n \vec{y}_{n+1}}{|<\vec{x}>_n||\vec{y}_{n+1}|} = \cos\left(\theta < \frac{\pi}{4}\right) \le \frac{1}{\sqrt{2}}\; \text{Q.E.D.}$$

Remarks

(1) Kalman weighted average has the gain $g \to \frac{1}{n+1}$ when the weight were uniform).

(2) Direction cosine is named as ***Vigilance parameter by*** Gail Carpenter-Steve Grossberg ART NI 103

(3) Adaptive Credit (Paul Werbos) Reinforcement Learning, Back Error Propagation : when further meaning is given to those classes (Control Theory: state space $\vec{x}$, etc.); (Paul Werbos 1974 Back prop) Parker (1982), Rumelhart (1981)

27

NI App #1 MPD Data Mining (Genome, Drug-Discovery, Financial, Intelligence)

Using Hetero-Associative Memory (HAM) applied to Real Time Computer Generated Hologram (CGH) using Acoustic Optical medium (e.g. Hologram or Real-Time cross-Surface Acoustic Wave (SAW)) and shining the light through to fusion Relational Data Basis $\vec{D}=(A,O,V)^T$ into Subliminal Bias, before Eureka Aha discovery.

The logic of "IF ,Then" can be implemented by MPD HAM: $\vec{B}=\left[\sum_{i}^{n}\vec{B}_i^T\vec{A}_i\right]\overrightarrow{A}$

Relational Data Basis: The color (Attribute) of Apple (Object) is red (Value).

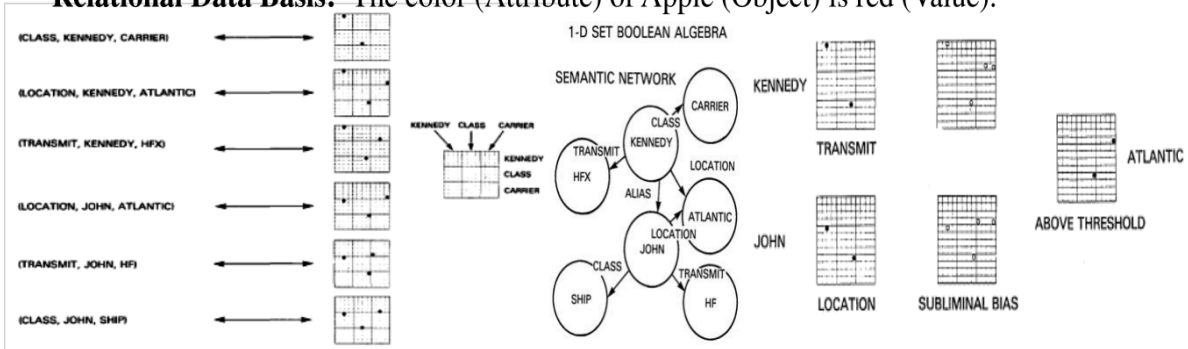

1. Szu H. & Caulfield J. " Optical expert System," Appl. Opt. 26, pp 1943-1947, 1987.
2. Szu H. & Caulfield J. "The Mutual Time-Frequency Content of Two Signals" Proc IEEE, 72, pp. 902-908, 1984

Auto-AM Write by outer product(150x150); Read by Inner Product; one step recovery test robustness

Fault Tolerance-AAM Write by outer product(150x150); Read by Partial Image Inner Product ; one step recovery

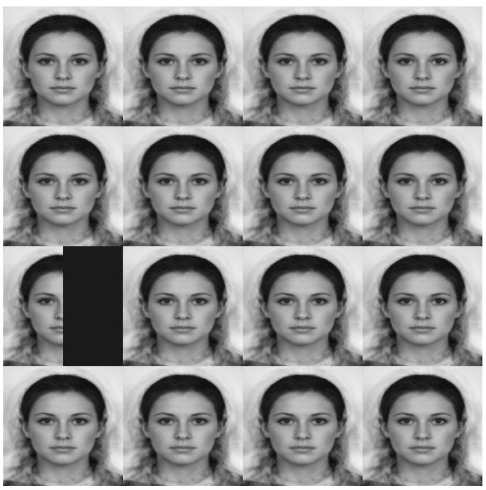

9/7/2023

30

Fault Tolerance-AAM Write by outer product (150x150); Read by Noisy Image Inner Product ; one step recovery

9/7/2023

31

Search and Rescue (SAR) in Forest requires heterogeneous BDA using Ultraspectral data (EO-IR, and RF (FOPEN & IFSAR)

H. Szu, C. Hsu" Ultra-spectral: Hyperspectral & RF features Registered by IFSAR," SPIE Proc. 4391 (2001, Orlando)

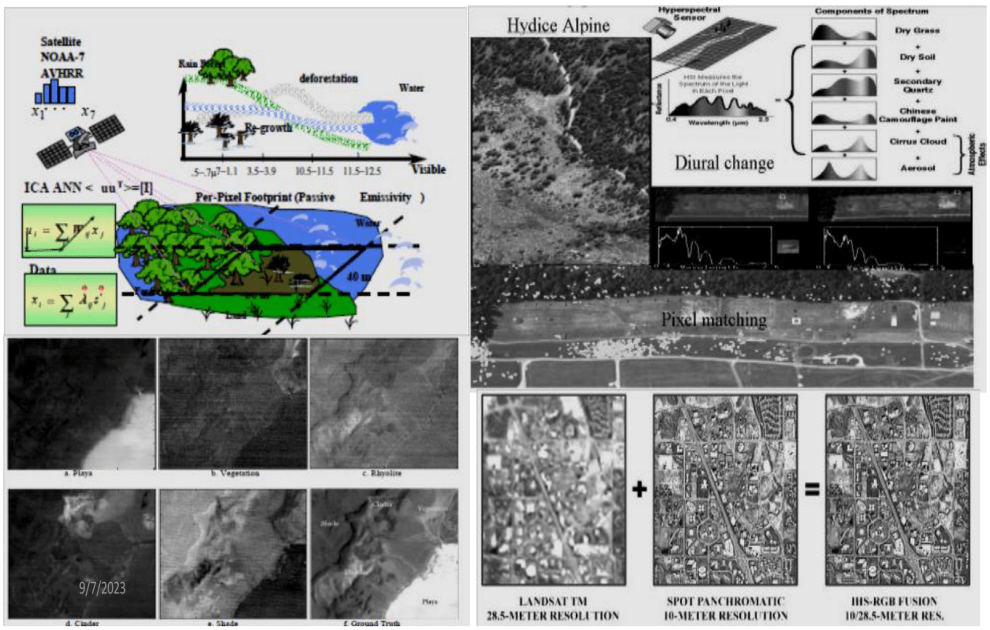

Users should demand Smartphone having 3-D sensitive IMU (by MEMS) wavelet preprocessing linked to Towers to USGS; IMU matured in every safety airbag. The 3-D proofing mass must be miniaturized. "When they build it, we will come."

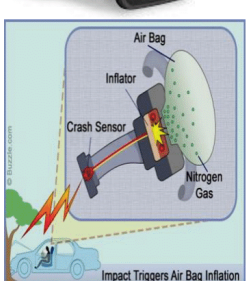

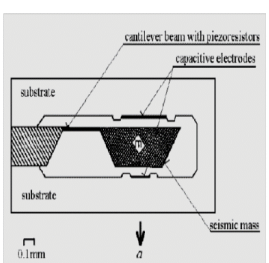

9/7/2023

33

More about BDA Cellular Towers (Archi-rithem Algo-tecture)

Kohonen SOM (Helsinki) & Carpenter-Grossberg (BU) ANN Model implemented "following the leaders self-clustering," that is embedded in FT MPD facilitating the ToA offsets necessary for BDA Nowcasting by NI.

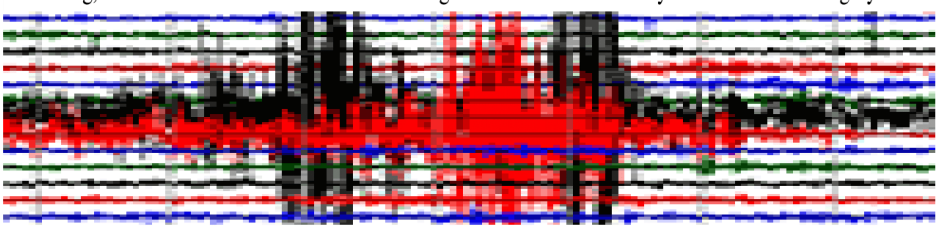

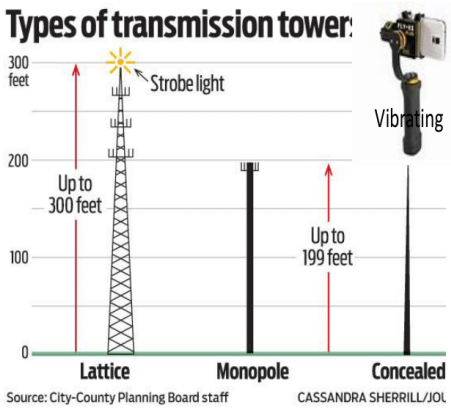

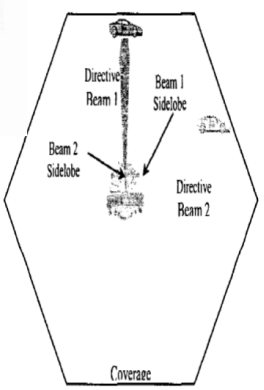

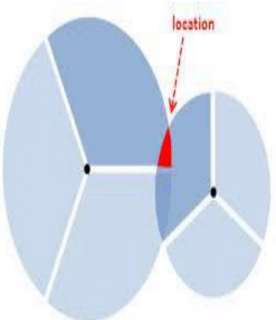

Cell phone detected within a certain distance of two cell towers with directional antennae.

9/7/2023 34

In conclusion,

BDA Nowcast stock "buy low, sell high" be rick, BDA not Nowcast Earthquakes to save life.

Given world 20% earthquakes at Japan; Smartphone coverage 99.%; Yet Japan Smartphone did not install IMU to sense Earthquakes. 4 years ago, March 11 2011, Earthquake Richet 9 Tsunami buried Fukushima Nuclear Power Meltdown worst than Chernobyl I^{131}, Cs^{137}.

WHO said ten fold Cancers and no Sashimi would be ever safe, not even deep sea farming.

♥, ♥, ♥, ♥,"WHENEVER WILL THEY LEARN? LONG TIME PASSING"♥, ♥, ♥, ♥, ♥, ♥, JOAN BAEZ

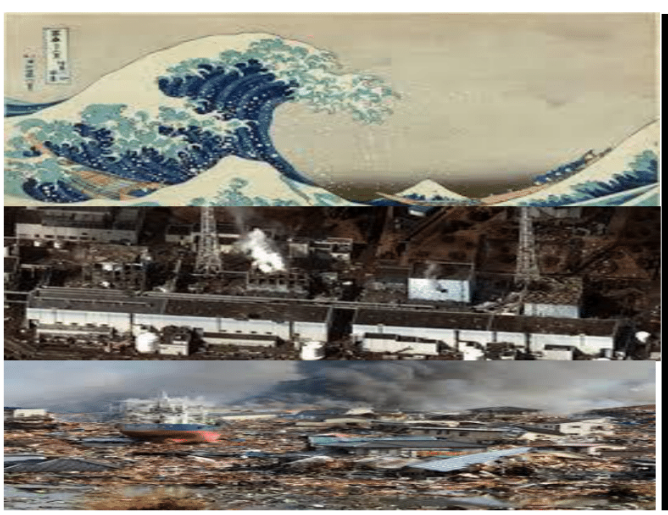

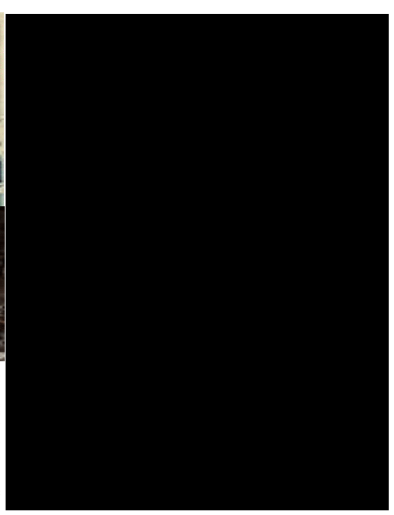

Conclusion/Summary

We have forecasted using Satellite Gravity Measurement data in public SPIE Orlando April 2008 where we exam a Saddle Point: Singular Stresses at in-situ Faulty Cracks at (21N, 103E) "Gold Sand Creek" upstream of Yangtze River Three Gorges Dam (21N, 113E). Nevertheless, the nightmare happened on May 12-15, 2008 Earthquakes at Richet scale 7.8 killed 80,000 people in Sichuan alone. Forecast was useless as life must go on.

We need Nowcast at a few minutes ahead to save lives. Animal survived in earthquakes. no 4-legs remains were found at Pompeii Rome. What do animals knows we don't. (i)Necessary Condition: Those animals roaming on the Earth must have isothermal brains, e.g. dinosaurs were cold blood animals and perished at ice age (ii)Sufficient Condition: All animals have pairs of legs and pairs of sensors. They do top-down and bottom up for guts felling in adaptive resonance and self-clustering of vector data time series X(t)=[A?]S(t)?

To guesstimate as deep learning de-convoluting for underlying $S(t)=[A]^{-1}X(t)=[W]X(t)$ with error $\Delta S=S_0-[W]X$ at MFE In short, Ludwig Boltzmann $S=k\,Log(W)=Ssub.+Senv.$; Inverse is Maxwell Probability $W=exp(S/k)=exp(ST/kT)$. From Energy conservation: Heat $Senv.T=-Esub$ internal energy: $W=exp(-Hsub/kT)$; Helmholtz MFE $H=E-TS$ leading D. O. Hebb bi-linear I/O product learning rule. Proof: MFE: $\Delta H=(\Delta H/\Delta S)\Delta S=\mu\Delta S\rightarrow 0$ implying $\Delta[W]/\Delta t=-\Delta H/\Delta[W]=\mu X$ implementing "following the leaders" in FT MPD)("Algo-tecture" or "Archi-rithm" Neural Nets): by Kosko Hetero AM, Kohonen Kalman-like SOM, Carperter-Grossberg ART, Werbos Adaptive Credit, Szu MFE Novelty Detection. Archeologically speaking,

We have designed Smartphone with IMU/MEMS in Nowcast Earthquakes. This network should now-cast the March 11,2011 Fukushima Nuclear Power Plant Meltdown. NI can build the next gen. Humanoids handling Nuclear Reactor Meltdown better than emotional human.

Appendix A Popular Science Books For Dummy

Dummy Book Series (Free Download)

Smartphone Nowcast

Next Big One[$]

Harold Szu, Ph. D.

***Fellows of IEEE, OSA, SPIE, INNS, AIMBE**

"In God we trust, all the rest show data;"

Evidence-based know-logic, *a dummy cannot be stupid*

Of course, we know "*devil, if any, is in the details.*"

Albert Einstein said well, in his one stone biography by Pairs,

"*Science has nothing to do with the truth, but consistency.*"

Accordingly, *engineering has nothing to do with the truth, but consistent approximations.*

We put together a common sense book, and offer it free. One pays for what one gets; not much, except the knowledge is the power, because "educated consumers are the best customers."

Origin of Universe, Big Bang, Dark Matter, Nucleus Physics, How Iron Formation, Earth Core Cooking Pot Origin of Earthquakes at Bernard cycle 24 years, Computational Mechanics, Computation Intelligence Smartphone Smart Sensor Web for Dummies.

*https://www.researchgate.net/profile/Harold_Szu2;

*http://www.ica-wavelet.org

*http://www.mathgeneology.org/harold_szu;

1. [$]Nowcast of natural resource and calamity warning, Harold Szu, **USPTO** 8392122 B2, Apr. 29, 2008;
2. Nowcast of natural resource and calamity warning, Harold Szu, Han-Shou Liu, Wavelet Proc. SPIE Aero-sense 2008 (Orlando FL)

Appendix B

Nowcast of natural resource and calamity warning US 8392122 B2; U.S. Pat. No. 7,366,564, issued on Apr. 29, 2008 & Oct. 28, 2010

(19) **United States**

(12) **Patent Application Publication**
Szu

(10) **Pub. No.: US 2010/0274493 A1**

(43) **Pub. Date: Oct. 28, 2010**

(54) **NOWCAST OF NATURAL RESOURCE AND CALAMITY WARNING**

(76) Inventor: **Harold Szu**, Potomac, MD (US)

Correspondence Address:
IP STRATEGIES
12 1/2 WALL STREET, SUITE E
ASHEVILLE, NC 28801 (US)

(21) Appl. No.: **12/756,621**

(22) Filed: **Apr. 8, 2010**

Related U.S. Application Data

(60) Provisional application No. 61/168,412, filed on Apr. 10, 2009.

Publication Classification

(51) **Int. Cl.**
G01V 1/00 (2006.01)
G06F 19/00 (2006.01)

(52) **U.S. Cl.** **702/15**

(57) **ABSTRACT**

A method of forecasting naturally-occurring phenomena, such as seismic activity, includes taking localized measurements of the Earth's gravitational force change using MEM inertial motion units. Trends in the measurements are interpreted and related to a phenomenon of interest, a likelihood of occurrence is predicted based on the relationship, and the likelihood is reported to interested parties, preferably automatically to emergency bulletin sources. Measurements can be taken from above the Earth's atmosphere. The trends can be interpreted by determining blind source separation information directed to the region underneath the Earth's mantle crust to determine composition and/or movement.

EARTHQUAKE CALAMITY WARNING FROM SPACE STATION--- ORBITAL DYNAMICS COUPLING GEOLOGY MANTLE CONVECTION

Harold H. Szu[a], *Fellows* (IEEE, SPIE, OSA, AIMBE, INNS), *& Academician* (RAS/NL),and[
Han-Shou Liu, *Senior Scientist*[b]
[b]NASA Goddard Space Flight Center, Greenbelt, MD 20771 USA
[a]GWU, Wash DC, NSWC, Duhlgren, VA, ONR, Arlington VA; Army NVESD, Ft. Belvoir, VA
(szu_h@yahoo.com)

ABSTRACT

It is not surprising that the earthquakes happened among clashing tectonic plate boundaries where numerous earthquake stations exist. Then, why do we need more? The significance of Sichuan and Tongshan earthquakes of China is a wakeup call that major earthquakes of logarithmic Richter scales beyond 7 could happen exactly within a single tectonic plate surprisingly. Thus, the previous border surveillance is broadened to areas coverage. Judging the success of archival survey of NASA with the gravitational potential by Liu et al., we review a unified earthquakes theory covering both the peripheral and the central plate in this paper, so that we can take seriously the need of a comprehensive global surveillance of natural calamity in the Space.

The earth surface crust, like a kitchen kettle lid, covers tightly the melted mantle rock layer, like a pea soup cooking in the kettle. Given the time they will all become bubbling, rattling & shaking, known as the Bernard instability. This instability is ubiquitous for any liquid state matter being heated from below, if and only if it has a real positive thermal expansion coefficient. Likewise, the earth mantle is being cooked from below by an enormously hot fireball of the size of a moon. The heat comes from the radioactive decay confined within the core over eon's age. Due to the enormous gravitation attraction being always real positive and additive, the inner core is bifurcated into 2 regimes, a heat-melted liquid metal regime, where the earth magnetic field is produced and predicted by Faraday induction law. And further inside there exists a tightly squeezed solid metal ball regime, due to the gigantic weight compression, as confirmed by sonar experiments. The complexity of earth Bernard instability is due to the extra rotational Coriolis force that makes the up-down thermal convection side-way, creating the mass imbalance and permitting in-situ measurements feasible at a distance.

We wish to propose a real-time *wide-area persistent surveillance system* on a *Space Station* for the now-cast, that is a real-time data acquisition system based on a distributed set of Inertial Motion Units (*IMUs*) embedded in the matured technology of Micro Electric Mechanical Systems (*MEMSs*). We watch for any diminishing of gravitational pulls upon the set of flying-over test-masses, due to the up-dwelling of much hotter and less denser melted mantle mass. The imbalanced proofing masses squeeze their neighborhood deformable piezoelectric materials generating the read-out currents. The currents feed an onboard min-supercomputer for Blind Sources Separation (BSS) smart algorithm $\vec{X}(t) = [A(\vec{x}, t)?]S(t)?$ solving the percentage of hot mass $S(t)$under the foot-print without knowing the system transfer function $[A(\vec{x}, t)?]$. Thus, one imposes the constraint of isothermal equilibrium physics at the minimum Helmholtz free energy [US PTO 7,355,182]. In cases of space invariant [A(t)], we apply the Independent Component (pixel-density) Analysis (*ICA*) based on the smoothness of higher order of statistics (HOS) [US PTO 7,366,564 references thereof]. These two classes of *BSSs* may happen in the localized crust stress singularity for earthquake, tsunami, including the magnetic N-S poles fluctuations and reversals.

We estimate that the device *SWaP* (Size, Weight and Power) and the cost, computing power; scanning swap within the payload cargo constraint of a Space Station. The space station will work with local in-situ seismic observations, when the ground truth is used to calibrate for the Space vector time series prediction. A preliminary design test bed is suggested to install over those cellular phone towers along the San Andrea Fault, California. The test bed can help accurately now-cast the natural calamity with powerful computer and precise modeling of the Earth mantle convection stress model.

KEYWORDS: Satellite gravity, crustal stress, mantle convection, geological stability, seismic precursor, origin of earthquake, tectonic plate theory, Three Gorges Dam, 2008 Sichuan Earthquake, China.

1. INTRODUCTION

The earthquakes were due to the imbalance generated by the earth fireball *core* about the size of moon, which is made of *liquid metal* layer generating electrical current producing by Faraday induction the geo-magnetic field of 50 μ Tesa in the North pole and a gravitationally compressed *solid metal* core freezing into a single giant

Independent Component Analyses, Wavelets, Neural Networks, Biosystems, and Nanoengineering VII, edited by Harold H. Szu, F. Jack Agee, Proc. of SPIE Vol. 7343, 73430W · © 2009 SPIE · CCC code: 0277-786X/09/$18
doi: 10.1117/12.820902

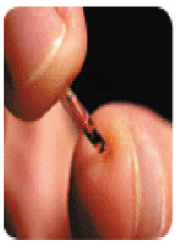

NI App #2 Data Basis Security by Smart Hybrid Card (US Patent Szu, US 8360315 B2) Jan 29, 2013

RFID roaming cows +MFID passports & books I/O=EMID 3D coding with RSA (Rivest, Samir, Adelman) factorial key for Friends or Fore's

Veri-Chip for Alzheimer at Delray Beach, Fla licensed by FDA

- N^3 (E x M x Theta) *Larger phase space* codec for secured communication link, PC access, memory
- RFID Capacitor coupling ~6m, Magnetic Coil coupling~1m, Smart Card (Passport, HK Sony Octopus-card shared no bank data) Hybrid Software & Hardware APS & NGI (128 bits)
- Radar Counter Counter-Measure (C-DRFM) led to pair of APS RFID's at $0.5 for tracking mass flow in real time inventory need.

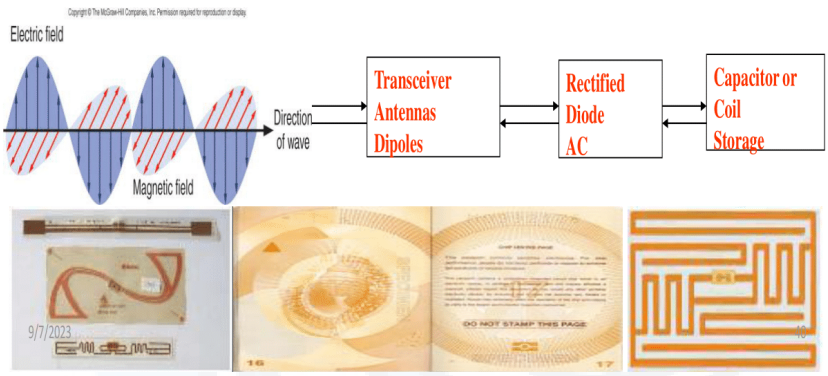

Brain Natural Intelligence combined both sides of brains Harnessing slow LHS & fast RHS thinking with Brainwave (Delta, Theta , Alpha, Beta: 5~30Hz) biofeedback with wireless EEG caps.

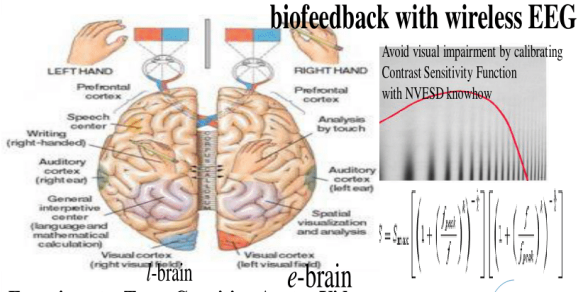

I-brain *e*-brain

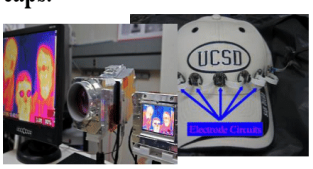

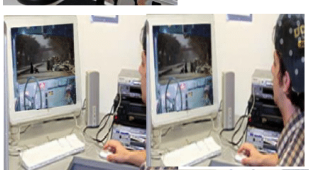

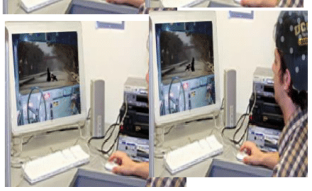

Experiments: Team Cognition Avatar Video

Apply psycholinguistics to increase partner communication and arrive at the optimum decision (tailoring to personality traits):

e-Brain: 1. harmless woman, 2. Let's wait & see;

***I*-Brain:** 1.Why the empty market? 2. why the burka woman leaving the farmer's market area?

Common Decision: *Check Fire!*

e-Brain views "mother-pushing a baby stroller"

I-Brain perceives, through HUMVV window, "Farmers' Market in Afghan"

NI App#4 Life or Death Remote Sensing:

During Korean & Vietnam Wars, ¼ Medics mortality were due to rushing & rescuing a dead comrades.

Casualty Sensor by Smartphone UV Raman (rotational coordinate) backscattering for Peri-Morten Scent (Mercaptan molecules in which oxygen is replaced by sulfur) (Szu et al. USPTO Patent issued 20150323464 A1)

•**Background**: Most researchers are addressing the problem based upon the presence or absence of vital signs. Absence of vital signs does not imply death, just unknown.

•Uniqueness Approach: Life-death is like phase transition. It has hysteresis loop, and is not a binary logic. No Vital Sign at high energy may not be dead "Negate the Converse False is not True"; However, at the low energy the present of Morten sign is mostly likely irrecoverable death.

•**Working Hypothesis:** Less uncertainty/fluctuations at lower energy states together with peri-mortal effluents e.g. Mercaptan molecule (oxygen is replaced by sulfur) indicating a rotten smell of death (UN Human Right Commission for massive graveyard detection)

•**Legal responsibility**. A drowned boy from high energy state has higher fluctuation. Thus, no pulses and no temperature might still be revived.

•**False Alarm Rate** in vital signs, such as brain waves still exit after irrecoverable death due to energy fluctuations (variance σ).

•**Benefits: Hand held Resonance Raman Scattering can** save lives of medics; Medic can spend more time on wounded

Mercaptan Thiol molecules (sulfur replaced oxygen C-S-H 90° breaking symmetry Raman active)

Nature already takes advantage of peri-mortal effluents

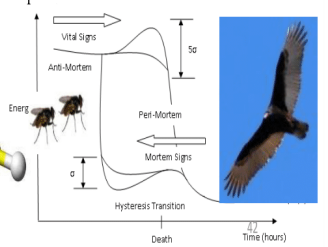

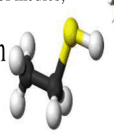

9/7/2023

NI App#3: Differentiate Animal or Human Crossing Digital Fence at Night by microwave interrogating & passive infrared imaging:

Szu, et al. (13 Authors, 10 Agencies)"OPTICAL DISPLAY FOR RADAR SENSING""ICA etc." Proc. of SPIE 9496 (Baltimore, 2015) (namely Harold Szu, Charles Hsu, Jefferson Willey, Joseph Landa, Minder Hsieh, Louis V. Larsen, Alan T. Krzywicki, Binh Q. Tran, Philip Hoekstra, John T. Dillard, Keith A. Krapels, Michael Wardlaw, Kai-Dee Chu)

Boltzmann implied Planck: $S_{tot} = k_B\, Log\, W$; $W = \exp(S_{tot}/k_B) = \exp(S_{tot}T_o/k_BT_o) = \exp(-H_{sub}/k_BT_o)$, use is made of energy conservation $\Delta E_{sub} = -T_o\Delta S_{env}$ to define Helmholtz free energy $H_{sub} \equiv E_{sub} - T_oS_{sub}$

$$H_{sub}\Psi_n = E_n\Psi_n \qquad E_n = \left(\frac{1}{2}+n\right)\hbar\omega; \omega \equiv 2\pi f. \qquad dos \equiv \frac{8\pi\omega^2}{|c_o|^3}$$

$$Q_{bb} = \sqrt{z}\sum_{n=0}^{\infty} z^n; z \equiv \exp(-\beta\hbar\omega); \beta \equiv \frac{1}{kT}, \quad < E_{bb} >_{Q_{bb}} = dos \cdot \left[\frac{\hbar\omega}{\exp\left(\frac{\hbar\omega}{kT}\right)-1}\right] \equiv U_{Planck}$$

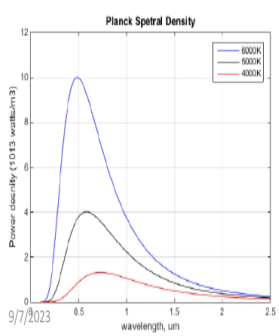

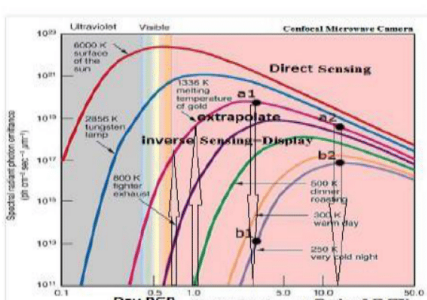

Q.E.D.

9/7/2023

43

Large Data Analysis (LDA) deals with (Genome, Epigenome, Drug Discovery, etc. data mining). While BDA requires feature extraction pre-processing of heterogeneous databases, LDA applies directly at relational data basis (e.g. Color of Apple is Red: vector (Color, Apple, Red)). Animal & Homosapien can capture surprising novelty events for survival reasons (flight or fight adrenaline hormone) when IQ are coded at LTM Hippocampus e-IQ at Amygdala, and integrated at STM Frontal Lobe

- NI App #1 MPD Data Mining (Genome, Drug-Discovery, Financial, Intelligence) **Novelty Detection**
- NI App #2: Data Basis Security by combining RFID, MFID with arbitrary phases, for Authentication, Privacy Security (APS) since the RSA factorial codec requires 3-D phase space
- NI App#3: Differentiate Animal or Human Crossing Digital Fence at Night, Synergistic active RF & passive IR
- NI App#4: Life or Death Remote Sensing: During Korean & Vietnam Wars, ¼ Medics mortality were due to rushing & rescuing a dead comrades.

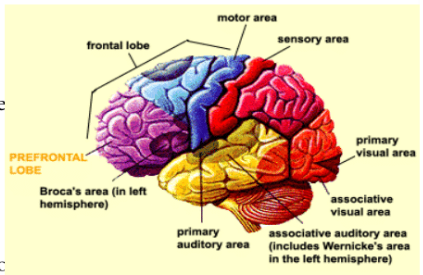

45

"Whenever will they learn? Long Time Passing,.❤❤❤",Joan Baez

- **Taiwan Lunar New Year 6.4 Richet magnitude Earthquake with 68 aftershocks at Culture & College Town Tainan, so far 116 body count in one collapsed tall building**
-

Biomedical Spontaneity Gibb's

Theorem 1 Minimum Helmholtz free Energy determines a stationary function of excited abnormal or malign state:

Given isothermal equilibrium system at the minimum Helmholtz free energy defined the departure from an individual baseline level satisfies a canonical ensemble average behavior, in terms of analytic input & output data ***X*** *and* ***S****. Then, the departure of the baseline according to minimum thermodynamics free energy one obtains*

H(isothermal free energy) = (info energy)E - (local temperature)T_o (Shannon entropy)S

$$E = E_o + \sum_{i=1,2} \frac{\partial E}{\partial s_i^{(o)}}(s_i - s_i^{(o)}) = E_o + \sum_{i=1,2} \mu_i (\sum_{i,j=1,2} [W_{ij}] X_j - S_i)$$

$$X(t) = a_o[A(t)?]S_o(t)$$

$$E = E_o + [\mu_1 \ \mu_2]\begin{bmatrix}(W_1^T, X) - s_1 \\ (W_2^T, X) - s_2\end{bmatrix}$$

$$= E_o + \mu_1(W_1^T, X) + \mu_2(W_2^T, X) - \mu_2 + (\mu_2 - \mu_1)s_1$$

$$H \equiv E - T_o S;$$

$$H = 0;$$

$$\frac{dH}{ds_1} = 0$$

$$s_1^* = 1 - \exp(-\frac{E_o^*}{K_B T_o})$$

Proof: Two State Exact Solution:

$$H = E - T_o S = 0 \qquad (1)$$

$$\frac{dH}{ds_1} = \frac{dE}{ds_1} - T_o \frac{dS}{ds_1} = 0 \qquad (2)$$

$$Shannon\ Entropy\ S = -s_1 \log s_1 - (1-s_1)\log(1-s_1)$$

$$\frac{dS}{ds_1} = -\log s_1 - \frac{s_1}{s_1} + \frac{1-s_1}{1-s_1} + \log\ (1-s_1) = \log(1-s_1) - \log s_1$$

$$\frac{d^2 S}{ds_1^{\,2}} = \frac{-1}{1-s_1} - \frac{1}{s_1} = \frac{-s_1 - (1-s_1)}{(1-s_1)s_1} = \frac{-1}{(1-s_1)s_1} \le o$$

$$Eq(1)\ gives\ E = T_0 S = T_o(-s_1 \log s_1 - (1-s_1)\log(1-s_1))$$

$$From\ linear\ E = \frac{dE}{ds_1} s_1 + E_o^* =_{(Eq(2))} T_o \frac{dS}{ds_1} s_1 + E_o^*$$

$$= T_o \{\log(1-s_1) - \log s_1\} s_1 + E_o^* / K_B$$

$$Thus\ \ E_o^* / K_B T_o = -\log(1-s_1^*) \qquad s_1^* = 1 - \exp(-\frac{E_o^*}{K_B T_o})$$

Appendix E

Capturing significant events with neural networks

Harold Szu*[a], Charles Hsu[b], Jeffrey Jenkins[a], Jefferson Willey[c], and Joseph Landa[d]

[a]*US Army NVESD, Fort Belvoir VA*

[b]*Trident Systems Inc. Fairfax VA*

[c]*US Naval Research Lab,. Washington DC.*

[d]*Briartek Inc. Alexandria VA*

Article Info

Article history:

Keywords:
Compressive Sensing
Associative Memory
Human Visual System
Compressive Video
Sampling

Abstract

Smartphone cameras sense all and keep all, contributing to digital data pollution. Our eyes sense all, reject many, and keep only the essential difference. To keep it requires an index. In this letter, a sparse index ones among zeros is generated by image changes. This is called Motion Organized Sparseness (MOS), rather than the purely random sparseness of compressive sensing (CS). Such a Non-overlapping Organized Sparse Event (NOSE) enjoys an independent degree of freedom satisfying the fault tolerance requirement of an associative memory (AM) matrix storage and retrieval without suffering cross talk. Following the NOSE criterion, we produced image matrix indices for rapid storage and retrieval from the information-compressive video.

Introduction-2

Tom Poggio et al. asked: "How many views does a monkey need in order to tell a good zookeeper from a bad one?" They discovered monkeys need 3 views: frontal, side views - and a 45° view.[1] Interestingly, humans need only 2 views; top and front to construct a 3-D building from architectural blueprints, front and side views are used for visualizing a human head, etc. According to the Central Slice Theorem,[2] the d.c. component of 1-D Fourier Transform of a parallel X-ray projected shadow-gram of a head tomography coincides with that of the 2-D Fourier Spectrum. Sufficient *M* number of 1-D projections can be combined into a 2-D rendering by means of the Theorem registering their 1-D Fourier spectrum at the same d.c. origin with the inverse reconstructed transformation, and then either a clear or a fuzzy interior picture appears. *A million-dollar question has been what is the optimal M value? (cf. Conclusion remarks).*

Computer vision based on frame differencing flow is inspired by but not necessarily the same as the biological vision, which seeks significant or abrupt changes when looking for food, mating, or selectively for survival reason. This is understandable from a Darwinian viewpoint. Marr et al. emphasized circa 1980 the importance of differential selectivity in early information representation of human visual systems (HVS). For example, driving in a rainy night we watch for pedestrians, but not the rain drops. When both eyes agree, it is a signal; if not, a noise. Such an experience is effortless requiring no memory supervision. Nonetheless, two eyes with brain can also solve the sophisticated image de-mixing problems (cf. conclusion remarks).[3] The lesson learned is stored and retrieved by the associative memory (AM) located at hippocampus. *For example, the HVS involves both the Hubel-Wiesel oriented edge map*[4] *and the distributive AM which build memory, motion, and changes. We refer to this* ***Memory-Motion-Changes*** *resulting in* ***Organized Sparseness*** *as* ***(MOS).***[5] *A modeling condition of this* ***MOS*** *is that we keep these salient changes orthogonal and thus independent to one another.* In Sect. 2, we review the simple matrix mathematics of outer-product write operations for AM storage and the inner-product read operations for AM retrieval. Such an AM approach to MOS is crucial for achieving both fault tolerance (FT) and generalization depending on user's a priori knowledge and viewpoint.

A **Nonoverlapping Organized Sparseness Event (NOSE)** insures comparison-selection of distinct scenarios among multiple sensory modalities that fuse over time. As a result, our **AM** model can build MOS ones and zeros where one represents major motions and zero represents stagnations at non-overlapping locations. This exploits the inherent mutual orthogonality, which is useful for video AM compressive or selective sampling and storage. Furthermore, our NOSE model does not randomly skip pixels without measuring, as Emmanuel Candes of Caltech, Justin Romberg of GIT Technology, Fields prize winner Terrence Tao of UCLA[2,6] and David Donoho of Stanford[7] introduced in 2006 their single frame compressive sensing (CS) *(cf. Conclusion remarks). In general, this MOS separates naturally salient parts of an event, which enables automatic graphic matrix indexing, which is more robust than the 1-D hashing index adopted in computer vision. Technically,* our ANN approach always senses all in full resolution; but rejects redundant frames (not pixels), keeps only distinctive different representations. Therefore, we have by-passed the need to develop a rapid and robust CS image recovery for real-time video. Our approach strives to be information-compressive sampling (CSp) like an automatic cliff notes with the goal of reducing the cost of a human analyst overcoming data pollution in the digital age.

Associative memory (1664 words, without Intro, graphs & Ref.)

We review how biological change generates attention and feature neurons. A mammalian strategy of paired sensors involves a short-term working memory for comparison and selection for input signal enhancement. Pazo-Alvarez et al in Neuroscience 2004[5] reviewed various modality of brain imaging methodologies, fMRI (Ahlfores '99), MEG, VEPs (Kremlacek '2001), ERPs, PET (Cunningham '90); Watson '93), to substantiate the *electric brain response* as a *differential response* of visual *event related potential* (ERP). They confirmed the possibility of automatic *comparison–selection* of motion direction changes. Furthermore, Todd and Marols in Nature 2004[9] summarized the capacity limit of visual short-term memory in human posterior parietal cortex where a single neuron, a grandmother neuron (i.e. a sparse neuronal representation), fires intensely for 1 second without disturbing others, supporting the independence strategy yielding the pseudo-orthogonality attribute.

Given facial images $\vec{X}_{N,t}$, three independent salient features representing the *eyes, nose,* and *mouth* were extracted. In the cool limit $K_B T \to 0$, McCulloch-Pitts sigmoid neuron is reducible to Von Neumann binary logic rounding off the maximum firing rate 100 Hz to one, and lower to zero: (*1, 0*) (*big, small*). When these neurons firing rates broadcast among themselves forming an Associative Memory [AM], e.g. 3x3 synaptic gaps junctions denoted by the matrix $W_{i,j}$ at the *hippocampus* (facilitating multi-sensory fusion through the Crick and Koch Claustrum communication underneath the Cortical layer[10] that consciousness begins at 30 Hz tuning ANN). When uncle and aunt are first introduced to a young child, the image of an uncle is compared with the image of an aunt. The child distinguishes the uncle by noticing him having a nose that is bigger than normal compared to that of the aunt and with his own mouth and eyes. These features can be expressed as firing rates $f_{old}(n_1, n_2, n_3)$ (*eye, nose, mouth*) (*0, 1, 0*), which turns out to be the coordinate $\hat{y}$ axis of the family feature space. Likewise, the perception of aunt has bigger eyes, smaller nose and smaller mouth (1,0,0), forming another coordinate axis $\hat{x}$, orthogonal to the coordinate $\hat{y}$ axis. Mathematically, this selection of saliency satisfies the NOSE criterion, as well as the Fisher's Mini-Max classifier criterion for intra-class minimum spread and inter-class maximum separation.[11,12] When the uncle is smiling at the child, the child generates through the same neural pathway of HVS a new input features f_{new} (n_1, n_2, n_3) (*eye, nose, mouth*) (*0, 1, 1*), then the responses arrive at the hippocampus where the AM system corrects effortlessly the new input back to the most likely relative, namely the big-nose uncle state (*0, 1, 0*), within the fault tolerance 45° cosine angle. Mathematically, this ANN classifier satisfies the nearest neighbor classifier principle. We write to AM by an outer-product between the uncle feature vector in both column and row forms, similarly the aunt. Then a smiling uncle is read by the child as a new input. The AM matrix–vector inner product represents three feature neurons (0,1,1) sending their 100 Hz firing rates through the AM architecture of Figure 1c, and the output (0,1,0) obtained after each neuron takes a sigmoid σ threshold remains to be the big nose uncle, despite of his smile.

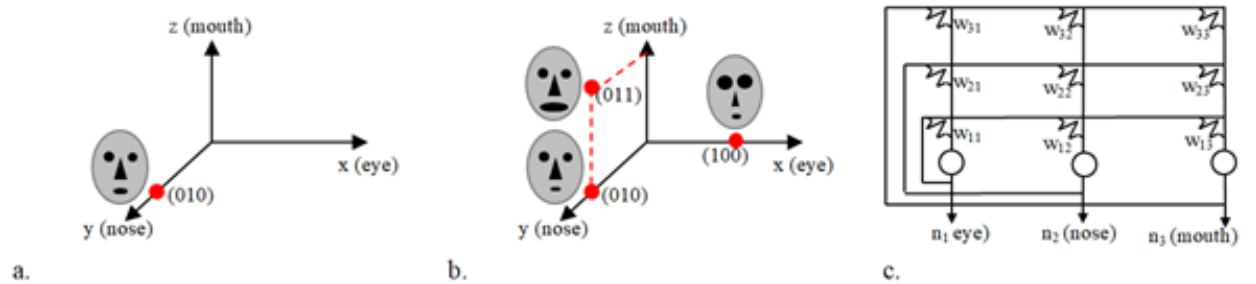

Figure 1 a, b, c Memory organized sparseness (MOS) may serve the fault tolerance attribute of a distributive matrix associative memory. When a child met for the first time his uncle and aunt, the child paid the attention to extract three feature neurons firing at 100 Hz or less represented by 1 or 0 respectively (shown in 1a). In the next time, the uncle was smiling at the child (indicated by (0,1,1) in the first quadrant) (shown in 1b), the child recognized by the vector inner product read procedure of the matrix[AM] and the new input vector (0, 1, 1). A smiling uncle is still the uncle as it should be. Mathematically speaking, the brain hippocampus storage is equivalent to the vector outer product of the feature vector (0, 1, 0) to itself at the matrix associative memory [AM]. The broadcasting communication network is called the artificial neural network (ANN) circuitry indicates learnable weight values $\{W_{ij}; i,j=1,2,3\}$ of the neuronal synaptic gaps among 3 neurons indicated by 9 adjustable wiggly resistances (shown in 1c) where both uncle and aunt feature memory are additively stored concurrently.

Write by the vector outer product to form a sparse memory [AM]. Orthogonal features are indicated in a 3-dimensional feature subspace.

$$[AM]_{big\ nose\ uncle} = \overrightarrow{output} \otimes \overrightarrow{input}$$

$$= \begin{bmatrix}0\\1\\0\end{bmatrix} \begin{bmatrix}0 & 1 & 0\end{bmatrix} = \begin{bmatrix}0 & 0 & 0\\0 & 1 & 0\\0 & 0 & 0\end{bmatrix}$$

$$[AM]_{big\ eye\ aunt} = \overrightarrow{output} \otimes \overrightarrow{input}$$

$$= \begin{bmatrix}1\\0\\0\end{bmatrix} \begin{bmatrix}1 & 0 & 0\end{bmatrix} = \begin{bmatrix}1 & 0 & 0\\0 & 0 & 0\\0 & 0 & 0\end{bmatrix}$$

$$[AM]_{big\ nose\ uncle} + [AM]_{big\ eye\ aunt} = \begin{bmatrix}1 & 0 & 0\\0 & 1 & 0\\0 & 0 & 0\end{bmatrix}$$

Read by the vector inner product recalling from the sparse memory template, and then use the nearest neighbor sigmoid threshold classifier to correct input data via the vector inner product:

$$\text{Recall Vector} = [AM][\text{error transmitted}]$$

$$\cong \sigma\left(\begin{bmatrix}1 & 0 & 0\\0 & 1 & 0\\0 & 0 & 0\end{bmatrix}\begin{bmatrix}0\\1\\1\end{bmatrix}\right) = \begin{bmatrix}0\\1\\0\end{bmatrix}_{uncle\ smiles}$$

The fault tolerant AM erases the one-bit error (the bottom bit) recovering the original state, which is equivalent to a semantic generalization: a big nosed smiling uncle is still the same big nose uncle. Thus, NOSE can produce either fault tolerance or generalization as two sides of the same storage coin according to the orthogonal or independent feature vectors.

Image Change Chip $\overrightarrow{ICC_t}$ is a mathematical procedure of information-selective compressive sampling defined as follows. If $\overrightarrow{ICC_t}$ is significant it must satisfy the requirement of pseudo-orthogonality described in Eq(1) to become admissible for AM storage Eq(2a). Then, the vector inner product is used for the retrieval from the AM the next significant change event index Eq(2b). The significant image change index is used to retrieve its high resolution image where another storage of Hetero-associative memory [HAM] matrix is defined by Eq(3a). Our dual storage strategy is more robust and efficient than early Kodak film preservation effort, which adopted a reduced dynamic range and resolution A/D-image to serve as the index of its own high resolution digital picture. We adopted NOSE notion to generate the pseudo-orthogonality $\overrightarrow{ICC_t}$ defined by the Dirac delta function:

$$(\overrightarrow{ICC}^T_{\tau\Delta t_S}, \overrightarrow{ICC}_{(\tau+1)\Delta t_S}) \cong \delta_{\tau,(\tau+1)} \quad (1)$$

where the superscript T denoted a transpose of a column vector to a row vector, and τ indicates a distinctive information flow when the CSp delayed time unit $\Delta t_S \gg \Delta t_{frame}$ compared to a video frame rate. Given one significant event index, the next significant event index follows without cross-talk:

$$[AM] = \sum_{\tau}\left[\overrightarrow{ICC}_{(\tau+1)\Delta t_S}, \overrightarrow{ICC}^T_{\tau\Delta t_S}\right]; \overrightarrow{ICC}_{(\tau+1)\Delta t_S} = \sigma\left([AM]\overrightarrow{ICC}_{\tau\Delta t_S}\right); where\ \sigma(x) = \frac{1}{1+e^{-x}} \quad (2a,b)$$

Then, a detail high resolution image is retrieved by the inner product from Hetero-Associative Memory [HAM] defined analogously as follows:

$$[HAM] = \sum_{\tau}\left[\vec{X}_{(\tau+1)\Delta t_S}, \overrightarrow{ICC}^T_{(\tau+1)\Delta t_S}\right]; \vec{X}_{(\tau+1)\Delta t_S} = \sigma\left([HAM]\overrightarrow{ICC}_{(\tau'+1)\Delta t_S}\right) \quad (3a,b)$$

The algorithm pseudo code is described as follows.

1. Read images (frame by frame, X_1, X_2, .., X_t, ...) from a video clip
2. Find the binary image changes (dX_1, dX_2, .., dX_t, ...) with a specific threshold, $dX_i = X_{i+1} - X_i$
3. Form a HAM using outer product of $[X_i dX_i]$.
4. Given a binary image change, retrieve data using inner product of $[HAM, dX_i]$.

Significant event storage and retrieval

We consider a high speed example:

i. Catching the glimpse of baseball pitching, and then a slow speed example

ii. Catching an Orchid punctuated blossoming at midnight

Figure 2 How we hit a curve baseball? A curve baseball takes about half a second to travel 60 ft. 6 in. at 80- 100 mph (113~140 ft/sec.) from the pitcher's mound to home plate. Good batters are taught to judge

(i) Catching 4 types of balls of the red seams at the swing distance arm-length away where Visual Contrast Sensitivity Function is optimal (fastball 90-mph topspin 1800 rpm, curveball 75mph, slider 85mph, and Screwball 75mph);

(ii) Taking the initial batting condition (e.g. 2 strikes against the batter situation the pitcher prefers a save slow speed foul out ball),

(iii) The batter watches the body & shoulder cue or hand hold clue from pitcher, as well as catcher last body movement language. When pitcher's fingers spin the top side of a fastball forwardly down during the release of the ball, it increases the top side's velocity with the spin, thus $V_{top} > V_{bottom}$. Since the air drag is proportional to the quadratic velocity $F_{top} \sim V_{top}^2$ (the first power comes from the air mass in the collision cylinder and the second power derives from the air mass momentum), the drag will produce a top heavy distribution function known as the Magnus effect in sports.[16] A topside-spin-forward ball generates a larger drag force at the top side; it pushes down the ball towards the home plate. The other physics effects are the lower air density the further it flies and the less humanity, the less drag, L. Bloomfield).

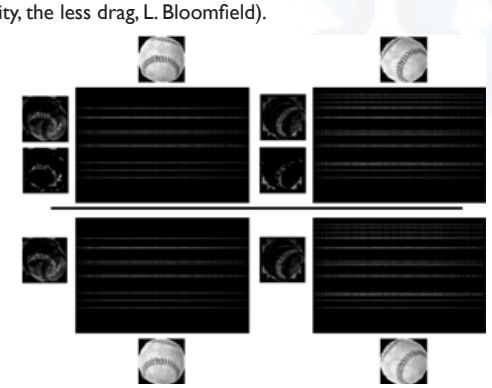

Figure 3 Top-Two 'writes' to HAM via an outer product of feature changes following a sigmoid σ -threshold operation. Two HAM writes and reads are displayed on the top, bottom respectively. Outer products of the feature changes (in binary mode after a threshold operation) and the object image is continuously updated in the [HAM] ('over-write' mode) shown on the top left. The top right shows the update of HAM with two different scenes (ball with top spin in this example). **Bottom-** Recalling an image from HAM via inner product with an arbitrary change vector (darker grayscale indicates zeros) with a sigmoid transfer function is used to recall the closet image, shown on the bottom left. The bottom right depicts another test result using a different change vector.

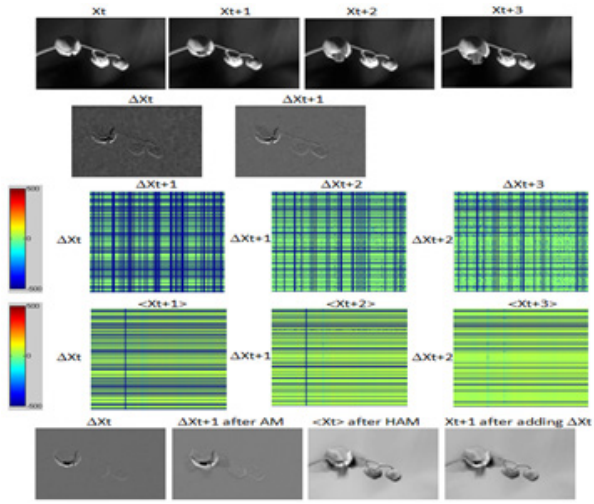

Figure 4 This HVS strategy ensures a sequence of blossoming orchid (1st row) that the updated change is a similar degree of sparseness and also exactly where the change happened (2nd row). In fact, a full sequence of sharp images (5th row) can be sequentially recalled from priming the [AM] sub-unit Eq(2a,b) (3rd row); [HAM] recall Eq(3a,b) (4th row).

Conclusion remarks

Two interesting remarks in comparisons with Compressive Sensing are given as follows.

Physics and mathematics challenges: Digital CT Scans of angiography (head) may be operated at 40% lower absorbed X-ray radiation than early models (at 500 milli unit of Wilhelm 'Roentgen equivalent man' (rem) or Int' Sys. U. at 5 milli Rolf Sirvert=1 Joule/kg). Candes, Romberg, Tao, and Donoho (*CRTD*) *Compressive Sensing (CS) methodology* developed originally for medical imaging is full of promises and challenges. In a simulation of the X-ray skull target, CRTD demonstrated that the amount of radiation exposure is reduced by another factor of ten, say from 300 slices of *X*-Ray projections to 30 slices at 1 cm apart reproducing an identical size and resolution image. *Such a feasibility of less radiation in less measurement holds promises for the medical community because it allows more patients to be examined at lower risk and less cost (i.e. wear and tear on equipment and technicians).* CRTD CS is not a traditional image compression. It happens at image acquisition pre-processing level. Compression is not desirable in the medical application because the patients would have already suffered from the radiation exposure. The reason that CRTD can sample much less than the Nyquist critical sampling rate, 2 per Fourier modes, is because the bio-tissue coupling tend to make an over-estimation of the independent number of Fourier modes. The adequate number of views M is proportional to the degree of freedom K. CRTD introduced a mask $[\Phi]_{M,N}$ which is a long rectangular matrix $M \cong K\,d.o.f. \ll N$ having K number of *1*'s (*1* means keep a pixel) distributed in a purely random fashion at arbitrary locations among numerous *0*'s. The sampling matrix is equivalent to a sparse CCD concept using M linear independent combination of image data which help recover the original image of N pixels. An original image should be filtered through a *random sparse sampling* mask; blocking X-rays or probing RF fields which is *physically impossible* and so far has escaped imaging community with the exception of optics. The *mathematical challenge* is that

given under-measurements of $\vec{y}_M : \vec{y}_M = [\Phi]_{M,N} \vec{X}_N$, finding the original larger set of image $\vec{X}_N$ was an *ill-posed inverse problem* without sufficient a-priori information. Any number of homogenous solutions, $[\Phi]_{M,N} \vec{X}'_N = 0$, could be added to an inhomogeneous solution $\vec{X}_N = [\Phi]^{-1}_{N,M} \vec{y}_M$ satisfying still the original set of measurements; but obviously this added homogeneous solution $\vec{X}'_N$ contributes a larger total magnitude and is therefore ruled out by the minimum l_1-norm constraint. This post processing is relatively *slow* but has inspired over 300 research and development papers in the world. Non-ANN readers may wish to skip the following remark and proceed directly to the summary paragraph without loss of insight.

ICA Linear algebra versus CS Linear algebra: The linear matrix $[\Phi][\Psi]$ used in ***CS*** should be compared to that used in Independent Component Analysis (***ICA***). We reviewed the ANN algebra to show how we can find this unknown mixing matrix $[A] \equiv [\ddot{O}][\O]$, as the Rosette stone, which can increase the supervised CS capability. When 2 eyes or 2 smart video cameras are used, one can factorize the joint probability density into a product of source densities without the *a-priori* knowledge of source mixing medium. How could we do that? The neural network community has followed the ICA factorization of *j-pdf* which is based on the Maximum of *a-posteriori* entropy $S_o = -\sum_{i=1}^{K} y_i \log y_i$ of de-mixed neural net weighted output $\vec{y} = [W]\vec{x}$ by Tony Bell, Terrence Sejnowski, Erkki Oja and Sunichi Amari (BSOA) circa 1997.[11] Concurrently, the present authors adopted the statistical mechanics approach maximizing the *a-priori* unknown sources $\vec{s}$ entropy $S_i = -\sum_{k=1}^{K} s_k \log s_k$ and minimizing the unknown mixing matrix $[A]$ error energy at an isothermal equilibrium. The Helmholtz free energy is the total energy E subtracting the none-workable source entropy $min.H = min.E - max.T_o S$ (e.g. brain temperature $T_o = 37^{\circ}C$). This mathematics is known as Lagrange Constrained Neural Networks[3] which was demonstrated with Math Lab code using 7 spectral band Landsat images over a Mediterranean desert city, and dual infrared spectral breast cancer images,[13] as well as a point-nonlinear space-variant mixture image.[12] Biologically HVS has dense photoelectric night vision rods of 140 million (grayscale) and 6.5 million day color cones arranged for multiple spectral CS in a seemingly random mosaic pattern at the retina in order to produce sparse information. All receptors compose overlapping, visual receptive fields of various sizes. If the intensity is over the prerequisite threshold held by an individual Ganglion cell connected to the receptive field, an action potential is fired from it to the brain. Ganglion receptive fields are not circular. They are in the shape of the Hubel-Wiesel (H-W) oriented edge maps,[4] known as Mexican hat wavelets (narrow ellipses, (+) on-center, (-) off-surround known as lateral inhibition). They extract edge features from an image and transmit them to the Visual Cortex (V1~V4 (edge, color, form, shape) regions). Hubel-Wiesel Mexican hat wavelet is the basis set $\{\psi_n\}$ denoted as sparse image edges column vectors applied to video compression.[14,15] Although $\vec{s}$ was a column vector of N components, with only K non-zeros wavelets is indexed by $n_k = 1,2,..,K \ll N$.

$$R^N = \vec{x} = \sum_{n=1}^{N} s_n \psi_n = \sum_{n_k=1}^{K} s_{n_k} \psi_{n_k} = [\Psi]\vec{s}\ ; \quad (4)$$

$$R^M : \vec{y} = \sum_{m=1}^{M} x_m \phi_m^T = [\Phi]\vec{x};\ \vec{y} = [\Phi][\Psi]\vec{s}\ . \quad (5)$$

Where M numbers of measurements represent the degree of sparseness of K ones among zeros $M \cong cK \ll N, where\, c \cong 1.3$. CRTD developed their linear programming algorithm under the constraint of the l_p-norm of total pixel value, $|\vec{x}|_p$:

$$|\vec{x}|_p \equiv (\sum_{n=1}^{N} |x_n|^p)^{1/p},\ \ 0 \le p < 2 \quad (6)$$

Where, $p = 2$ was Least Mean Squared (LMS); $p = 1$ is Manhattan, or city-block, window-rim distance; $p = 0$ promotes the sparseness of non-zero elements. CRTD recovered an optimal image $\vec{x}$ if $0 < p \le 1$. A smaller l_p-norm value rules out any superfluous homogeneous uniform solutions which reduce the contrast of the true image, $\vec{x}_N$. Instead of using the computationally intractable (or NP complete) l_0-norm (counting non-zero elements), or LMS l_2-norm for the Moore-Penrose pseudo-inverse, their minimization procedure was a compromise at the l_1-norm, promoting sparseness, eliminating the homogenous solutions, and recovering the unique in homogeneous solution.

CS community adopted the wavelet bases in column vectors forming long rectangular matrix $[\Psi]$, and a wide rectangular sampling matrix $[\Phi]$ which is filled with randomly scattered ones among zeros. Their product $[A] \equiv [\Phi][\Psi]$ turns out to be the unknown mixing matrix in ICA.

$$\vec{y} = [\Phi]\vec{x} = [\Phi][\Psi]\vec{s} \equiv [A]\vec{s} \quad (7)$$

1. *Symmetric Wiener Whitening in* ensemble average *matrix*,

$$[W_z]^T = [W_z] = \left\langle [\vec{y}\vec{y}^T] \right\rangle^{-\frac{1}{2}}$$

By definition $\vec{y}' \equiv [W_z]\vec{y}$ satisfying $\left\langle \vec{y}'\vec{y}'^T \right\rangle \equiv [W_z]\left\langle \vec{y}\vec{y}^T \right\rangle [W_z]^T = [I]$

$$\because [W_z]\left\langle \vec{y}\vec{y}^T \right\rangle [W_z]^T [W_z] = [I][W_z] = [W_z];$$

$$\therefore [W_z]^T [W_z] = \left\langle [\vec{y}\vec{y}^T] \right\rangle^{-1};\ [W_z] = \left\langle [\vec{y}\vec{y}^T] \right\rangle^{-\frac{1}{2}} \quad \text{Q.E.D}$$

2. **Orthogonal transform:** $[W]^T = [W]^{-1}$

By definition

$$[W]\vec{y}' = [W][W_z]\vec{y} = [W][W_z][\ddot{O}][\O]\vec{s} \equiv [W][W_z][A]\vec{s} = \vec{s}$$

$$\because [W] < \vec{y}'\vec{y}'^T > [W]^T \equiv [W][I][W]^T = \left\langle \vec{s}\vec{s}^T \right\rangle \cong [I];$$

$$\therefore [W]^T = [W]^{-1}\ \text{Q.E.D}$$

Reducing ICA to orthogonal rotation, allow ANN seeking a simple geometrical solution as the killing vector orthogonal to all the row vectors $[W_z][A] = [W_z][\ddot{O}][\O]$ except one, produces a correspondingly independent source along that direction.[11,12] Besides our MOS criterion, this ICA algebra might help design new sparsely sampling matrix deterministically.

In summary

For video compressive sampling, we do not use purely random sparse mask of ones among zeros to insure the independence. The

locations of ones have additional useful information which helped us rapidly and robustly recover original imagery. We have made sure that the frame sampling time $\Delta t_S \geq\geq t_F$ is delayed enough to allow motion displacement generate non-overlapping ones among zeros. This was a graphical indexing concept forming an ICC matrix storage called the Associative Memory (AM) in an Artificial Neural Network (ANN), as well as the outer product of ICC with the corresponding image itself called the Hetero-Associative Memory (HAM) without suffering cross talk. This is how we can instantaneously recall any image, without the need of search and slow image recovery iteration.

References-1

1. Giese MA, Poggio T. Neural mechanisms for the recognition of biological movements. *Nat Rev Neurosci*. 2003;4(3):179–192.
2. Candes EJ, Romberg J, Tao T. Robust uncertainty principle: exact signal reconstruction from highly incomplete frequency information. *IEEE Trans IT*. 2006;52(2):489–509.
3. Szu H, Kopriva I. Comparison of LCNN with Traditional ICA Methods. WCCI/IJCNN. 2002; Szu H, Chanyagorn P, Kopriva I: Sparse coding blind source separation through Powerline. *Neurocomputing*. 2002;48(1–4):1015–1020; Szu H. Thermodynamics Energy for both Supervised and Unsupervised Learning Neural Nets at a Constant Temperature. *Int J Neural Syst*. 1999;9(3):175–186; Szu H, Hsu C. Landsat spectral Unmixing à la superresolution of blind matrix inversion by constraint MaxEnt neural nets. *Proc. SPIE 3078.* 1997:147–160; H. Szu H, Hsu C. Blind de-mixing with unknown sources. *Proc Int Conf Neural Networks.* 1997;4:2518–2523.
4. Hubel DH, Wiesel TN. Receptive fields and functional architecture in the cat's visual cortex. *J Physiol*. 1962;160(1):106–154.2.
5. Pazo-Alvarez P, Amenedo RE, Cadaveira F. Automatic detection of motion direction changes in the human brain. *Eur J Neurosci*. 2004;19(7):1978–1986.
6. Candes EJ, Tao T. Near-optimal signal recovery from random projections: universal encoding strategies? *IEEE Trans IT*. 2006;52(12):5406–5425.
7. Donoho DL. Compressive sensing. *IEEE Trans IT*. 2006;52(4):1289–1306.
8. Cohen EH, Barenholtz E, Manish Singh M, et al. What change detection tells us about the visual representation of shape. *J Vis*. 2005;5(4):313–321.
9. Todd JJ, Marols R. Capacity limit of visual short-term memory in human posterior parietal cortex. *Nature*. 2004;428(6984):751–754.
10. Crick FC, Koch C. What is the function of the Claustrum? *Phil Trans of Royal Soc B-Bio Sci*. 2005;360(1458):1271–1279.
11. Bell AJ, Sejnowski TJ. A new learning algorithm for blind signal separation. *Adv In Inf Proc Sys*. 1996;8:7547–7763; Hyvarinen A, Oja E. A fast fixed-point algorithm for independent component analysis. *Neu Comp*. 1997;9:1483–1492; Amari SI. Information Geometry. *Contemporary Math* (ed. Nencka & Bourguignon). 1997;203:81–95.
12. Szu HH, Kopriva I. Unsupervised learning with stochastic gradient. *Neurocomputing*. 2005;68:130–160.
13. Szu H, Miao L, Qi H. Unsupervised learning with mini free energy. *Proc SPIE ICA, Wavelets, Neural Networks*. 2007;6576:14; Miao L, Qi H, Szu H. A maximum entropy approach to unsupervised mixed-pixel decomposition. *IEEE Trans Image Proc*. 2007;16(4):1008–1021.
14. Hsu C, Szu H. WaveNet processing brassboards for live video via radio. *Journal of Electronic Imaging*. 1998;7(4):755–768.
15. Szu H, Hsu CC, Thaker P, et al. Image Wavelet transform implemented with discrete wavelet chips. *Optical Engineering*. 1994;33(7).
16. Adair RK. The Physics of Baseball. (Perennial NY, 3rd Ed, 2002); L. Bloomfield. The Physics of Everyday Life.

References-2

1. Szu HH, Liu H–S. Earthquake calamity warning from space station: orbital dynamics coupling geology mantle convection. Proc SPIE 7343, Independent component analyses, Wavelets, Neural Networks, Biosystems, and Nanoengineering VII, 73430W. 2009.
2. Szu H. Thermodynamic learning rule. *INNS Natural Intelligence Magazine*. 2013;2(1):19–27.
3. O'Keefe JA. Zonal harmonics of the Earth's geopotential field and the basic hypothesis of geodesy. *J Geophys Res*. 1959;64(12):2389–2392.
4. Chandrasekhar S. *Hydrodynamics and hydromagnetic stability*. Oxford U Press. 1961:306.
5. Runcorn SK. Satellite gravity measurements and laminar viscous flow model of the Earth's mantle. *J Geophys Res*. 1964;69(20):4389–4394.
6. Runcorn SK. Flow in the mantle inferred from the low–degree harmonics of the geopotential. *Geophys J Int*. 1967;14(1–4):375–384.
7. Arfken G. *Mathematical methods for physicists*. Academic Press, New York. 1966:423.
8. Turcotte DL, Oxburgh ER. Finite amplitude convection cells and continental drift. *J Fluid Mech*. 1967;28:29–42.
9. Schubert G, Turcotte DL, Olson P. Mantle convection in the earth and planets. Cambridge U Press. 2001:956.
10. Liu HS. On the breakup of tectonic plates by polar wandering. *J Geophys Res*. 1974;79(17):2568–2572.
11. Liu HS, Chang ES, Wyatt GS. Small scale mantle convection system and stress field under the Pacific plate. *Phys Earth Planet Inter*. 1976;13(3):212–217.
12. Liu HS. Convection pattern and stress system under the African plate. *Phys Earth Planet Inter*. 1977;15(1):60–68.
13. Liu HS. Mantle convection and subcrustal stress field under Asia. *Phys Earth Planet Inter*. 1978;16(3):247–256.
14. Liu HS. Convection generated stress concentrations and seismogenic models of the Tangshan earthquake. *Phys Earth Planet Inter*. 1979;19(4):307–318.
15. Liu HS, Mantle convection and subcrustal stresses under Australia. *Modern Geology*. 1979;7:29–36.
16. Liu HS, Chang ES. On the selection of station sites for observing strain steps and earthquake forerunners in California. *Bull Seismological Soc Am*. 1979;69(6):1989–1994.
17. Liu HS. Convection generated stress field and intraplate volcanism. *Tectonophysics*. 1980;65(3–4):225–244.
18. Liu HS. Mantle convection and subcrutal stresses under the United States. *Modern Geology*. 1980;7:81–93.
19. Liu HS. Mantle convection pattern and subcrustal stress field under South America. *Modern Geology*. 1980;7(3):161–169.

20. Liu HS. Geodynamics of Cenozoic deformation in Central Asia. *Phys Earth Planet Inter*. 1981;25(1):64–70.
21. Liu HS. Ore deposits in Africa and their relation to the underlying mantle. *Modern Geology*. 1981;8(1):23–36.
22. Liu HS. Geodynamics of the Baikal–Stanovoy seismic belt. *Phys Earth Planet Inter*. 1983;31(1):77–82.
23. Liu HS. A dynamical basis for crustal deformation and seimotectonic block movements in central Europe. *Phys Earth Planet Inter*. 1983;32(2):146–159.
24. Liu HS. Satellite–determined stresses in the crust of Europe. *Seismic Activity in Western Europe*. 1984;19–36.
25. Liu HS. Geodynamical basis for crustal deformation under the Tibetan Plateau. *Phys Earth Planet Inter*. 1985;40(1):43–60.
26. Liu HS. Satellite detection of the convection generated stresses in the Earth. *Recent Res Devel Geophysics*. 2003;5:117–137.
27. Gilert S, Borre K. Linear algebra, geodesy and GPS. Wellesley–Cambridge Press. 1997.
28. H Szu. ICA-an enabling technology for intelligent sensory processing, IEEE circuits and systems newsletters. 1999;14–41, December 1999; H. Szu, Progresses in unsupervised artificial neural networks of blind image demixing, IEEE Ind Elec Soc Newsletter. 1999;7–12.
29. H Szu, Zhang LM. Intel image proc blind sources. Shanghai Sci Ed Publ. 2003. In: Computational Intelligence, Ch 16: H. Szu Unsupervised Learning ANN, IEEE CI Society, The IEEE Press 2004.
30. Wagner CA, Lerch FJ, Brownd JE, et al. Improvement in the geopotential derived from satellite and surface data (GEM 7 and 8). *J Geophys Res*. 1977;82(5):901–914.
31. Lemoine FG, Kenyon SC, Factor JK, et al. The development of the joint NASA GSFC and the national imagery and mapping agency (NIMA) geopotential model EGM96. 1998;NASA/TP 1998–206861.
32. Tapley, BD, Bettadpur S. The gravity recovery and climate experiment: mission overview and early results. *EOS Trans AGU*. 2001;82(47):F286.
33. Candes EJ, Romberg J, Tao T. Robust uncertainty principle: exact signal reconstruction from highly incomplete frequency information. *IEEE Trans IT*. 2006;52(2):489–509.
34. Candes EJ, Tao T. Near-optimal signal recovery from random projections: universal encoding strategies? *IEEE Trans IT*. 2006;52(12):5406–5425.
35. Donoho D. Compressive Sensing. *IEEE Trans IT*. 2006;52(4):1289–1306.
36. Szu H, Miao L, Qi H. Unsupervised learning with minimum free energy. *Proc SPIE*. 2007;6576.
37. Szu H, Hsu C. Landsat spectral unmixing a la superresolution of blind matrix inversion by constraint maxent neural nets. *Proc SPIE Int Soc Opt Eng*. 1997;3078:147–160.
38. US PTO Patent Harold Szu. Infrared multi–spectral camera and process of using infrared multi–spectral camera. US PTO 7366564. 2008.
39. Szu H, Buss JR, Kopriva I, et al; Nonlinear blind demixing of single pixel underlying radiation sources and digital spectrum local thermometer. 2008.
40. Szu H, Hsu C, Jenkins J, et al. Capture significant events with neural networks, *Neural Networks*. 2012;29–30:1–7.
41. Appleby R, Coward P, Sanders JN. Evaluation of a passive millimeter wave imaging for wide detection in degraded visual condition. *Proc SPIE Int Soc Opt Eng*. 2009;7309.
42. Coward P, Appleby R. Comparison of passive millimeter–wave and IR imagery in a nautical environment. *Proc SPIE Int Soc Opt Eng*. 2009;7309:1–8.
43. Cha JH, Abbott AL, Szu H. Passive ranging redundancy reduction in diurnal weather conditions. *SPIE Defense, Security, Sensing*. 2013.
44. Hsu C, Hsu MK, Cha J, et al. Adaptive compressive sensing camera. *SPIE Proc*. 2013.
45. Vahidinia S. Regolith radiative transfer model; applications to saturn's icy rings. PhD 2010 UC Santa Cruz.
46. Mustardm JF, Hays JE. Effects of hyperfine particles on reflectance spectra from 0.3 to 25 microns. *Icarus*. 1997;125(1):145–163.
47. Payan V, Royer A. Analysis of temperature emissivity separation (TES) algorithm applicability and sensitivity. *Int J Remote Sensing*. 2004;25(1):15–27.
48. Vernazza P, Carry B, Emery J, et al. Mid–IR spectral variability for compositionally similar asteroids; implications of asteroid particle size distribution. *Icarus*. 2010;207(2):800–809.
49. Hapke B. Bi-direction reflectance spectroscopy: I. theory. *Geophysical Rev*. 1981;86:3039–3054.
50. Ren H, Szu H, Buss J. Lagrange constraint neural network for fully constrained subpixel classification in hyperspectral imagery. *Proc SPIE*. 2002;4738:184–190.
51. Kopriva I, Szu H. Fast LCNN ica for unsupervised hyperspectral image classifier. *Proc SPIE*. 2002;4738:169–183.
52. Ren H, Chang CI. Target–constrained interference–minimized approach to subpixel target detection for hyperspectral images. *Opt Eng*. 2000;39(12):3138–3145.
53. Chang CI, Heinz DC. Constrained subpixel target detection for remotely sensed imagery. *IEEE Trans Geosci Remote Sensing*. 2000;38(3):1144–1158.